DEVELOPMENT OF A PHYSIOLOGICAL FLOW LOOP SIMULATOR FOR GRAFT COMPLIANCE TESTING

JORDI REDDY

CARDIOVASCULAR RESEARCH UNIT

UNIVERSITY OF CAPE TOWN

February 2010

Supervisor: Dr Thomas Franz

Co-supervisor: Dr Deon Bezuidenhout

Submitted to the Department of Human Biology, University of Cape Town, for the degree

MSc (Med) in Biomedical Engineering

I. Declaration

I declare that this dissertation contains only my work and that all significant contributions from external sources have been cited and referenced.

_____

Jordi Reddy

II. Acknowledgements

I thank the following people:

Foremost, Dr Thomas Franz, for his superb supervision, input, advice and guidance concerning almost every aspect of the project throughout its duration

Dr Deon Bezuidenhout, for his out-of-the-box thinking and contributions to the design phase of the project

My parents, for their continued support, interest and input

Raymond Michaels, for his assistance with various pieces of equipment and the relevant operating procedures

Special thanks to Bruno Orlandi for contributing his incredible manufacturing skills and engineering experience to the mechanical aspects of the project

This project was supported financially by the National Research Foundation (NRF) of South Africa

III. Table of Contents

IV. List of Figures

V. List of Tables

VI. Table of Symbols

	Symbol	SI Unit	Industry / medical unit
Area	A	m^2	
Linear piston acceleration	a	m/s^2	
Compliance	C		%/100mmHg
Graft internal diameter	D	m	mm
Tube diameter	d	m	mm
Force	F	N	
Pulse frequency	f	Hz	bpm
Needle valve gate height	h	m	mm
Mass	m	kg	
Fluid pressure	P	kPa	mmHg
Volume flow rate	Q	m^3/s	cc/s
Tube radius	R	m	mm
Crank radius	r	m	
Torque	T	Nm	
Time	t	s	
Flow velocity	u	m/s	cm/s
Linear piston velocity	v	m/s	
Linear piston displacement	x	m	mm
Crank angle	θ	rad	degrees (°)
Fluid viscosity	μ	Ns/m^2	
Density	ρ	kg/m^3	
Sector angle	φ	rad	degrees (°)
Crank angular velocity	ω	rad/s	rpm

VII. Glossary

AAMI: Association for the Advancement of Medical Instrumentation.

AIH: Anastomotic Intimal Hyperplasia. Excessive thickening of the intimal tissue in the peri-anastomotic region of vascular grafts.

BDC: Bottom-dead-centre. Crank position relative to the piston plunger when fully withdrawn.

Check valve: One-way valve. Valve that allows fluid to pass in one direction only.

CVRU: Cardiovascular Research Unit (University of Cape Town, Cape Town, South Africa)

Cracking pressure: The pressure required to open a check valve.

DIPT: Disposable Integrated Pressure Transducer.

EMI: Electromagnetic interference.

PID controller: Proportional-integral-derivative controller. Closed loop control for use in a feedback system.

TDC: Top-dead-centre. Crank position relative to the piston plunger when fully extended.

Tricuspid valve: Tri-leaflet atrioventricular heart valve between the right atrium and the right ventricle.

Dictrotic wave: A small pressure peak caused by the reflection of a pressure wave after closure of the aortic valve.

Chapter 1: Introduction and Problem Description

1.1 Description of the Problem

The long-term success of tissue-engineered medical implants comprising synthetic materials depends largely on the host response. In vascular grafts, replacing or bypassing diseased arterial blood vessels, radial compliance is one of the key factors for long-term graft success [Seifalian et al., 1999]. Vascular prostheses should ideally mimic the mechanical behaviour of healthy native arteries which adapt the diameter in response to the blood pressure changes. Non-compliant (i.e. stiff) vascular grafts which do not show this diameter adaptation behaviour may lead to physiological problems after implantation. One such problem is anastomotic intimal hyperplasia (AIH), the excessive thickening of intimal tissue in the peri-anastomotic region of vascular grafts. This is caused by variations in flow and shear stresses aggravated by compliance mismatching between the host artery and prosthetic implant, and often results in long-term graft failure.

The characterization of radial compliance, i.e. the change in luminal graft diameter with change in internal pressure, is therefore a crucial part in the design and development process of vascular grafts. While computational methods have become more important in theoretically predicting the mechanical behaviour of graft prototypes, the experimental testing of prototypes and materials utilised is also necessary. Experimental tests, conducted in-vitro under simulated physiological conditions, serve the measurement of material properties of graft components and the

characterization of the structural mechanical properties of graft prototypes, such as the radial compliance. The results of these experiments for the structural properties of graft prototypes may be utilized directly in the design process and feature as input and validation data for computational methods.

The simulation of physiological conditions of the cardiovascular system in an *in vitro* setup is a non-trivial task and requires comprehensive consideration of the nature of the physiological blood flow and properties of the arterial circulation.

1.2 Significance of the Project

The focus of this research is aimed at cardiovascular diseases and development of this project will contribute to the testing and further development of graft prototypes and materials that may be used to treat such diseases. The outcomes of this project will provide the Cardiovascular Research Unit with a valuable technology and equipment for ongoing and future research into vascular grafts aimed at incorporating leading research topics such as tissue regeneration and tissue engineering. The significance of this project is high since cardiovascular diseases are becoming one of the leading causes of death, and are expected to supersede infectious diseases by the year 2020.

1.3 Scope and Objectives of the Project

Compliance mismatching between the graft and the host artery is recognised as one of the main contributors to graft failure. Thus, effective testing of vascular grafts requires the determination and assessment of graft compliance. In order to measure the graft compliance *in vitro* it is necessary to develop a system to simulate the physiological conditions of a patient, namely blood pressure, viscosity, temperature, flow rate, pulse frequency, stroke volume and host artery compliance. Accurate simulation of these conditions ensures that the behaviour of the graft in the testing system closely represents the behaviour of the graft once it is implanted in the patient. By designing the system to simulate these conditions at different regions of the arterial tree, it would be possible to assess the grafts in the context of their intended implant location in the patient. These requirements stipulate that the system be able to reproduce variable dynamic physiological conditions that may be adjusted with respect to the type of graft being assessed.

The above specifications form the scope of this project, the outcome of which is an *in vitro* system that provides a time-correlated pressure profile to be used, together with a corresponding diameter profile, for compliance measurement of synthetic vascular grafts. The diameter measurement system design and integration does not form part of this project and is the basis for future work, wherein the combination of pressure and diameter profiles will be integrated such that the graft compliance can be calculated. Thus the objective of this project was to produce a working prototype such that graft specimens could be subjected to physiological dynamic pressure and flow conditions by the end of the project duration. The milestones associated with this objective were defined as follows:

- Determination of the physiological properties of the cardiovascular system, such that the design requirements of the electro-mechanical system could be established
- Electro-mechanical bottom-up design of the circulatory system. This entailed development of a pulse duplicator, relevant measurement devices and control system to produce and maintain the circulatory system conditions as close to the physiological conditions as possible

- Manufacture of custom designed components and assembly of subsystems
- Development of the control system and graphical user interface to control the flow loop parameters
- Output an optimized time-correlated pressure profile, expressed graphically and numerically, for future integration with a diameter measurement profile
- Output the best flow profile approximation with respect to physiological conditions, such that the optimized pressure profile was not compromised

Despite the exclusion of the graft diameter measurement system from the project scope, it was required that the flow loop simulator be designed with an ultrasound diameter measurement system in mind. Thus the electro-mechanical design process considered the system as a whole in order to facilitate the future integration of the two systems.

What follows is a discussion of the background theory and literature relevant to compliance testing, followed by a detailed description of the design process (Chapter 3) and outcomes (Chapter 4). Chapter 5 presents a discussion of the design outcomes, after which conclusions and recommendations for future work are outlined in Chapter 6.

Chapter 2: Background Theory and Literature Review

2.1 Vascular Compliance Theory

The radial compliance of a vascular graft is a measure of the change in the internal diameter of the graft relative to a change in applied internal pressure, and may be expressed as follows:

$$\mathrm{C_{radial}} = \frac{\Delta \mathrm{D}}{\mathrm{D}\Delta \mathrm{P}} \times 100\% \times 100\ \mathrm{mmHg}$$

where C_{radial} is the radial compliance, D is the internal diameter and P is the applied internal pressure. As mentioned previously, the scope of this work concerns the dynamic change in pressure, ΔP. Future integration of a diameter measurement system will contribute the dynamic change in internal diameter, ΔD, to yield the graft compliance.

2.2 Compliance Testing

There have been relatively few prior attempts at producing a working compliance tester system. The systems presented in previous art have highlighted some significant factors regarding the simulation of physiological conditions, with the goal of *in vitro* assessment of an implantable device. The areas of primary concern in the design of such a system are the reproduction of physiological conditions and measurement of the behaviour of the device under investigation. The most complex physiological conditions to reproduce are the flow, pressure and volume waveforms. Thus, the focus of initial research was concerned with exploring the possibilities surrounding hydraulic actuation and drive mechanisms. Additional significance was placed on researching the measurement apparatus that is required to monitor dimensional changes in the device under investigation, such that they could be factored into the design process.

2.2.1 Drive Devices

Various drive devices and mechanisms have been used to produce flow in a hydraulic system, the majority of which are pumps that make use of an electric motor. Previous designs propose solutions to the problem of producing accurate physiological flow waveforms by mechanical means. Some of the literature also discusses the ability of the designs to produce physiological pressure waveforms.

Normann [1977] simplified a balloon-activated blood pump, intended for use as a ventricular assist device. A balloon fitted inside a tube is inflated with pressurized gas to expel fluid from the region between the balloon and the outer tube. Pulsatile flow is generated by periodic pressurization of the balloon.

Werneck, et al. [1984] proposed that the pump be designed as an ideal flow source such that impedance can be added to the system to more closely represent the heart. The proposed pump comprised two sections, the first to convert electrical information to mechanical movement, and the second to convert the mechanical movement to fluid velocity. The former was designed for position control since velocity control becomes too complex at low frequencies. The latter incorporated a printed armature motor for its fast response and linear voltage-to-velocity characteristic.

Brant, et al. [1986] developed a cam and roller-follower pump system to minimize discontinuities in the pump motion that could produce non-physiological accelerations of the fluid in the system. Maintenance of flow continuity is largely attributed to the roller maintaining multiple points of contact with the cam. A potential problem with the cam-follower system is that the roller may uncouple from the cam due to insufficient contact force. The authors proposed that a return spring be incorporated to maintain the contact force.

Law, et al. [1987] designed a roller pump system to produce physiological pulsatile flow. A complication with the roller pump was that for constant rotor speed, flow varies over each revolution. This is because as one roller leaves the tube, the end of the tube regains its uncompressed shape. The fluid delivered by the other roller will be absorbed by the expanding tube section and reduce the overall flow rate. This problem was overcome by adding a metal insert to the pump assembly to allow the tube to expand more slowly. The limitations of this system were outlined by the authors:

- The output flow rate is determined by the diameter of the tubing
- The roller pump and motor are expensive

Improvements to the system were proposed:

- A stepper motor with more steps per revolution would allow for increased control
- Closed-loop control could provide a better match between input and output waveforms
- A position sensor installed on the rotor would provide useful information that could be used as the control input

Peterson, et al. [1990] discussed a pump device capable of displacing a stroke volume accurate to within 0.5 microlitres (µl). The device comprises a variable speed DC motor which drives a bellows to displace fluid into and out of the graft, thus producing a sinusoidal change in internal pressure.
The shortcomings of various pump types were discussed by Holdsworth, et al. [1991] in an attempt to develop a more suitable pump for physiological flow simulation. The authors' comments were as follows:

- Gear pumps produce damage to suspended particles and are sensitive to cavitations due to the action of the gears
- Peristaltic pumps simulate flow waveforms by mechanical control of the pump back-plate or computer control of the roller. This type of pump can only produce a limited number of waveforms and is not well suited to producing steady or reverse flow
- Cam-driven piston pumps are also problematic when trying to programme new waveforms or produce steady flow
- Servo-driven piston pumps act as an ideal flow source, but are poorly suited to producing uninterrupted constant flow

The above pumps all require flow-monitoring as feedback to determine the output waveform, whereas the pump developed by the authors has sufficiently stable open-loop performance to remove the requirement for continuous feedback control. The developed pump is a modification of the servo-driven piston pump that produces physiological blood flow waveforms, including reverse and steady flow. The error is negligible at low flow rates and is a maximum of 250µl/s at the maximum flow rate of 60ml/s. This maximum flow rate is limited by insufficient torque at high rotation rates.

Runge [1994] proposed a cardiopulmonary bypass pump comprising a compression plate that compresses the pump ventricle against the exterior wall. The compression plate mechanism is a mechanical system that translates rotational motion into axial translation, via a rotating shaft with helical grooves that are tracked by a follower pin on the plate. Thus a compressive force is produced.

Qian [1996] conducted research into an alternative to the diaphragm pump as a means of producing pulsatile flow. The pulsatile blood pressure and flow rate is achieved by changing the rotational speed of the impeller periodically by introducing a square wave voltage into the motor coil. The focus of the research was to design the impeller blade profile to eliminate haemolysis of blood cells. The device caused no damage to blood cells when tested on pigs. The pump produces pulsatile flow like a diaphragm pump and does not produce any backflow.

An infinitely variable pneumatic pulsatile pump was conceived by West [1996]. The pump does not require electrical actuation of its components and it is capable of producing slow pulsatile flow as well as high-frequency pulses and steady flow. The pneumatic control circuit comprises compression chambers, controlled by tactile pneumatic response switches, to produce oscillating pressure to drive the system.

Conti, et al. [1997] devised a means of producing pulsatile flow by driving a bellows with an adjustable DC rate motor to control fluid volume ejected in the circulatory system. There is minimal published information on the system's effectiveness with respect to pressure and flow waveform simulation.

Wright [1997] stipulated that a roller pump produces ripple flow rather than pulsatile flow. The author modified the roller pump concept by using high torque motors and electronic control to intermittently start and stop the pump rotor. This allows for adjustment of the pulse duration, frequency and speed, as well as the proportion of pulsatile to continuous flow. The design limits the flow pulse production to 10% of that capable by the human left ventricle. The author commented on the rectification of a sine wave flow waveform with the use of a one-way valve at the system inlet from the pump.

Charara et al. [1999] combined a stepper motor and piston configuration to produce positive fluid displacement. The emphasis was on producing laminar parabolic flow profiles over a variable velocity range. This computer-controlled pump system showed significant attenuation at high frequencies as well as a phase lag that resulted in the system response differing from the command. Discussion of other pump types revealed their shortcomings as determined by the authors:

- Roller pumps produce uncontrolled sine wave flows
- Gear pumps are difficult to sterilize and can damage the fluid particles
- Piston pumps deviate from the system transfer function and the axial distension of the vessel segment cannot be easily adapted

The focus of most of the aforementioned literature was primarily on physiological flow simulation. There was minimal discussion regarding the ability of the designs to produce accurate waveforms of both flow *and* pressure. However, Dynatek Dalta Scientific Instruments (Galena, Missouri, USA) has developed commercial devices capable of accurately producing both waveforms.

One such device is the MP3 Pulse Duplicator designed to produce physiological flow and pressure waveforms for heart valve testing [Dynatek]. The pulse duplicator comprises a stepper- or servo-motor drive system and divides each cycle into a number of steps. The programmable nature of this drive system allows for high resolution control of the waveforms produced at the pump output.

The pulsatile ventricular assist device [Dynatek] is designed to emulate *in vivo* flow rates and pressures to test artificial hearts and assist devices. It provides mechanical equivalents for the left ventricle, aortic valve, compliant aorta, atrium and mitral valve. The pumping system comprises a servo-motor and linear actuator which drives a piston as the pump output.

These devices from Dynatek Dalta may serve as intellectual input for this project with respect to the development of a drive system for the compliance tester, as well as a comparative tool for the assessment of the developed device.

2.2.2 Measurement of Graft Diameter

The change in graft diameter due to change in internal pressure is known as the radial compliance of the graft. The most significant physical property of the graft with respect to radial compliance measurement is change in *internal* diameter, since this is the most direct result of internal pressure changes. Taking into account the intention to incorporate the flow loop simulator with a diameter measurement system for compliance calculation, it was necessary to consider methods of

monitoring the dimensional changes of a vessel graft, due to changes in internal pressure and flow of the circulating fluid.

Measurement of internal diameter changes may be conducted directly or indirectly (from outer diameter and wall thickness), and it is preferable to conduct the measurements non-invasively, i.e. minimal physical contact with the vessel, to minimize the error introduced by the measurement device. Thus far, various diameter measurement methods and apparatus have been researched.

One of the first techniques for measuring the external diameter of a vessel was proposed by Fung [1966]. The design comprised a collimated light beam that was aimed at the vessel such that it cast an enlarged silhouette on a photo cell. The photo cell was used to track rapid changes in the external margins of the vessel by detecting changes in the light intensity. In addition to external diameter measurement, the vessel tension was measured using strain gauge force transducers. The author commented that the region over which the vessel holds the closest approximation to a cylinder is short relative to its length. This is due to tapering at the extremities as a result of the vessel elasticity.

Learoyd, et al. [1966] also made use of a light beam and photoelectric cell to measure the external diameter of arteries. The authors commented that the light source drifted when driven by a 12V battery. The solution was to replace the battery with a DC power supply stable to within 5mV.

Murgo, et al. [1971] designed a cantilever system with strain gauges to measure the external diameter of arteries between 1mm and 20mm. The cantilevers required physical contact with the vessel and exerted nominal loads on the vessel walls (approx. 600mg) that acted as a restoring force at the point of contact. This resulted in an underestimate of the vessel diameter. This system suffered additional problems with drift and was susceptible to permanent damage due to over deflection.

White, et al. [1986] used Electromagnetic Rheoangiometry (ER) to determine the compliance of small diameter arterial prostheses. This technique was used to measure continuous intraluminal diameter, pulsatile diameter and pulse pressure of the vessel segment. The diameter measurements were measured using a quadrangular loop probe and external magnetic field.

An ultrasonic echo tracking device was developed by Tardy, et al. [1991] that allows continuous recording of the internal diameter of peripheral arteries. The diameter is measured 300 times per second with a resolution of 2.5 micron. The arterial pressure was measured using a light-plethysmograph with accuracy of 0.25kPa. Hysteresis occurred in the diameter-pressure curve due to the finite pulse wave velocity of the ultrasound, and different diameter and pressure measurement sites.

Meister, et al. [1992] were able to measure the internal diameter and wall thickness at the same location on an artery using ultrasound. With reference to [Tardy et al., 1991], this technique could minimize the effects of the finite pulse wave velocity and reduce hysteresis.

Greisler, et al. [1992] determined the external diameter of bioresorbable vascular grafts using a helium-neon laser micrometer. The scanning range of the micrometer was between 0.254mm and 50mm.

Li, et al. [1993] highlighted the limited achievable resolution of ultrasound as one of the primary errors in diameter measurement. The wavelengths of ultrasound with frequencies 3MHz, 5 MHz and 10 MHz are 0.5 mm, 0.3 mm and 0.15 mm respectively, thus the error in area estimation on small vessels can be very high. To measure blood vessel diameters the authors measured the external vessel diameter using a microscope, and the inner diameter with cursors on a B-mode ultrasound image.

Conti, et al. [1997] incorporated a linear voltage displacement transducer (LVDT) into their compliance testing system for length-to-voltage conversion to measure change in graft length. Compliance was calculated as a function of change in graft length and the known volume of fluid ejected by the aforementioned bellow pump system.

Two complications associated with laser and ultrasound measurements of vascular grafts during high-speed testing were outlined by Conti, et al. [1998]. The first is the resultant error due to vibration of the device. This can be overcome by using a high sampling rate. The second concerns the roughening of the graft due to its radial and longitudinal compliance. This roughening alters the physical properties of the grafts and, in the case of ultrasound, the interaction of the measurement medium with the graft.
The principle of ultrasonic flow measurement relies on the frequency shift of an ultrasound signal when it is reflected by suspended particles in the fluid [Omega, 2009]. This implies an additional consideration that the fluid contain at least 100 parts per million of 100 micron suspended particles or gas bubbles such that the flow velocity can be measured.

Yeoman [2004] utilized two separate methods of diameter measurement. Digital imaging of the graft comprised a digital camera connected to a microscope such that the images could be analyzed using signal processing. The wall thickness of the graft was measured from cross-section samples and subtracted from the digital measurement of the external diameter to determine the internal diameter. This method ignores the change of wall thickness due to internal pressure. Ultrasound imaging was used to measure the internal diameter non-invasively and directly. However, the image resolution was poor and the recorded results were difficult to use due to scattering of the reflected ultrasound by the porous graft structure.

An advancement on non-invasive echo-tracking measurement was designed by Cinthio et al. [2005] to measure arterial wall movements in two-dimensions. Two high-resolution triangulation lasers were used to track movements along two axes. The test results show an inaccuracy of 2.5% full scale deflection, reproducibility of 8 micron and a resolution of 5 micron. Significant use of image processing and development of an echo-tracking algorithm was required to analyze the results of this setup.

Pampel, et al. [2007] discussed a radiometric measurement technique for dynamic thickness measurements in industry. A transmitter and receiver on either side of a measurand determine the thickness of the measurand by measuring the amount of radiation transmitted through it.

Binu, et al. [2007] developed a fibre optic displacement sensor of measurement of the amplitude and frequency of vibrations. The optic sensor can measure vibration amplitudes of 0.008mm to 0.74mm, and has a frequency range of 75Hz to 275Hz. However, these measurement ranges are not centred on the regions of interest for cardiovascular studies, thus the device is not ideal for the purposes of this project. Interference of ambient light and airborne particles are additional considerations with respect to this measurement technique.

The Venturi effect can be used as an indirect method of measuring the volumetric flow of a fluid. The concept uses Bernoulli's principle to determine the reduction in fluid pressure across a constriction in the fluid flow path, given the known velocities of the fluid on either side of the constriction. Conversely, if the pressures on either side of the constriction are measurable, it is possible to calculate one of the fluid velocities if the other is known.

None of the aforementioned devices and methods provides a complete solution to the problem of non-contact, non-invasive measurement of the internal diameter of a cardiovascular vessel graft. The concepts and principles presented provide insight into the design of such a device or technique, and provide substantial information on measurement devices that may be used together to arrive at a suitable measurement system.

2.2.3 Alternative Methods of Compliance Measurement

Other techniques for measuring compliance have been proposed, that offer alternatives to direct measurement of vessel diameter. One such approach is the injected volume technique that involves monitoring of the pressure-volume relationship of the vessel under investigation [Conti, 1990]. A rod is used to determine the initial volume of the vessel lumen. A known volume is injected into the vessel and the change in pressure is recorded. The new volume can be calculated to determine the pressure-volume relationship. This method is only suited to static measurement of vessel compliance. It is also problematic for open-mesh structures in which the latex/silicon liner bulges through the mesh openings, resulting in inaccurate volume calculations.

Kok, et al. [2000] measured bladder pressure and urine flow rate to determine changes in urinary bladder compliance due to urethral obstruction. A blood flow meter was used to measure urethral flow. The measured pressure and flow rate were plotted and the maximum flow rate, pressure at the maximum flow rate and pressure at half the maximum flow rate were determined. Thus the urethral resistance could be determined. Compliance was calculated as the increase in bladder pressure between two boundaries during a filling cycle, as a function of the infused volume.

For the flow loop simulator, it was necessary to consider the aforementioned devices and techniques to determine the most accurate and versatile method of flow and pressure profile production, such that they could be incorporated into the system design or serve as input into the development of a more suitable method.

2.2.4 Additional System Considerations

The practical implications associated with *in vitro* graft testing posed some relevant design considerations. These considerations are outlined below and were factored into the design process as described in detail in the following chapter.

- Open-mesh grafts require sealing, whether by clotting or insertion of a non-porous tube, which affects the structural stiffness of the graft, and consequently the deformation
- *In vivo* arteries are held in longitudinal tension. Thus to improve the accuracy and applicability of the *in vitro* testing procedure it was necessary to consider pre-straining the test grafts in the flow loop simulator
- Rigid mounting of a graft produces end effects at the attachment sites, thus the future diameter measurement system should be positioned where the end effects are at a minimum,

i.e. in the mid region of the graft. This implied design considerations with respect to graft positioning in the flow loop simulator.

- Graft manufacture should consider a high length-diameter ratio such that the end effects are negligible in the graft mid region, thus accommodation was to be designed for relatively long graft specimens in the flow loop simulator
- It was important to realise that the graft mounting method was non-trivial, and that diameter discontinuities could interfere with the pressure and flow profiles, such that the produced profiles would not be adequately translated to within the graft or otherwise suffer significant losses. This implied the design requirement of a thin-walled mount on either side of the graft specimen.

Chapter 3: Design Process

3.1 Derivation of System Specifications

Figure 1 provides approximations as to the physiological profiles of pressure and flow velocity in a healthy patient. For the purposes of CVRU it was desirable to be able to test a range of artificial artery grafts between 1.6 and 8mm inner diameter. The average range of physiological conditions associated with arteries of this size as observed in healthy patients are summarized in Table 1. Additionally, Table 1 summarizes the desired testing range of the flow loop simulator, with respect to these physiological values. The desired testing range exceeds the limits of the physiological conditions since it was valuable to assess the grafts beyond these limits and potentially determine their failure conditions. During development of the flow loop simulator, the system was optimized to test grafts of 4mm diameter at 72bpm cycle frequency.

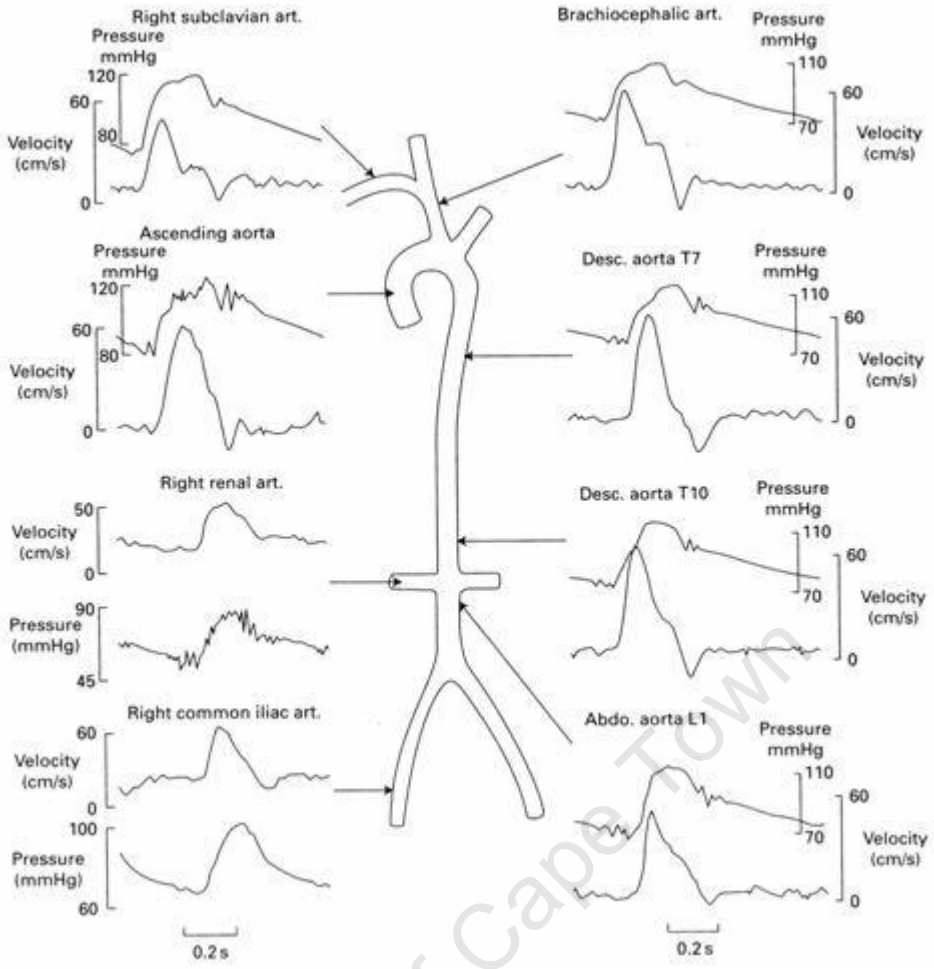

Figure 1: Approximations of pressure and flow profiles at different points of the arterial tree [Mills et al., 1970]

Table 1: Summary of the physiological conditions and compliance tester specifications associated with grafts between 1.6 and 8mm inner diameter. The critical values associated with the worst case scenario for patients are shown in brackets.

	Physiological conditions	**Flow loop simulator specifications**
Compliance [%/100mmHg]	3 – 4 [Conti and Strope, 2002]	0 - 15
Fluid pressure [mmHg]	80 - 120 (160) [Conti and Strope, 2002]	0 - 200
Cycle frequency [bpm]	–50 – 180 (200) [Conti, 1990]	0 - 200
Flow velocity [cm/s]	0 – 60 [Charara et al., 1999]	0 - 100
Temperature [°C]	37 [Conti and Strope, 2002]	37
Fluid viscosity [Ns/m^2]	Blood: 0.0049 [Rosenson et al., 2002]	Water: 0.0006 Glycerine saline solution: 0.0049

3.2 Pump System Design

3.2.1 Pulse Duplicator Mechanical Overview

To accurately produce physiological flow and pressure profiles, corresponding to different regions of the arterial tree, it was necessary to design and develop a pulse duplicating pump system. Specification of such a pump system required detailed discussion and evaluation of the intended components. These components include a motor and mechanical conversion system (to convert the motor output into the required mechanical form), as well as a hydraulic conversion system (to convert mechanical movement into hydraulic actuation). Tables 2, 3 and 4 consider the characteristics and properties of the components relevant to the pump system design. Figure 2 illustrates diagrammatically the mechanical construction and linkages of the various designs.

Table 2: Comparison of characteristics and limitations concerning motor selection

Motors			
Type	Stepper motor	DC motor	Linear motor
Type of motion	Rotational	Rotational	Linear
Max. torque	High (over wide range of speeds)	Low to Moderate (decreases with increasing speed)	High (over wide range of speeds)
Max. Speed	Moderate	High	Low to Moderate
Controllability	Position control related to resolution determined by number of rotor steps. Speed control related to stepping rate.	Speed control related to voltage across motor coils	Position control related to resolution determined by number of coil steps. Speed control related to stepping rate.
Accuracy	Very high (with micro-step position control)	Moderate	Moderate to High (position control)
Stability	Internal position control - stable in open loop	Requires external rotational speed control	Internal position control - stable in open loop
Cost	Moderate to High: increases with increasing holding torque and torque range	Low to Moderate: increases with output power / torque	High

Table 3: Comparison of characteristics and limitations concerning mechanical converter selection and design

Mechanical converters				
Type	Crank and connecting rod	Scotch Yoke	Cam	Cam with internal profile
Function	Convert rotation to linear motion	Convert rotation to linear motion	Convert rotation to linear motion	Convert rotation to linear motion
Friction	Low	Moderate	Moderate	High
Component wear	Minimal wear on bearings/bushings due to rotational friction	Moderate wear on crank pin and slot due to continuous translational friction	Moderate wear on cam and piston due to collision at the point of contact	High wear on pin and slot due to continuous translational and rotational friction determined by the slot profile
Behaviour	Produces near-sinusoidal conversion. Variable profile with different points of attachment along crank length.	Produces exactly sinusoidal conversion by simple harmonic motion due to the basic construction. Variable profile with variable location of crank pin.	User defined profile based on perimeter shape. One profile per cam. Requires return mechanism to reinstate cycle start point.	User defined profile based on milled detail within perimeter. Does not require return mechanism to reinstate cycle start point.
Suitability	Not ideal for continuous flow	Not ideal for continuous flow	Not ideal for continuous flow	Not ideal for continuous flow

Table 4: Comparison of characteristics and limitations concerning hydraulic converter selection and design

Hydraulic Converters				
Type	Bellows	Piston	Diaphragm	Roller pump
Friction	None	High (between piston head and cylinder)	None	Minimal
Control	Relate compression to ejected volume	Relate piston translation to ejected volume & piston velocity to flow rate	Diaphragm flexion and velocity relates non-linearly to ejected volume & flow	Ejection rate determined by motor rotational speed
Characteristics	Few moving parts	Requires accurate construction	Direct coupling between actuator and diaphragm	Direct hydraulic conversion by tube compression
Behaviour	Energy conversion involves chamber compression	High wear rate on seal between piston head and cylinder. Energy conversion involves volume compression within incompressible cylinder.	Energy conversion involves flexure of diaphragm	Produces continuous flow by default. Not well suited for static pressure production.

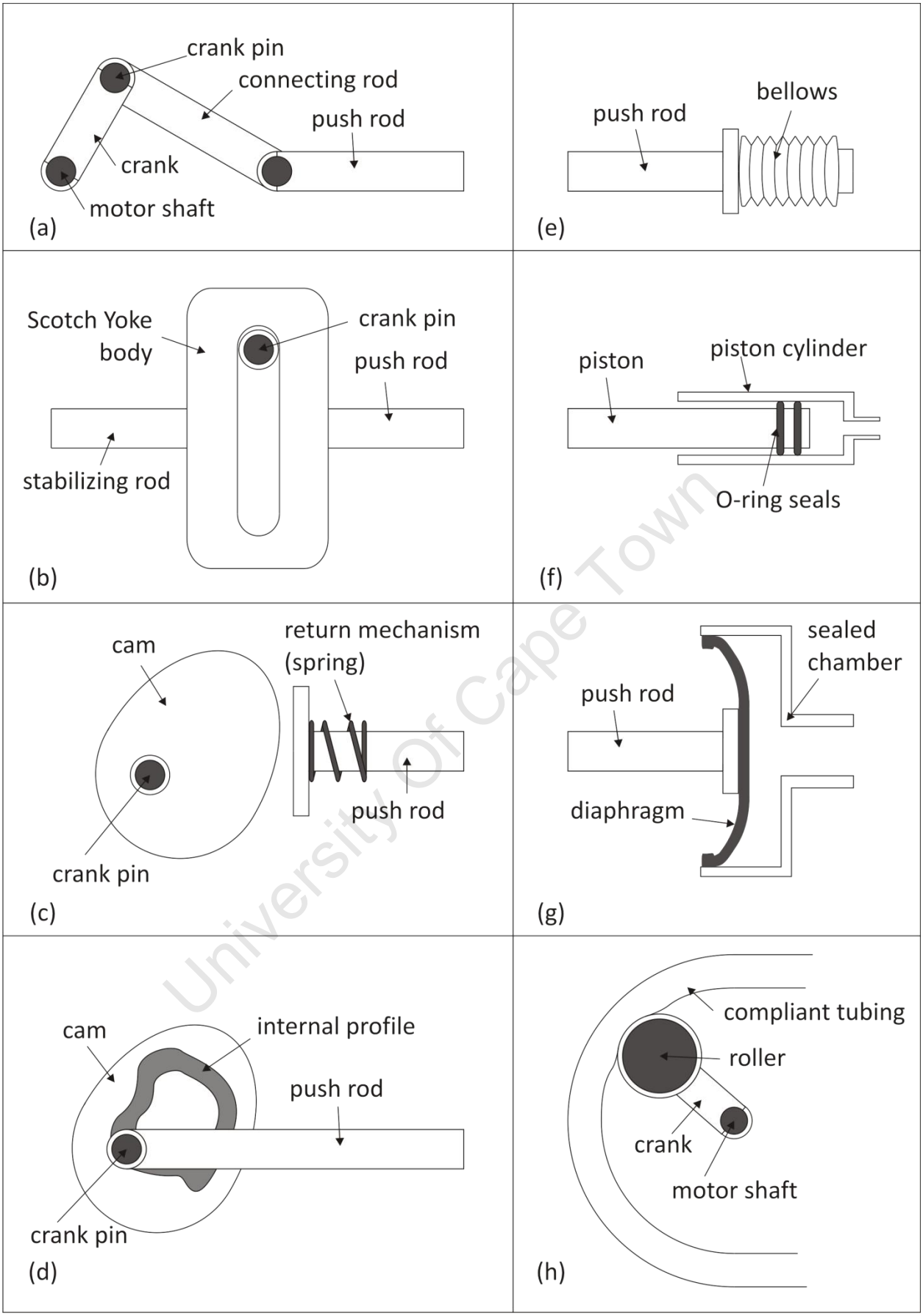

Figure 2: Schematic diagrams showing the mechanical construction of the (a) crank and connnecting rod, (b) Scotch Yoke, (c) cam with return mechanism, (d) cam with internal profile, (e) bellows, (f) piston, (g) diaphragm and (h) roller pump.

All of the aforementioned apparatus are capable of producing the mechanical requirements, albeit with varying degrees of difficulty. The primary factors in choosing the optimal apparatus for the assembly were therefore based on accuracy, ease of control and cost. Since it is unlikely that a system component is ideal in terms of all of these factors, a compromise was essential to make the most suitable design decision. Thus the best compromise for the motor, mechanical conversion and hydraulic conversion elements were chosen.

A stepper motor was chosen as the most suitable motor due to its favourable torque-speed characteristic such that the motor will provide sufficient torque over the desired speed range. Additionally, the shaft speed and position are controlled digitally via a computer thus eliminating the requirement for external components in order to change the actuator profile, e.g. discrete cams for different actuator profiles.

A crank and conrod arrangement offers good linearization of the shaft rotation with minimal losses and wear effects. However, in practice it is complicated to linearize a pushrod of small diameter and long stroke if driven by a conrod. This is due to the forces oblique to the pushrod's axis of linear motion at all times other than at top-dead-centre and bottom-dead-centre. The bearings required to maintain smooth linear motion would be subjected to these oblique loads thus increasing wear, decreasing performance and introducing a high likelihood of bearing failure due to the angles of the applied loads. For these reasons it was preferable to use a Scotch Yoke arrangement to linearize the crank rotation. A Scotch Yoke offers entirely linear motion along the piston shaft length, without the oblique linkage of the conrod. The linear piston motion is also much smoother with a Scotch Yoke and exactly sinusoidal, unlike a crank/conrod arrangement. The point at which the crank pin meets the Scotch Yoke slot is the only site of significant friction, and the wear due to this friction was taken into account in the design. This system is suitably versatile when coupled with a variable crank, thus allowing the end stroke to be varied and eliminating the requirement of additional components.

A piston provides the least complicated and most efficient method of hydraulic conversion with respect to this project, since the piston cylinder is non-compliant and of fixed volume. However, the most prominent limitations of the piston design are friction and leakage, which directly affect system performance in terms of pressure and flow production. A bellows system is an attractive alternative; however, it introduces other complications. Primarily, the ejected fluid volume is difficult to quantify and control due to the complex wall profile and compliance of the flexible walls. Thus the piston configuration was determined to be preferable to drive the flow loop since accuracy is of great importance. The limitations of the piston configuration required the design of accurate and efficient sealing in the piston cylinder to minimize friction and leakage between the piston and the cylinder wall.

Since the stepper motor, crank, Scotch Yoke and piston system are not ideally suited to producing unidirectional flow conditions; an additional output valve stage was required after the hydraulic conversion. This valve stage was designed as an arrangement of one-way check valves such that there is an inlet and outlet for the respective intake and ejection phases of the pumping cycle.

3.2.2 Static Motor Torque Requirements

In order to derive the required motor specification it was necessary to consider the pump system as a whole, and refer the flow velocities and pressures in the flow loop through the piston, Scotch Yoke and crank to the motor shaft. The Scotch Yoke system was modelled as in Figure 3, where O is the motor shaft, B is the crank pin, A is the point of application of the reaction force, F_A, of the fluid on the piston, θ is the crank angle and r is the crank radius.

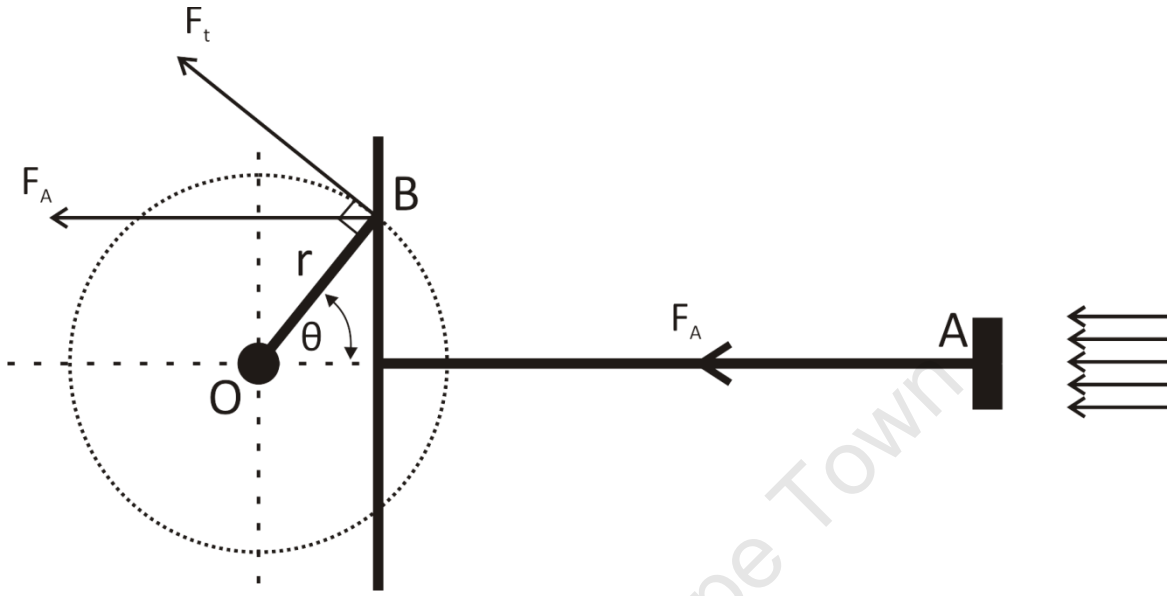

Figure 3: Force model of the Scotch Yoke pump system

To determine the static torque requirements of the motor, a free body force diagram was developed as in Figure 4 below:

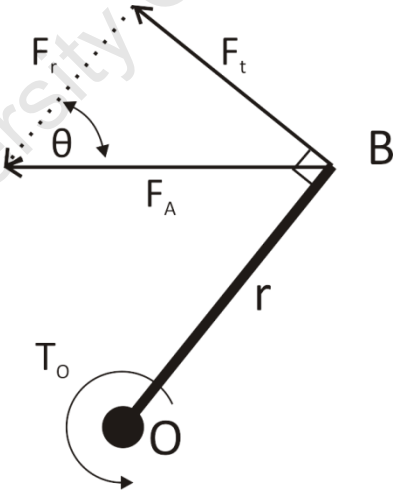

Figure 4: Scotch Yoke pump system free body force diagram

The holding torque, T_O, about point O was calculated in terms of F_A and θ as follows:

$$T_O = F_t \cdot r \quad (1)$$

$$F_t = F_A \cdot \sin\theta \quad (2)$$

$$T_O = F_A \cdot r \cdot \sin\theta \quad (3)$$

To define the specifications of the system components it was necessary to compute the maximum values of the system variables and choose components capable of withstanding or producing the required maximum values within a safety factor, such that the components do not operate at their limit.

The maximum crank radius was set at 25mm, to minimize wear due to friction and produce the required flow velocity and pressure waveforms accurately. The fluid reaction force, F_A, was calculated as a point force on point A due to the maximum applied fluid pressure of 33kPa (~250mmHg) on a circular piston surface area. The system dimensions and specifications were calculated for various piston diameters by varying the crank radius whilst keeping the piston diameter constant. Thus a range of crank radii could be derived in order to produce the required ejected volumes, relative to a range of graft sizes, from each particular piston size. The minimum crank radius was optimized in terms of practicality and ergonomics to 5mm, thus yielding a total crank radius range of 20mm. The design constraint implied by this range restriction was that in order to test a large range of graft sizes, the system would require a number of discrete pistons. Each piston diameter was chosen as the most versatile match for its associated range of graft sizes. Thus during development, using a 4mm graft, a piston diameter of 10mm was selected.

To determine the maximum motor torque requirement it was necessary to consider the system in terms of the largest graft sample intended for testing in the flow loop simulator. Thus it was found that grafts of 8mm diameter require a piston diameter of 40mm such that the system is able to operate within the optimal crank radius range. The maximum static torque about the motor shaft associated with these dimensions was found to be 1.1Nm. It was desirable that the system component specifications allow for upgrades in the future, possibly including a wider range of graft sizes in the testing range. Thus, it was found that increasing the piston diameter to 60mm would allow for testing of grafts up to 13.3mm diameter. The revised torque requirement was then calculated as 2.4Nm.

3.2.3 Motor Speed Requirements

To ensure that each piston size was capable of moving fluid through all graft sizes at the maximum desired rate of 100cm/s [1m/s] it was necessary to specify the required maximum speed of the stepper motor. The range of graft diameters that could be tested by each discrete piston was determined, such that the piston diameter was always greater than the graft diameter.

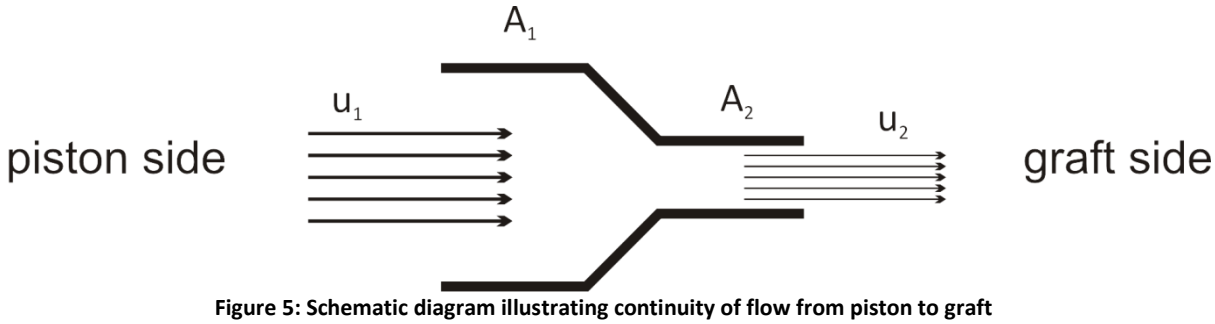

Figure 5: Schematic diagram illustrating continuity of flow from piston to graft

Figure 5 thus illustrates the concept of continuity of flow, which explains that the flow velocity in the piston is therefore less than that in the graft if the fluid is assumed to be incompressible. This is explained using the equation for continuity of flow,

$$\rho_1 A_1 u_1 = \rho_2 A_2 u_2 \tag{4}$$

where ρ is the density of the fluid, A is the cross-sectional area of the conduit, and u is the velocity of the fluid. Since the fluid is the same throughout the flow system, $\rho_1 = \rho_2$. It follows that a decrease in cross-sectional area results in an increase in fluid velocity, i.e. if $A_1 > A_2$ then $u_2 > u_1$. This implies that the speed requirements of the motor are reduced in order to produce the desired flow velocity in the graft.

Since the fluid velocity on the piston side is directly related to the piston velocity, the maximum required piston velocity, v, can be expressed as

$$v = u_1 = \frac{A_2 u_2}{A_1} \tag{5}$$

Thus for the maximum piston diameter of 60mm and graft diameter of 13.3mm, the maximum required piston velocity was found to be $v = 49.14 \times 10^{-3}\ \mathrm{m/s}$.

Figure 6 illustrates that the piston velocity can be related to the motor shaft angular velocity as follows:

$$x = -r\cos(\theta) \tag{6}$$

$$v = \frac{dx}{dt} = r\sin(\theta) \cdot \frac{d\theta}{dt} \tag{7}$$

$$\therefore v = \omega r\sin(\theta) \tag{8}$$

$$\omega = \frac{v}{r\sin(\theta)} \tag{9}$$

where x is the linear displacement, v is the piston velocity in the x-direction, ω is the angular velocity of the motor shaft and θ is the angle or rotation of the motor shaft.

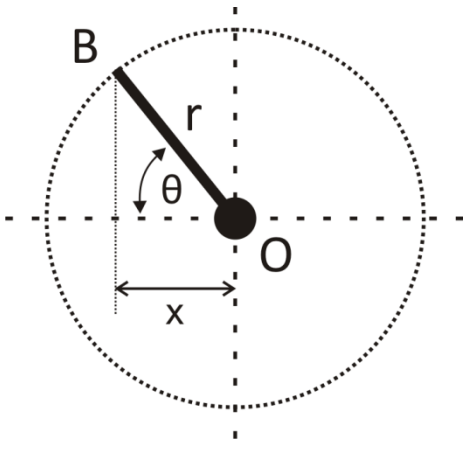

Figure 6: Schematic diagram showing the angle relation between linear and angular velocity of a crankshaft

In the Scotch Yoke arrangement, consider that at angles approaching $\theta = 0^{\circ}$ and $\theta = 180^{\circ}$ the angular velocity of the crank must increase in order to maintain the maximum linear velocity of the piston, since at these angles $\sin(\theta)$ approaches zero. Therefore to specify the maximum required

rotational speed of the motor, the system was considered at $\theta = 5^{\circ}$as an angle close to the described limits, during which it is likely that a high linear velocity may be required (i.e. beginning of a pulse).

Substituting for $v = 49.14 \times 10^{-3}$ m/s, $\theta = 5^{\circ}$[0.087 rad], r = 25mm yields that the maximum required rotational speed of the motor shaft is approximately $\omega = 22.6$ rad/s [~215rpm].

3.2.4 Dynamic Motor Torque Requirements

The dynamic system behaviour is characterized by the combined momentum of the Scotch Yoke and piston members; as well as the effect of the fluid momentum on the piston head.

As determined above, the maximum required piston velocity of the Scotch Yoke members was 49.14×10^{-3} m/s during the ejection phase. It was arbitrarily specified that the intake speed be roughly 4 times the ejection speed, i.e. 0.2 m/s, since it was preferable to minimize the intake duration such that the time between ejection phases was minimized. Thus the crank top-dead-centre position was chosen as the region of maximum acceleration, and hence maximum instantaneous torque.

To determine the estimated maximum torque requirements in order to accelerate the Scotch Yoke and piston members it was assumed that the members would be made of Stainless Steel (ρ = 8000kg/m^3) with a mass of approximately 0.5kg, and that the change of direction between ejection and intake phases would take 1ms. This was a generous assumption since the momentum of the mechanical members was to be considered, despite stepper motors being capable of accepting much shorter pulse durations.

The instantaneous torque requirement at the crank top-dead-centre was derived algebraically as follows:

$$v_{intake} = v_{eject} + at \tag{10}$$

$$\therefore a = \frac{v_{intake} - v_{eject}}{t} \tag{11}$$

$$T = Fr = mar = \frac{mr(v_{intake} - v_{eject})}{t} \tag{12}$$

Thus the maximum torque requirement was found to be $T = 3.125$ Nm.

To address the effect of fluid momentum on the dynamic system behaviour, it was noted that the fluid ejected through the valve stage outlet by the piston is isolated from the fluid drawn through the inlet from the reservoir. This is due to the system of one-way valves and implies that the piston interacts with separate volumes of fluid, moving them from rest during the draw and ejection phases of each cycle, thus limiting the effects of the fluid momentum in the flow loop on the piston. It is a reasonable assumption that the fluid inertia is negligible with respect to the fluid pressure reaction force applied on the piston, since the volume of fluid in the piston cylinder is small and the fluid mass therefore minimal. Based on this reasoning it may be assumed that the motor torque specifications established thus far are suitable for the dynamic requirements of the system, once a safety factor has been applied.

The above torque specifications could be met either with a large motor with a high torque rating, or a smaller motor suitably geared to increase the torque. Based on the factors compared in Table 5, a standard stepper motor was chosen as the most suitable option to drive the flow loop simulator pump system. A large standard stepper motor was able to provide the required torque over the

desired speed range with greater accuracy. The step accuracy was improved with the use of a micro-stepping driver to divide the standard step angle, thus increasing the number of steps per revolution and hence the position accuracy of the stepper motor. This was achieved without sacrificing the motor torque or speed capabilities.

Table 5: Comparison of standard and geared stepper motors

Motor type	Standard stepper motor	Geared stepper motor
Lifespan	Lasts longer due to fewer moving parts	More susceptible to wear due to increased number of moving parts
Accuracy	Accuracy decreases as torque rating increases	Tolerance between the gear teeth mechanically decreases position accuracy
Torque vs. speed	Greater speed capabilities for the desired torque	Gearing to increase torque requirements reduces the speed capabilities of the motor
Cost	Cheaper	More expensive

The equipment chosen for the pump system based on the above specifications is as follows:

- Ocean Controls MOT-132 FL86STH80-6004B Bipolar Stepper Motor (MOT-132 FL86STH80-6004B, 8.7Nm, Ocean Controls, Seaford, Australia)
- Ocean Controls SMC-005 MD882 Micro-stepping Stepper Motor Controller
- Ocean Controls SMC-101 48V Power Supply

The motor holding torque of 8.7Nm allows for a safety factor of 3.5 with respect to the static system specifications, and 2.8 with respect to the dynamic system specifications. This will account for any torque required to overcome additional loading on the piston due to the actual forces that were considered theoretically above, as well as the loading that was considered minimal and neglected in the above calculations. The maximum loaded rotational speed of the motor shaft is quoted by Ocean Controls as 2250rpm, thus the speed requirements of the flow loop simulator are very much within the motor capabilities.

Figure 7 shows the Solidworks render of the pump assembly. The stepper motor (a) was mounted on an 8mm thick aluminium plate (b) with two 16mm thick aluminium brackets (c). The variable crank (d) was fixed along the motor shaft with a grub screw at the key. Two aluminium pillars (e) serve as longitudinal alignment of the Scotch Yoke assembly (f), and Teflon bushings were used to minimize friction between the Scotch Yoke and the pillars. Large washers and Teflon discs were also placed on the front and back face of the Scotch Yoke to minimize friction against the variable crank and the head of the crank pin (g). The piston plunger (h) was screwed onto the Scotch Yoke pushrod (i) to actuate the fluid in the hydraulic system.

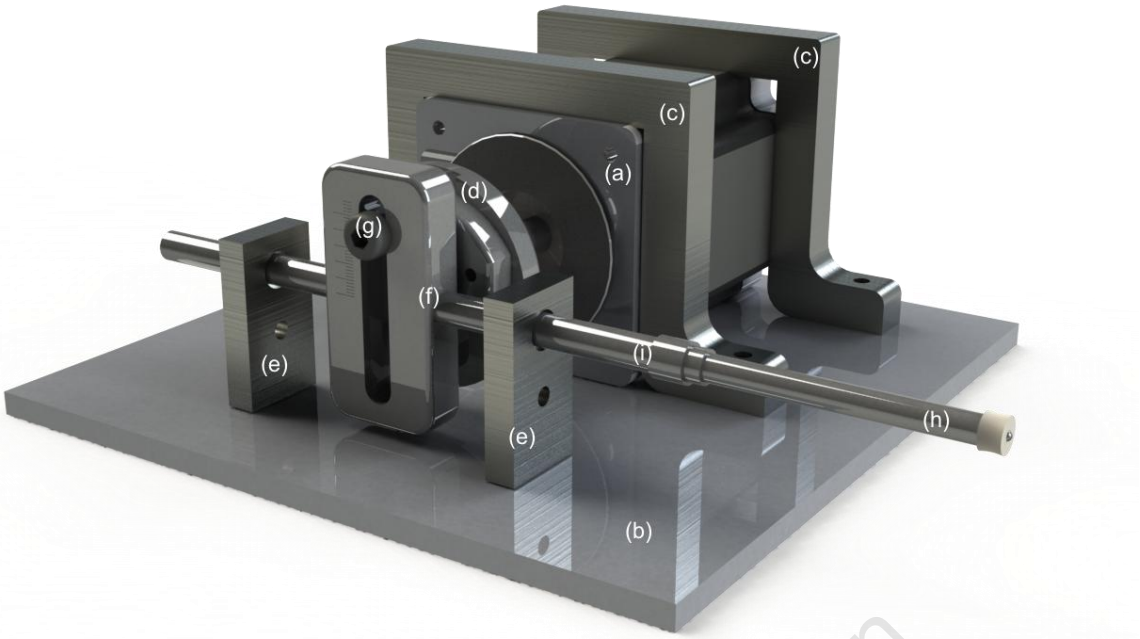

Figure 7: Solidworks render of the pump assembly: (a) stepper motor, (b) aluminium base plate, (c) aluminium brackets, (d) variable crank, (e) support pillars, (f) Scotch Yoke body, (g) crank pin, (h) piston plunger, (i) Scotch Yoke pushrod

3.3 Flow System Design

3.3.1 Flow System Overview

The flow system was designed to circulate and pressurize a solution of salt and glycerine to match the density and viscosity of blood. This specification allowed for the most accurate replication of graft behaviour as would be experienced while circulating blood, but without the associated complications, i.e. clotting, flow inhibition, cleaning, hygiene, etc.

Figure 8 shows the Solidworks design of the overall flow system and Figure 9 indicates the flow paths through the system. The fluid in the flow system is supplied from an elevated reservoir (a) at the centre of the loop. Directly below, a separate reservoir (b) serves as a water bath in which the graft sample is submerged. Both the upper and lower reservoirs are designed to be heated to maintain a temperature of 37°C in the circulating fluid and graft sample material respectively. The upper reservoir is adjustable in elevation so as to produce a static baseline pressure, associated with the resulting head of water, in the flow system.

The flow path from the pump to the graft was designed to be straight to maintain flow integrity. The only curved tubing in the system is at the flow intake (c) and bypass (d), and distal to the graft location (e) where flow integrity is non-essential. Where possible, the length of the flow loop was minimised to reduce heat loss, and heat insulating materials were used for the flow loop components, i.e. polyurethane tubing and machined Perspex. Stainless steel was used for its non-corrosive properties in saline environments and where machining precision and structural rigidity were especially important. In addition to its thermal insulating properties, non-compliant polyurethane tubing was used as the most suitable non-corrosive material to contain saline and glycerine solutions at 37°C. Alternative readily available flexible tubing was only designed for a maximum of 30°C; thereafter the risk of tube rupture became unfavourable to the system design.

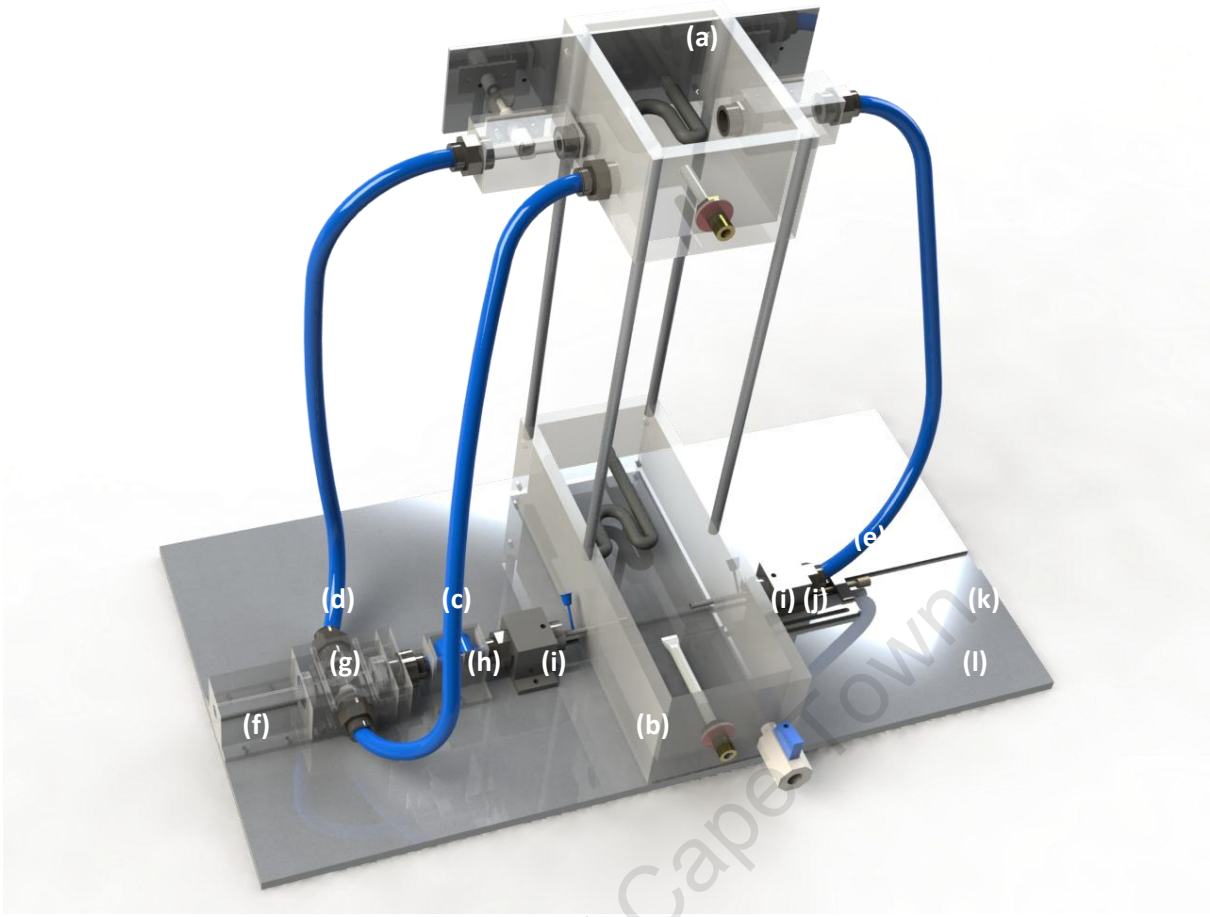

Figure 8: Solidworks render of the flow loop system: (a) upper reservoir, (b) lower reservoir, (c) intake tube, (d) bypass tube, (e) distal ejection tube, (f) piston cylinder, (g) valve stage, (h) flow measurement stage, (i) graft adapters, (j) pre-strain mount, (k) longitudinal track, (l) aluminium base plate

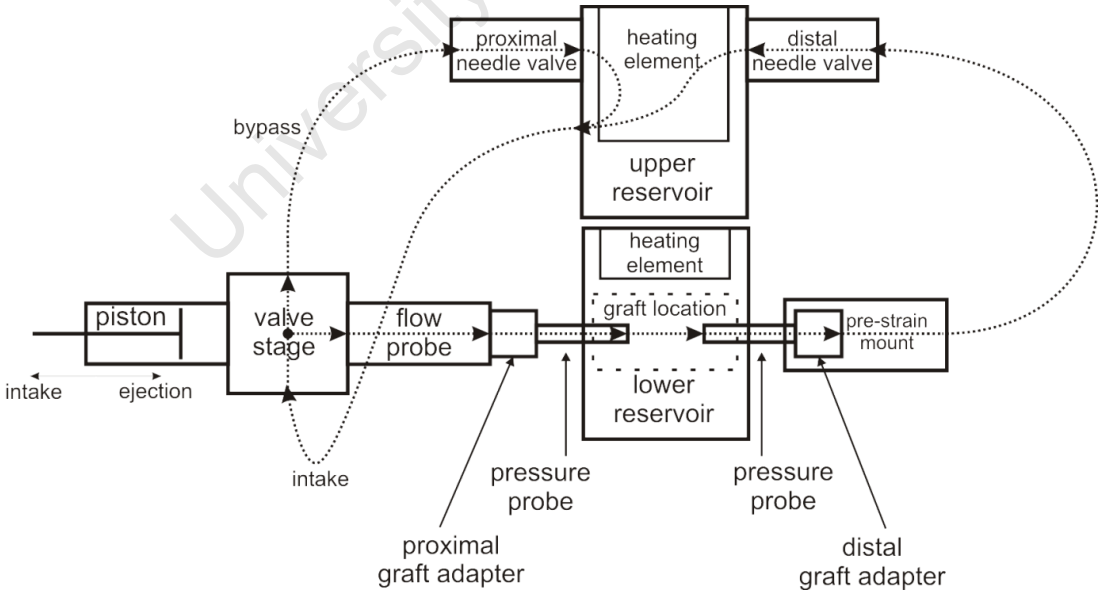

Figure 9: Schematic overview of the flow loop system

The flow system components were designed in a modular setup to allow for ease of replacement or redesign of discrete components based on experimental testing during the design process. The main straight flow path comprises a piston cylinder (f), valve stage (g), flow measurement stage (h), graft adapters (i) and pre-strain mount (j), all of which are fixed along a recessed track (k) to ensure

correct axial alignment and operational ergonomics. Perspex was used for the piston cylinder, valve stage and flow measurement stage such that a visual inspection could reveal the presence of air bubbles in the system. O-ring seals were used between flow loop modules to prevent leakage at the joins. The entire flow system is mounted on an 8mm thick aluminium base plate (l).

The flow system was designed to be driven by the pump system previously described. The piston cylinder may be defined as the interface between the pump and flow systems. The aforementioned piston diameter of 10mm, associated with 4mm diameter grafts selected for system optimization, defined the standard bore of 10mm for all flow system components before and after the graft adapters. The flow system components may thus be described as follows:

3.3.2 Piston Plunger and Cylinder

The piston plunger comprises a machined stainless steel rod of 9mm diameter, and a 10mm diameter Teflon disc affixed to the front of the rod with a screw. Teflon was chosen to minimize the friction between the plunger and cylinder wall. The Teflon disc is scored concentric to its outer diameter such that the outer diameter flares slightly when the disc is tightened against the front face of the rod, as illustrated in Figure 10. This ensures that the plunger seals properly against the cylinder wall in both directions for intake and ejection of fluid.

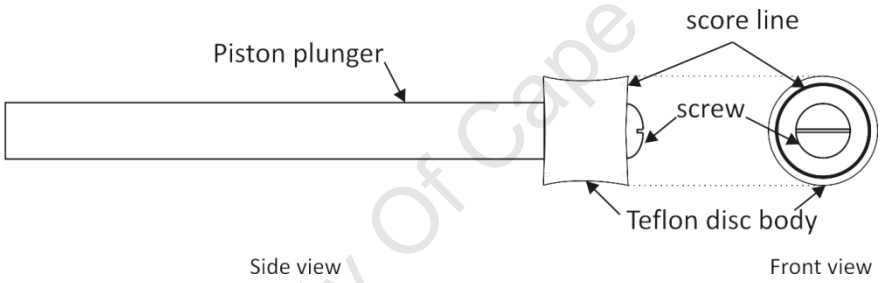

Figure 10: Schematic of the piston plunger and scored Teflon disc

The 10mm diameter piston cylinder is 60mm long to accommodate the full stroke of the Scotch Yoke and the additional thickness of the Teflon disc on the piston plunger. Polishing the inner surface of the cylinder served to further minimize friction between the plunger and cylinder wall, thus ensuring smooth actuation of the piston and reducing wear on the Teflon disc.

3.3.3 Valve Stage

The valve stage was designed to facilitate unidirectional flow through the flow loop when driven with the Scotch Yoke/piston pumping mechanism. This stage comprises three custom check valves that operate as illustrated in Figure 11.

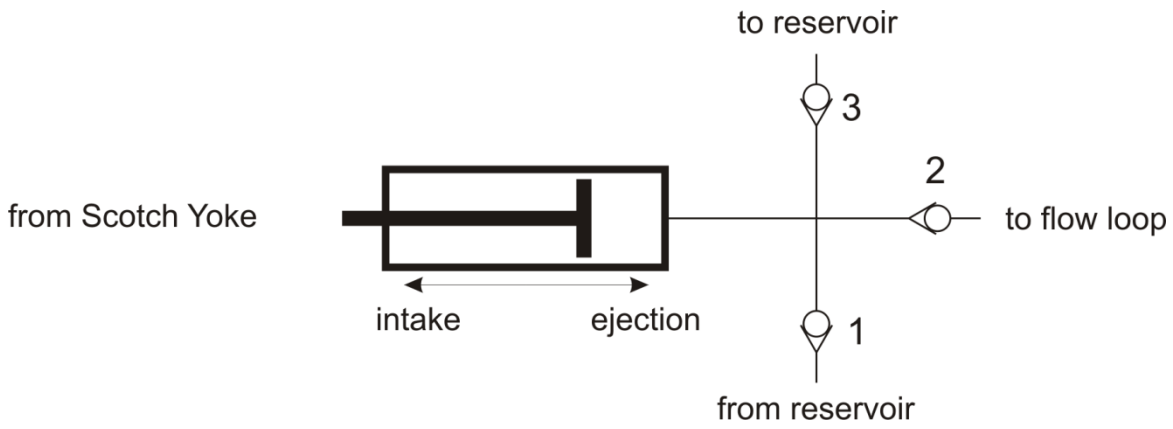

Figure 11: Schematic showing the valve stage operation with piston actuation

During the intake phase, valve 1 allows fluid to be drawn from the reservoir into the piston cylinder. During the ejection phase, valve 2 allows fluid to be pumped into the main flow loop, and valve 3 acts as a bypass, shunting fluid back to the reservoir. The bypass valve was coupled with a needle valve such that the optimal volume of fluid could be bypassed in order to maintain favourable piston stroke, thus ensuring accurate production of flow profiles.

Standard spring-loaded check valves require large pressures, relative to the operating conditions designed in this assembly, to be actuated. Additionally, the volume passed through the valve during the opening and closing phases represents a significant percentage of the volume pumped from the piston. Therefore, to accommodate the relatively low pressures in the system and prevent excessive leakage due to mechanical operation, the check valve construction in the valve stage avoids the use of standard components. The construction instead comprises a 0.5mm latex sheet and a wire mesh clamped between two flanges on the sides of the valve stage body. A Y-shaped cut in the latex sheet allows it to open similar to a tricuspid heart valve in the intended direction of flow, while the wire mesh acts as a scaffold and prevents opening in the opposite direction. The light latex material allows for reduced actuation pressures and a faster response to the piston motion. Therefore, it facilitates minimal fluid wastage and negligible dead spots in the pressure profile during opening and closing. Additionally, the check valves were designed with an outer diameter of 21mm, to ensure effective and secure mounting and that the valve leaflets exposed sufficient area when open so as not to constrict fluid flow with respect to the 10mm bore of the valve stage conduits. This is illustrated in Figure 12.

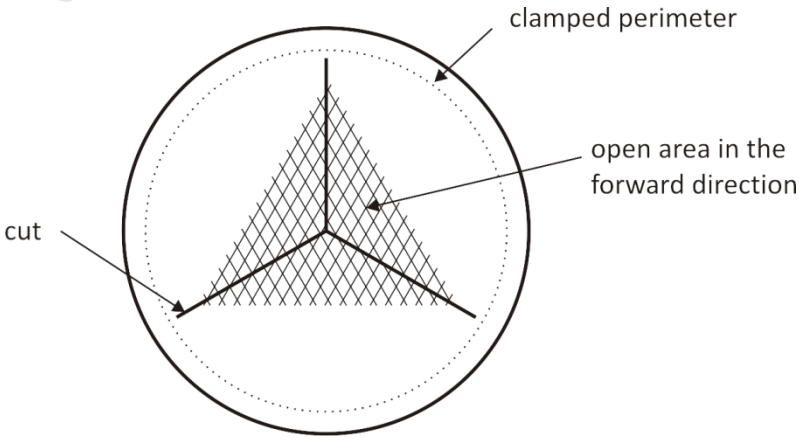

Figure 12: Schematic of the custom check valve design

3.3.4 Flow Measurement

Figure 13: Transonic T108 Ultrasound Volume Flowmeter

Measurement of the fluid volume flowrate was performed using the T108 Transonic Volume Flow Meter (Transonic Systems Inc., New York, USA), as shown in Figure 13, and occurs before the graft adapter due to space constraints relative to the size of the ultrasound flowmeter probe, as well as the potential need to remove the probe from the system easily. Using the principle of continuity of flow, this measured volume flowrate is referred from the 10mm tube diameter to the graft in order to arrive at an estimate of the volume flowrate through the graft. The volume flowrate as measured by the T108 is output in real time via a dynamic output on the device.

3.3.5 Graft Adapter

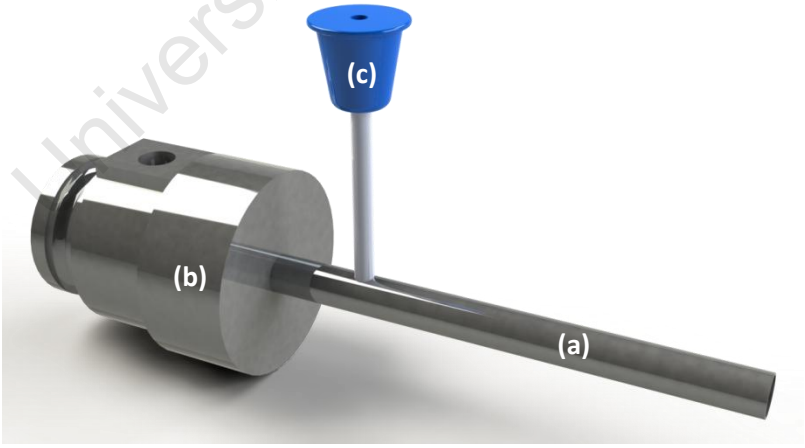

Figure 14: Solidworks render of the graft adapter: (a) hypodermic tube, (b) machined Stainless Steel body, (c) Luer needle

Accommodation of different graft sizes in the flow system was achieved by designing interchangeable graft adapters that fit in an adapter mount machined to a standard size. These adapters serve to decrease the flow tube diameter to that of the particular graft, and provide a point of attachment for the graft with minimal diameter tolerance. Minimising the tolerance between the adapter output and the graft minimises the errors that occur at the interface. These errors include

fluid turbulence, vortex formation, reflected waves, flow inconsistencies and pressure discontinuities.

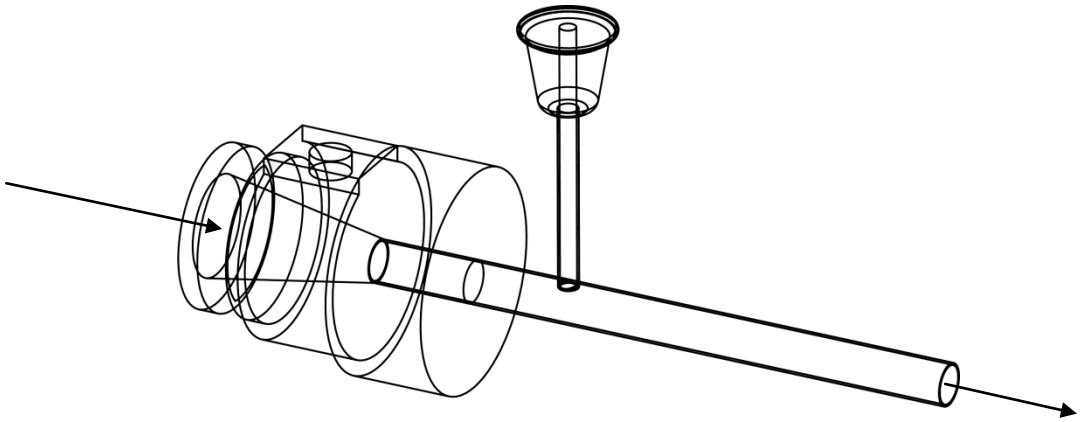

Figure 15: Hidden-line drawing of the graft adapter design, showing the flow direction and diameter reduction

The graft adapter design incorporates a conical diameter reduction, Figure 15, machined from Stainless Steel, such that the circular cross-section of the tubing is maintained and fluid turbulence is minimised. The low tolerance between the adapters and the adapter mount serves to minimise mechanical discontinuities in the flow path and thus limits the formation of vortices and reflected waves. The graft adapter output comprises a Stainless Steel hypodermic tube (a), brazed into the machined adapter (b), as shown in Figure 14. The various adapter sizes incorporate the appropriate diameter of hypodermic tubing at their output. The hypodermic tubing was chosen such that the inner diameter was centred around the most common graft sizes likely to be tested, and with the lowest ratio of wall thickness to outer diameter such that the diameter discontinuity between the tubing and the graft was minimised. The wall thickness range of the various diameters of the chosen hypodermic tubing is between 0.4mm (for 1.5mm outer diameter tubing) and 0.51mm (for 5.2mm outer diameter tubing).

The hypodermic tubes located in each graft adapter penetrate the respective walls of the lower reservoir to facilitate mounting of the graft within the reservoir. The holes through which the hypodermic tubes pass were sealed with O-rings to fit the outer diameter of the hypodermic tubes and prevent leakage of the contained fluid.

Graft specimens are mounted to the graft adapters at each end by means of a sleeve sutured to the graft body. The grafts are secured by slipping tight-fitting O-rings over the graft sleeve and hypodermic tubing.

3.3.6 Pressure Measurement

Pressure measurements are performed using two Disposable Integrated Pressure Transducers (DIPT), (Elcam Medical, BarAm, Israel), as shown in Figure 16. Since pressure measurement and monitoring is invasive by definition, it was not possible to place a pressure probe inside the graft without disturbing the flow conditions. For this reason, a pressure transducer was hydraulically routed to each end of the graft, such that the average of the two pressures would provide a good approximation of the pressure inside the graft. This was achieved by silver soldering a hypodermic Luer needle (c), Figure 14, orthogonally into the hypodermic tubing of each graft adapter. This was the closest permissible point to the graft at which pressure could be measured without disturbing the testing conditions, and allowing sufficient physical space for the manual connection of non-compliant pressure tubing.

Figure 16: Disposable Integrated Pressure Transducer (DIPT) [Elcam, 2008]

The pressure tubing conducts the fluid pressure from each Luer needle to an individual DIPT. The transducers provide pressure measurements up to 300mmHg and a maximum operational duration quoted as 96 hours [Elcam Medical], after which the transducers should be replaced. These pressure transducers are cost-effective and the response time is well suited to the task of dynamic pressure measurement. The small footprint allowed for unobstructed integration into the flow system and easy access for manual setup procedures. The electrical signal corresponding to the measured pressure is output via an RJ11 jack on the DIPT.

3.3.7 Graft Pre-strain Mount

In vivo, native arteries are subjected to inherent strain due to their interconnection and location throughout the body, as well as the longitudinal stretching undergone during growth. This strain contributes to regulating changes in artery length due to blood pressure and viscous drag forces during the cardiac cycle. To replicate this phenomenon, the graft adapter mount distal to the graft specimen is threaded and mounted on a base plate such that the longitudinal position of the adapter can be adjusted accurately with a screw. Once the graft is attached to the adapters both proximally and distally, turning the screw clockwise will apply a longitudinal strain to the graft thus simulating the approximate longitudinal loading that the graft would experience *in vivo* once sutured to the host arteries. The increase in length, i.e. increase in strain, of the abdominal aorta is approximately 1%, and the pulmonary and ascending aortas increase by 5-11% during the cardiac cycle [Chuong and Fung, 1983]. The pre-strain mount was thus designed to apply longitudinal strain of up to 30% to grafts with a length of 50mm, such that the graft specimens could be tested beyond physiological strain levels.

3.3.8 Needle Valves

The distal needle valve is located on the upper reservoir, distal to the graft sample in the main flow loop. The flow loop cross-sectional area is thus adjusted distal to the graft sample to produce back pressure within the graft. The proximal needle valve is located between the bypass check valve and the upper reservoir. Bypassing a controlled volume of fluid from the main valve stage affords the piston a larger stroke length whilst ejecting no more volume than is required for the specific graft specimen. Friction and stiction at the piston plunger mitigates very small piston movements; therefore a longer stroke length is desirable since it allows for more accurate control of the flow velocity out of the piston cylinder, due to greater piston travel per step of the drive stepper motor shaft.

Both needle valves perform much like a sluice, inhibiting flow through the flow tubing by decreasing the cross-sectional area via a linear gate, as illustrated in Figure 17. where h is the linear position of the needle valve gate and R is the tube radius. The back-pressure produced in the system is a measure of the fluid force interacting with the gate area blocking the tube cross-section; therefore the back-pressure may be controlled by controlling the gate height.

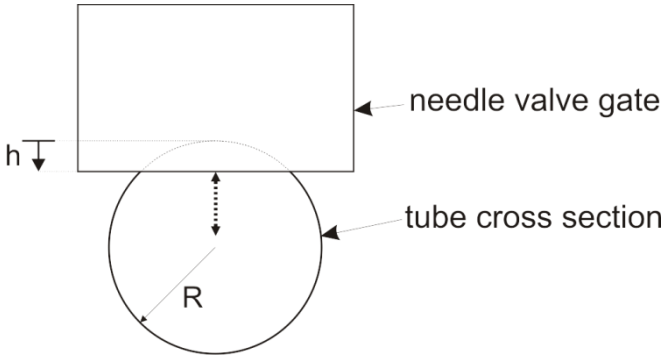

Figure 17: Schematic illustration of needle valve operation

The gate of each needle valve is coupled to a mini-stepper motor (FL39ST34-0306A, 0.013Nm, Mantech Electronics, Cape Town, South Africa) by a threaded stainless steel rod, mounted on the motor shaft. Each mini-stepper motor is actuated via an L297 Stepper Motor Control Board [Julian Mayer, Electrical Engineering, University of Cape Town]. The needle valve gates are cylindrical and machined from Teflon, as illustrated in Figure 18, to minimize friction against the Perspex needle valve body and ensure smooth operation along the length of the stainless steel thread. Since the gates are cylindrical, they are constrained to linear motion by means of a slot along their length and guiding pin. This slot simultaneously prevents accumulation of fluid in the space behind the gate, due to leakage, by shunting fluid around the gate and back into the flow loop.

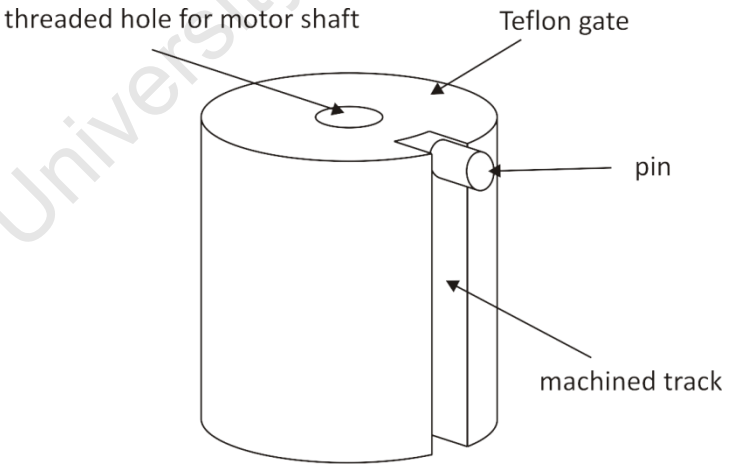

Figure 18: schematic diagram of the needle valve gate showing the slot and pin

3.3.9 Heating Element

A custom submersible heating element (650W, Hotflo, Cape Town, South Africa) was designed to maintain fluid temperature at 37°C. The design was such that the addition of glycerine/salt to the fluid solution would not result in burning at the element. Glycerine imposed the greatest limitation with respect to dissipated power relative to surface area at 5.5W/m^2 to prevent burning. The fluid temperature is measured with a PT100 Temperature Probe (Switchrite, Cape Town, South Africa)

and controlled using a Delta DTD PID Temperature Controller (Electromechanica, Cape Town, South Africa). The PT100 Temperature Probe is housed in a sealed conductive enclosure to prevent contact with the fluid.

Fluid circulation around the heating element is achieved passively by the intake and ejection of fluid between the reservoir and the rest of the flow loop for each pumping cycle. This is facilitated by the placement of the flow loop ports in the reservoir wall on either side of the heating element such that fluid flows across it during pumping. The pump intake draws fluid from near the heating element, where it is slightly warmer than in the rest of the reservoir, thus passively maintaining a relatively small temperature difference inside and outside the graft specimen as the fluid cools along the flow path.

3.4 Integrated assembly

3.4.1 Mechanical Construction

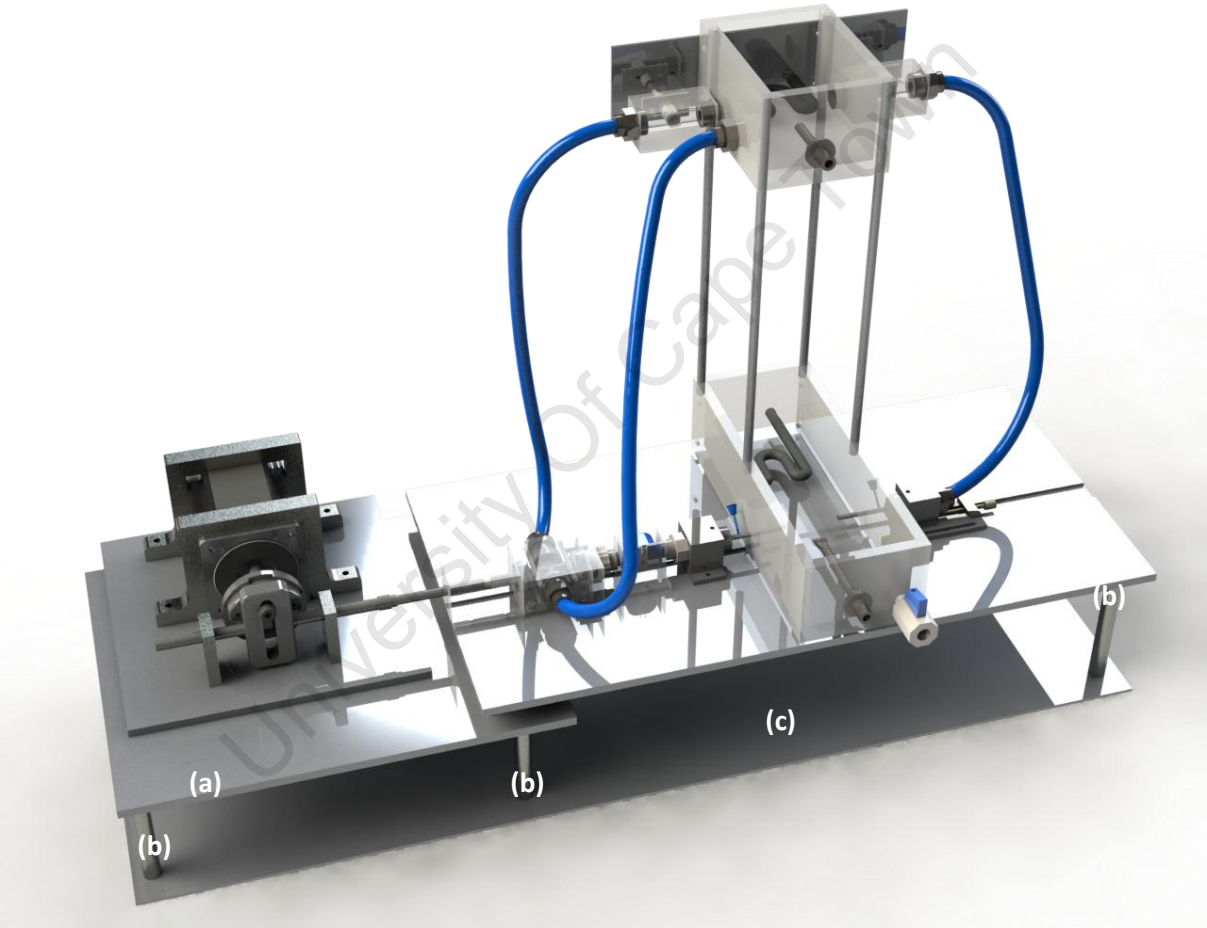

Figure 19: Solidworks render of the integrated mechanical assembly: (a) aluminium extension platform, (b) aluminium support rods, (c) parcel shelf

Figure 19 shows the integrated mechanical assembly of the flow loop simulator as designed in Solidworks. An 8mm thick aluminium extension platform (a) is rigidly connected 21.5mm below the flow loop base plate with four bolts and solid aluminium rod spacers. Locating dowels serve as alignment when disassembling and reassembling the extension platform from the flow loop base plate.

The drive motor assembly is mounted on the extension platform, with four bolts through its base plate, and located in slotted holes in the extension platform. The base plate and extension platform

are assembled such that they have the capacity to accept thin aluminium spacers between them. Together with the slotted holes, this enables exact alignment of the piston plunger in three dimensions.

The entire aforementioned assembly is elevated approximately 100mm by six aluminium rods (b). A 1mm thick parcel shelf (c) extends the full length of the assembly and is attached to the bottom of the rods. All electronic components, with the exception of the T108 Flowmeter, are located on the parcel shelf.

3.4.2 Electrical Interface

All electrical actuation and measurement signals are interfaced with a PC via the USB-6251 Data Acquisition Device (DAQ) [National Instruments, Texas, USA], as shown in Figure 20.

Figure 20: National Instruments USB-6251 Multi-function Data Acquisition Device [National, 2009]

The DAQ comprises digital and analogue interfacing capabilities as outlined in Table 6.

Table 6: Overview of USB-6251 specifications

Analog Inputs	Max Rate	Analog Outputs	Max Rate	Digital I/O	Counter/ Timer
16 SE/8 DI (16 bit)	1.25 MS/s	2 (16 bit)	2.86 MS/s	24 (8 clocked)	2

3.4.3 Signal Routing

The interconnection of the flow loop simulator hardware through the DAQ is illustrated in Figure 21 with the electrical subsystems categorized according to their function. The entire system is powered from a 230V wall outlet. Fully assembled, the only connections that require user handling are the 230V power plug, USB plug from the DAQ to the PC, and the two RJ11 jacks from the DPT pressure transducers (only when replacing the transducers).

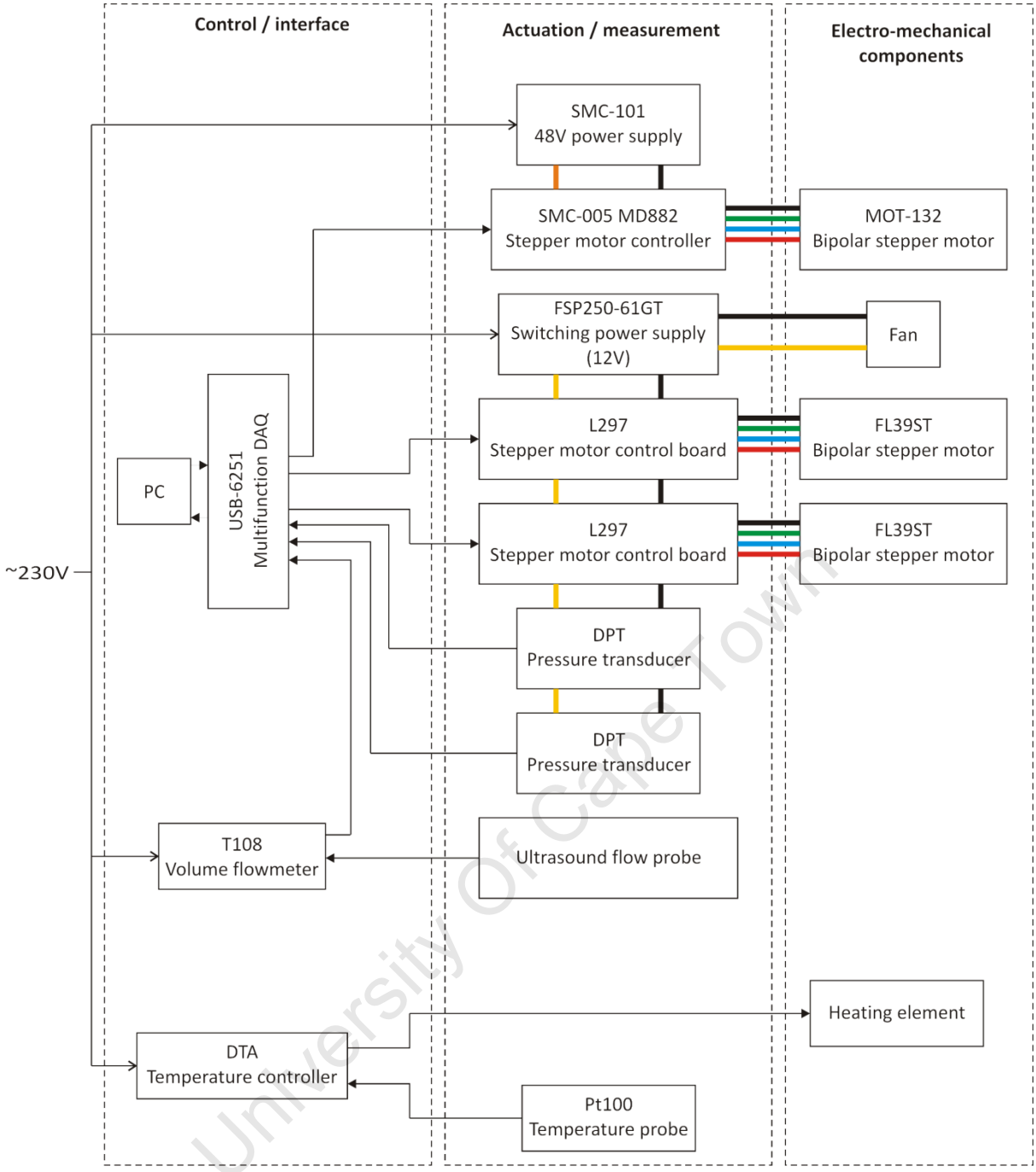

Figure 21: Schematic overview of the electrical signal routing

3.5 Actuation and Measurement System Design

3.5.1 System Overview

The integrated system is software controlled and was programmed using LabVIEW8.2 graphical programming software with DAQmx8.8 [Both National Instruments, Texas, USA] drivers installed.

The actuation section considers the control of mechanical elements, namely the drive stepper motor and the two mini-stepper motors coupled to the needle valves. These elements are actuated via the DAQ in response to software instructions. A graphical user interface (GUI) allows for user-adjustment of various system parameters.

The measurement section of the control system considers the acquisition of data from measuring points along the flow loop, namely the ultrasound flow measurement and the two pressure

measurements on either side of the graft sample. The measured signals are processed and displayed in real-time for user assessment.

3.5.2 Actuation System Design

3.5.2.1 Flow and Pressure Profile Construction

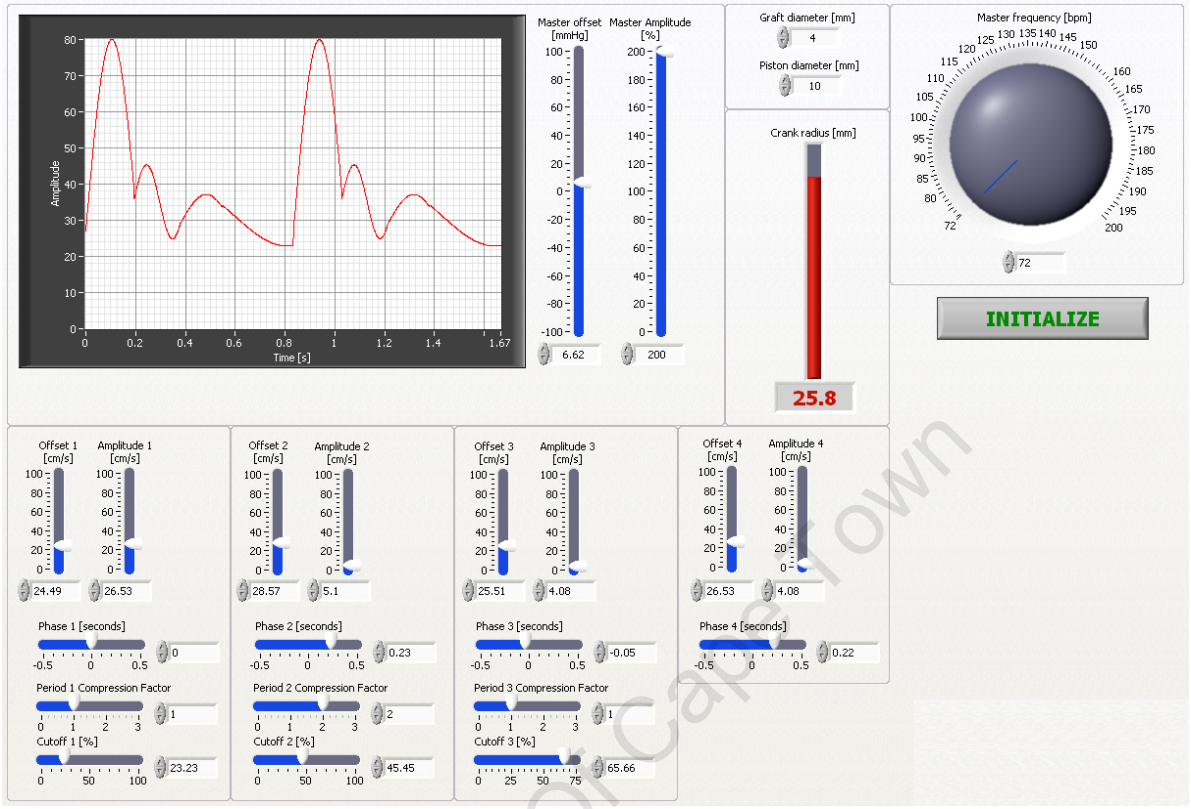

Figure 22: Screenshot of the LabVIEW graphical user interface

The slider-based GUI, Figure 22 (see Appendix A for the associated code segment), allows the user to define the desired flow and pressure profiles relative to the proposed region of implantation of the particular graft, as illustrated in Figure 23. The sliders divide each profile into four sections such that typical profile geometries can be constructed using a combination of four separate curves. The first three curves take the form of sine waves adjustable in amplitude, offset, cutoff and phase, as well as four discrete period settings. These controls allow the user to construct an approximation of the peaks, troughs and minor undulations observed in physiological arterial flow and pressure measurements.

The fourth curve only has controls for the amplitude, offset and phase as it is specifically designed to address the decay phase of the profile. There is significant interest in this particular phase of the profile, and indeed its actuation, as it allows the user to programme the profile decay. This capability is an alternative to adjusting a mechanical Windkessel compliance component as is most common in flow loop designs to date.

Construction of the flow and pressure profiles, based on the slider settings, is achieved by concatenating the four user-defined sine wave sections. The sine wave sections are inter-related with respect to their cutoff points. This allows each section to be modified independently, whilst ensuring that there are no discontinuities in the concatenated profile.

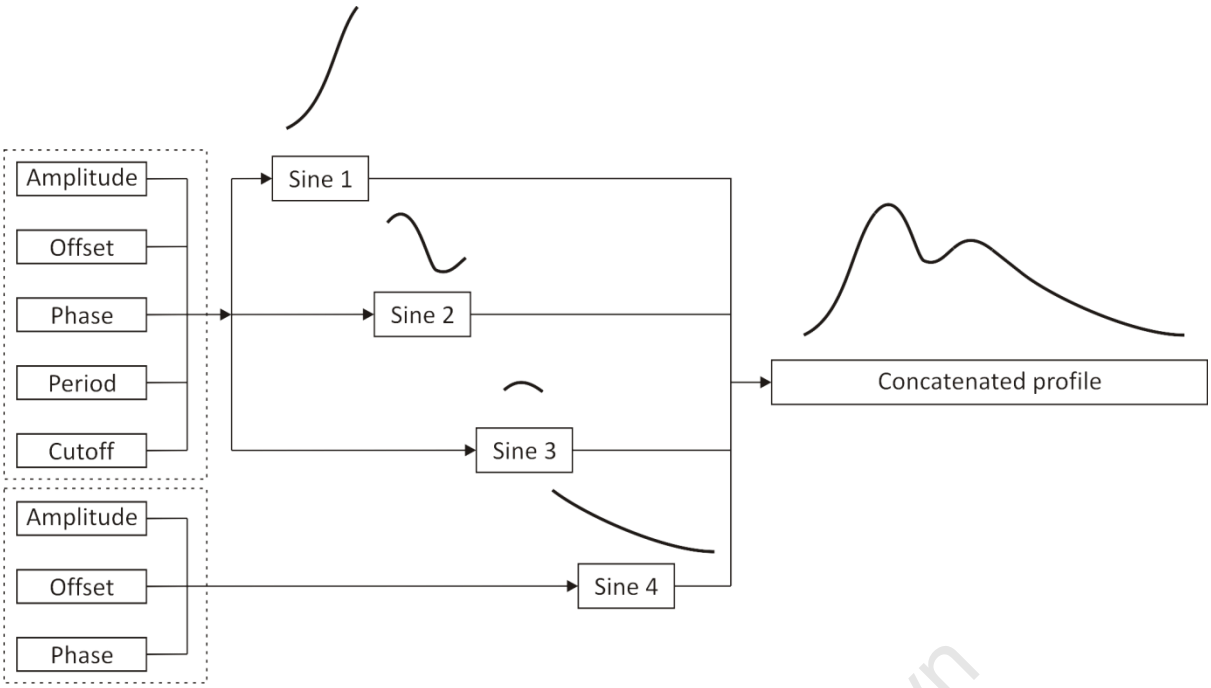

Figure 23: Block diagram showing sinewave manipulation for custom profile generation in the graphical user interface

The user may also enter the graft and piston diameters selected for the test. The crank radius is then determined, using the equation for continuity of flow (Eq. (4)), such that the piston stroke is optimized for the particular setup. The output based on the user-defined parameters comprises the crank radius readout and a LabVIEW waveform that is manipulated to control the main drive stepper motor.

3.5.2.2 Drive Stepper Motor Algorithm

Once the flow profile output is defined, it is analyzed and converted into a squarewave pulse train that serves as instruction for the drive stepper motor. Analysis of the LabVIEW waveform divides it into 100 samples, each of which corresponds to the desired instantaneous flow velocity in the graft sample. For each instantaneous flow velocity the required piston speed is calculated, once again using the equation for continuity of flow (Eq. (4)). This piston speed is related through the Scotch Yoke and crank members to compute the required instantaneous rotational speed of the drive stepper motor as in Eq. (9).

The rotational speed of stepper motors corresponds directly to the rate at which the motor is pulsed. Thus the above required instantaneous rotational speed is converted to a train of squarewave pulses at a single corresponding frequency. The pulse train is then divided further into an array of 1000 samples such that the pulse train may be output using a clock source of constant frequency. This process is repeated for each of the 100 sections of the LabVIEW waveform, converting each flow velocity to its respective single-frequency pulse train, and manipulating it to correspond to the constant-frequency clock. The 100 single-frequency pulse trains are then concatenated to build the final pulse train of varying frequency, output entirely using the constant-frequency clock source. Figure 24 illustrates the sequence of operation of the conversion algorithm (see Appendix A for the associated code segment).

Justification of using a single clock source arises from the need to control the rate at which the flow profile is actuated by the drive stepper motor, i.e. the “heart rate”. Since the entire flow profile corresponds to a single clock source, adjusting the rate of actuation only requires adjustment of the

clock source to the desired constant frequency. This maintains the relationship between the profile's constituent pulse trains, and only adjusts the rate at which they are actuated overall. The final squarewave pulse train is sent to the drive stepper motor as a logic signal (0-5V) via the DAQ (see Appendix A for the associated code segment).

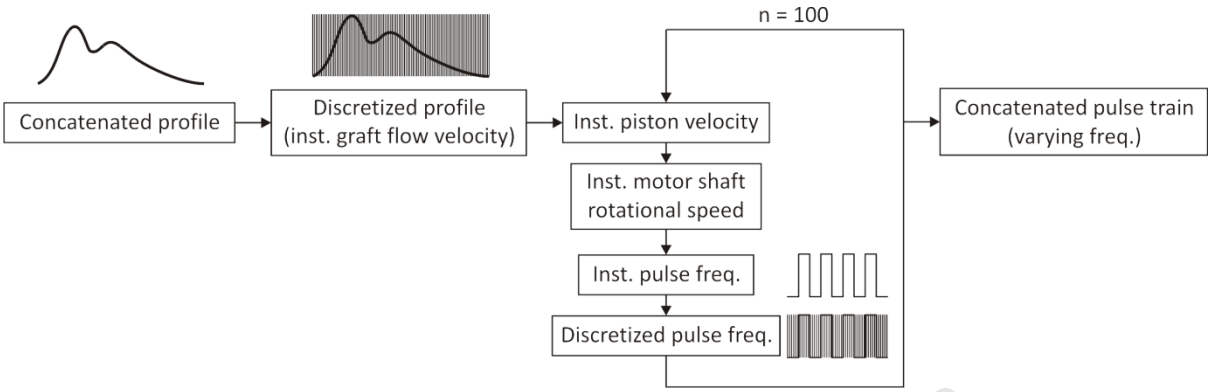

Figure 24: Block diagram of the conversion algorithm sequence

3.5.2.3 Drive Stepper Motor Actuation

Actuation of the drive stepper motor involves an ejection phase from 0° to 180°, and an intake phase from 180° to 360°. The ejection phase constitutes the active pumping of fluid through the flow loop, whereas the intake phase concerns re-filling the piston cylinder for the subsequent ejection phase. During the ejection phase the aforementioned squarewave pulse train, as prepared by the drive stepper motor algorithm, is output to the drive stepper motor via the DAQ. An optical sensor at the 180° position signifies when the crank is at top-dead-centre (TDC). The optical sensor monitors the motor crank rotation and ends the ejection phase when it is triggered. Thereafter, the intake phase is initiated, during which the motor rotates at constant speed to draw fluid from the reservoir into the piston cylinder. At the 360° position is a second optical sensor that signals when the crank is at bottom-dead-centre (BDC). The intake phase halts when the BDC optical sensor is triggered, and signifies the start of the subsequent ejection phase.

3.5.2.4 Mini-stepper Motor Control

Digital control of the needle valve mini-stepper motors is achieved via the DAQ, in response to the user-defined pressure profile set in the GUI.

The distal needle valve controls the back pressure in the graft sample by adjusting the tube cross-sectional area relative to the flow profile. Since the piston moves fluid through the flow loop with a predefined profile, changing the cross-sectional tube area distal to the graft sample does not affect the flow profile proximal to the graft. However, the relationship between the axial pumping force of the piston and the change in tube cross-sectional area distal to the graft is significant, since at any instant along the flow profile the distal needle valve gate position will produce a back pressure associated to the piston force applied at that instant. Therefore it was critical to establish the best compromise of gate position such that the best approximation to the desired pressure profile was established relative to the desired flow profile.

The proximal needle valve in the bypass path operates in a similar manner, except the gate position corresponds to volume rather than pressure. Contrary to the distal needle valve, the proximal needle valve is closed by default. Its gate is opened relative to the volume of fluid to be bypassed

from the main valve stage. Determination of the bypass volume required for optimal flow profile production considers that the piston stroke should be as large as possible. However, maintaining a large piston stroke, and hence a large volume of fluid ejected from the piston cylinder, requires that a large percentage of fluid is bypassed for smaller diameter graft samples. It was worth considering a compromise of smaller piston stroke lengths, and associate appropriate bypass volumes to them such that the flow profile was most accurately produced for a given graft diameter.

3.5.2.5 Mini-stepper Motor Calibration

In order to control the gate height using the mini-stepper motor, it was necessary to relate the gate height to the stepper motor shaft position. More specifically, the shaft position may be described in terms of the number of steps that the shaft has turned from a zero point. The gate height is related to this step number by virtue of the pitch of the shaft thread. It was measured that 2800 steps were required to move the gate the 10mm from fully open to fully closed positions in the needle valve assembly. Thus the ratio of gate to shaft position could be expressed as 3.57×10^{-3} mm/step.

The proximal and distal mini-stepper motors were calibrated using the same procedure, with a full range of 2800 steps, since the needle valve construction is identical.

To compute the area of obstruction of the needle valve gate when h>0 (see Figure 17) the obstructed area was defined as a segment of the circular tube cross-section. Therefore, it was necessary to derive the relationship between segment area and gate height in order to compute the change in tube cross-sectional area with respect to gate height. With reference to Figure 25, the segment area, $\mathrm{A_{seg}}$, is defined as:

$$\mathrm{A_{seg}} = \frac{\mathrm{R^2}}{2}(\varphi - \sin\varphi) \tag{13}$$

The angle φ may be described in terms of the gate height, h, as:

$$\varphi = 2\arccos\left(\frac{\mathrm{R-h}}{\mathrm{R}}\right) \tag{14}$$

Substituting φ into Eqn. (17) yields:

$$\mathrm{A_{seg}} = \frac{\mathrm{R^2}}{2}\left[2\arccos\left(\frac{\mathrm{R-h}}{\mathrm{R}}\right) - \sin\left(2\arccos\left(\frac{\mathrm{R-h}}{\mathrm{R}}\right)\right)\right] \tag{15}$$

This may be simplified as:

$$\mathrm{A_{seg}} = \mathrm{R^2}\left[\arccos\left(\frac{\mathrm{R-h}}{\mathrm{R}}\right) - \left(\frac{\mathrm{R-h}}{\mathrm{R}}\right)\sqrt{\frac{2\mathrm{Rh-h^2}}{\mathrm{R^2}}}\right] \tag{16}$$

Thus the unobstructed tube cross-sectional area, $\mathrm{A_{open}}$, was defined in terms of the segment area as

$$\mathrm{A_{open}} = \pi\mathrm{R^2} - \mathrm{A_{seg}} \tag{17}$$

$$\therefore \mathrm{A_{open}} = \pi\mathrm{R^2} - \mathrm{R^2}\left[\arccos\left(\frac{\mathrm{R-h}}{\mathrm{R}}\right) - \left(\frac{\mathrm{R-h}}{\mathrm{R}}\right)\sqrt{\frac{2\mathrm{Rh-h^2}}{\mathrm{R^2}}}\right] \tag{18}$$

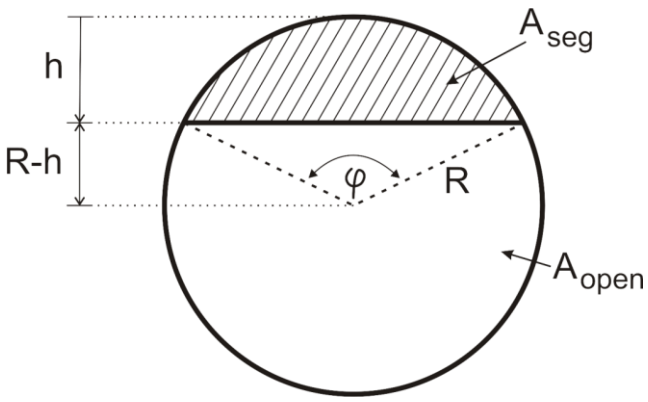

Figure 25: Schematic diagram showing the tube cross-sectional area with angle φ related to needle valve gate position

Eqn. (18) expresses the unobstructed tube cross-sectional area relative to the gate height for the case where the gate is fully open by default. To characterize the back pressure relative to the gate height, it was beneficial to transform this relationship to the converse case since the distal needle valve is fully closed by default. Thus Figure 26 illustrates the characteristic curves of the open and obstructed tube cross-sectional areas relative to the distal needle valve gate height. The relationship is well-defined but non-linear over the full range of gate positions from 0 to 100%, i.e. fully open to fully closed across the 10mm bore of the needle valves.

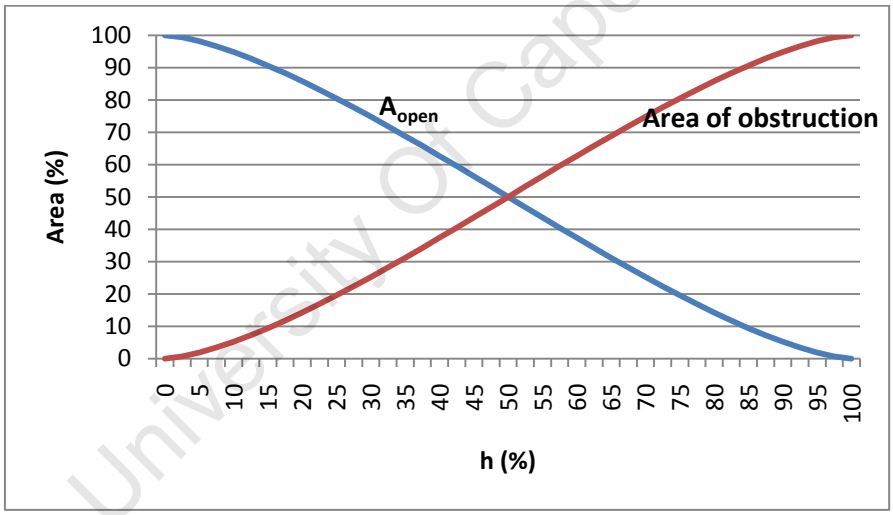

Figure 26: Graph showing the open and obstructed tube cross-sectional areas relative to the distal needle valve gate height h from fully open to fully closed positions

Since the back pressure associated with the distal needle valve is a measure of the instantaneous fluid reaction force per unit area imposed on the tube cross-section by the gate, the non-linearity with respect to the gate height implied that the change in pressure would be similarly non-linear. Thus a uniform change in gate height would yield a non-linear change in the pressure response of the system.

3.5.3 Measurement System Design

3.5.3.1 Pressure Transducer Calibration

Once integrated into the flow loop system, the proximal and distal DIPT output signals were interfaced with the DAQ using two analogue input ports and a sample rate of 1kHz. The average of the two DIPT signals was computed as an approximation of the pressure at the midpoint of the graft.

The integrated DIPT signal suffered from significant electromagnetic interference (EMI), predominantly from the drive stepper motor and coupled through the aluminium base plates. Before any signal processing was possible, it was essential to reduce the effect of the EMI on the DIPT transducers.

EMI reduction entailed decoupling the motor from the aluminium base plates by wrapping it in thin insulating plastic. Thereafter the motor was enclosed in a copper mesh cage which was grounded to the ground pin of the motor power supply. Figure 27 is a plot of the averaged DIPT signal over a time period of 15 seconds to illustrate the effect of the motor EMI and subsequent decoupling and shielding. At time t=0 the unprocessed DIPT signal noise can be seen with power removed from the motor. At t=4.5s the motor power supply was switched on and the motor driver noise was superimposed on the pressure signal. The driver switched on the motor current supply at t=6.5s and the resulting unshielded EMI-related noise amplitude exceeded the intrinsic transducer noise by a factor of 10. Connecting the copper mesh cage to ground at t=11.5s reduced the noise significantly.

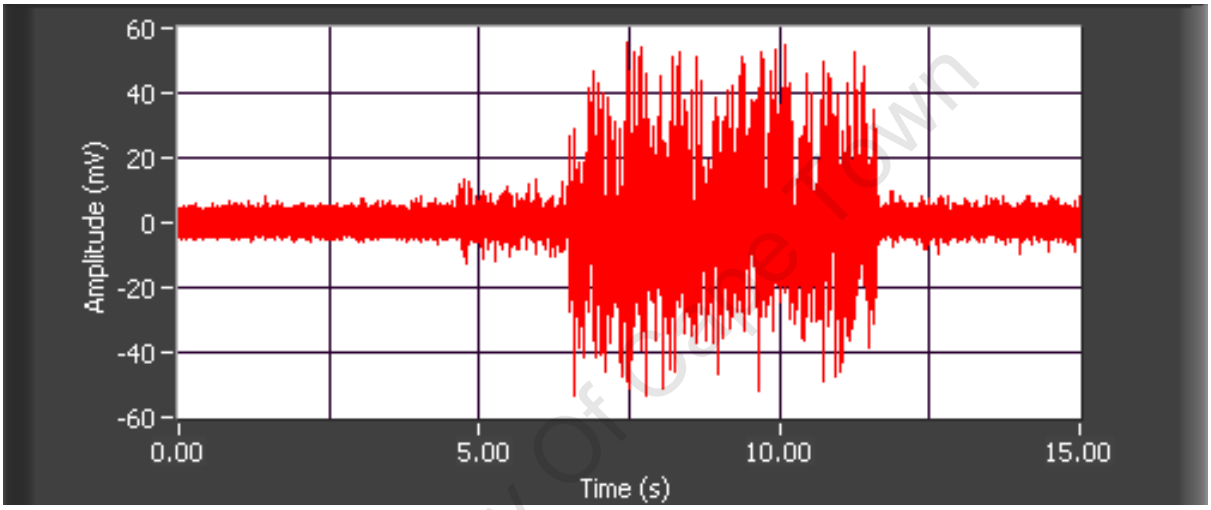

Figure 27: LabVIEW plot of the raw DIPT pressure signal, showing the effect of EMI on signal noise

A quantitative assessment of the DIPT signal noise was conducted after decoupling and shielding. Figure 28(a) shows the signal of Figure 27 from t=12s where the raw transducer noise amplitude was measured as 20mV peak-to-peak.

Incorporating the DIPT transducers into the measurement system of the flow loop is a non-standard use for these devices. The transducer output does not include any filtering or averaging thus it was essential to introduce these processing steps in the signal path in order to convert the raw signal to useable data.

Since the pressure profiles were not expected to vary at frequencies any higher than the flow profiles, a low pass filter was implemented in software with a cutoff frequency of 15Hz. It was experimentally verified that the cutoff frequency removed as much signal noise as possible, without degrading the profile integrity. Re-examining the signal noise from time t=12s, it was found that low pass filtering reduced the noise amplitude by 92% to 1.6mV peak-to-peak, as shown in Figure 28(b).

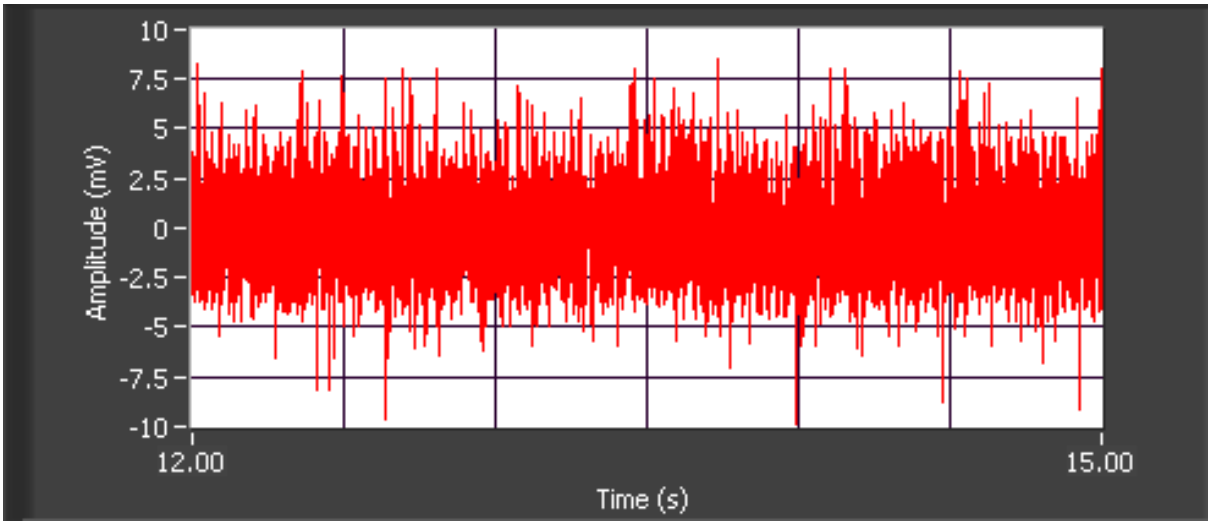

(a)

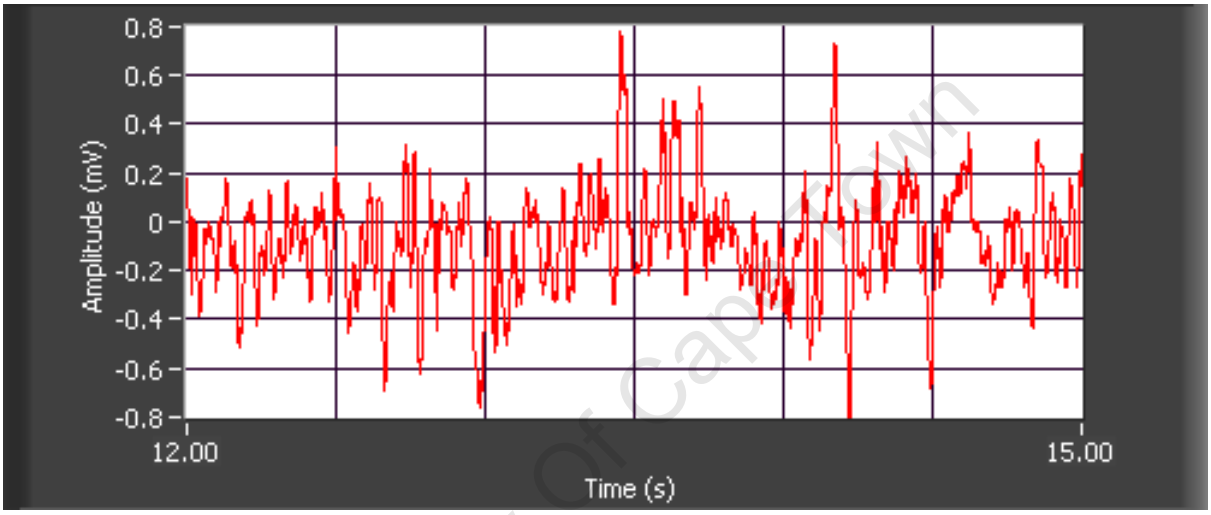

(b)

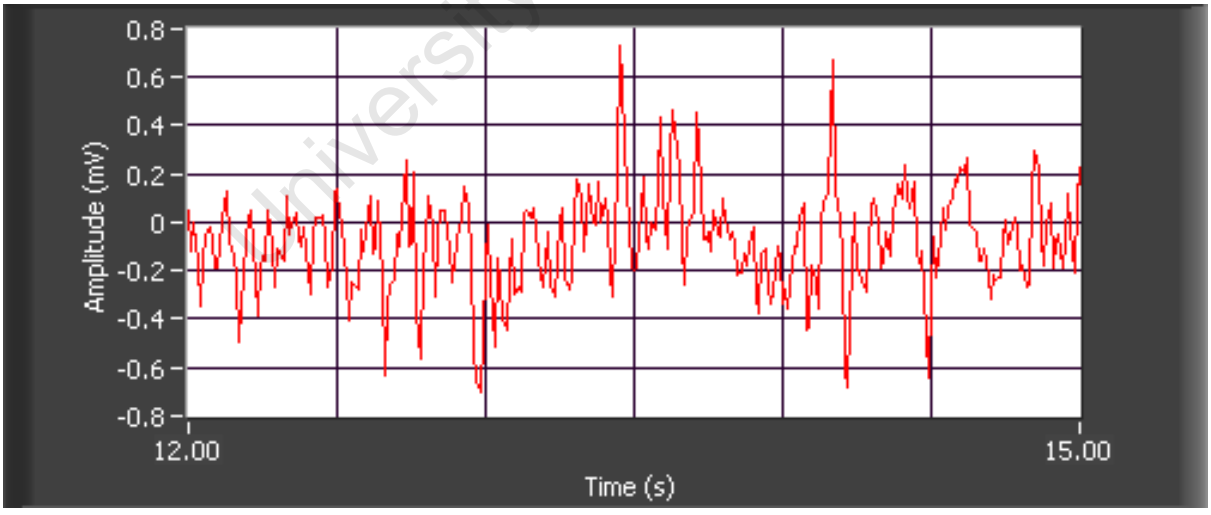

(c)

Figure 28: LabVIEW plot of the (a) raw, (b) filtered and (c) averaged DIPT pressure signal from time t=12s

Due to random voltage spikes present in the DIPT output, an averaging algorithm was written and implemented after the low pass filter. The algorithm computes the average of every 10 samples, thus reducing the sample rate to 100Hz. This ensured that the net sample rate maintained the measurement profile integrity and that the effect of any large spikes on the measurement error was

reduced. Thus the filtered noise amplitude was attenuated further, resulting in the final noise amplitude of 1.3mV peak-to-peak, as shown in Figure 28(c).

To determine the resolution and peak voltage output of the current setup, the system was calibrated using a column of water. By incrementing and then decrementing the height of the water column, the ascending and descending curves of the transducer output voltage could be recorded to develop the associated hysteresis loop.

Height restrictions prevented full scale calibration using the water column method. However, the instrument datasheet states the following combined non-linearity and hysteresis conditions:

$$\text{Error} = \begin{cases} \pm 1\text{mmHg}\ (-30 - 200\text{mmHg}) \\ \pm 1.5\text{mmHg}\ (200 - 300\text{mmHg}) \end{cases}$$

The desired maximum system pressure was specified as 200mmHg (see Table 1), therefore it was assumed that a voltage-pressure gradient established within this range would be sufficient to characterize the entire linear range from 0 to 200mmHg. Since the specific gravity of mercury is 13.546, the gradient established using a column of water was scaled by this factor to obtain the voltage relative to pressure in millimetres of mercury (mmHg). Thus the DIPT hysteresis loop and best fit straight-line calibration curve are shown in Figure 29.

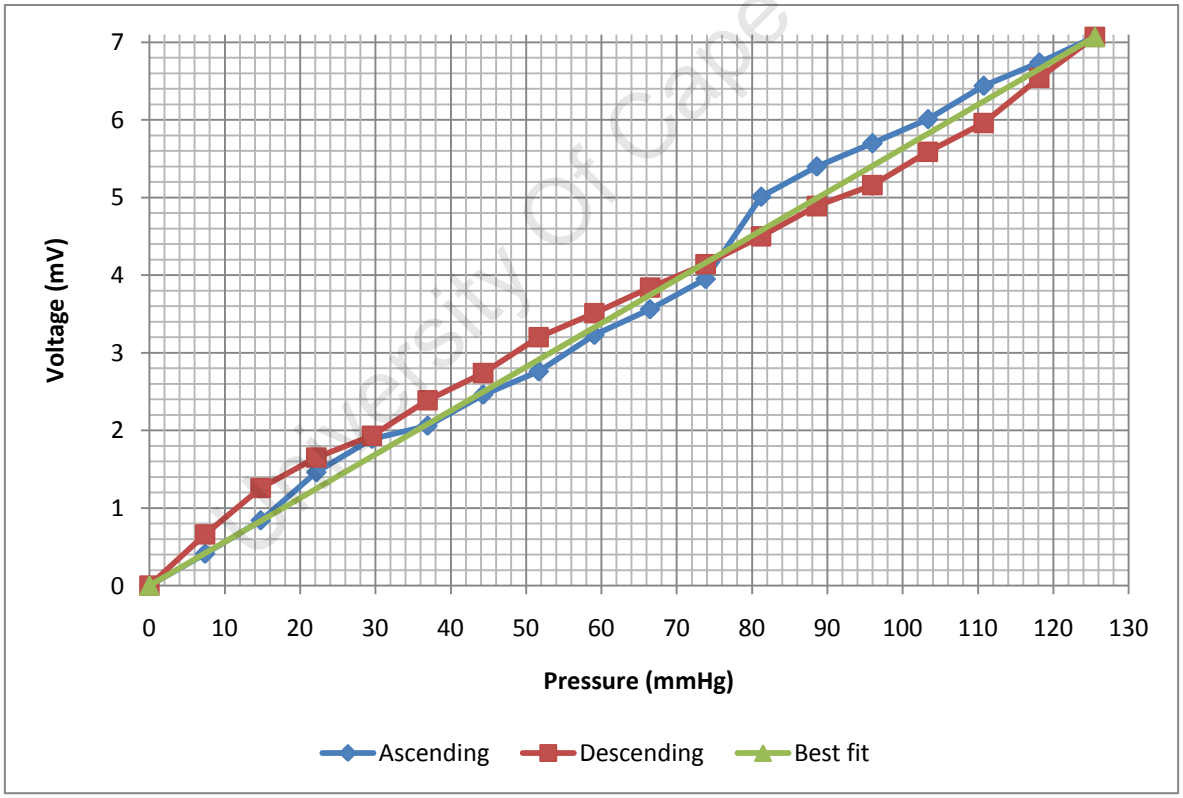

Figure 29: Hysteresis loop and best fit straight line of the pressure transducer output voltage vs. pressure, correlated relative to a height of mercury

Based on Figure 29, the voltage-pressure gradient was found to be 0.056335mV/mmHg, thus the maximum required voltage relative to 200mmHg was calculated to be

$$200 \times 0.056335 = 11.27\text{mV} \approx 12\text{mV} \tag{19}$$

Thus the noise of 1.3mV peak-to-peak, as shown in Figure 28(c), could be expressed as a percentage of this maximum voltage:

$$\frac{1.3}{12} = 10.8\% \text{ of the peak voltage} \tag{20}$$

Therefore, for a peak pressure of 200mmHg, this equated to an associated error of 22mmHg peak-to-peak, i.e. $\pm$11mmHg.

3.5.3.2 Flow Sensor Calibration

A pulsatile flow profile may be accurately represented by the first 10 harmonics of the signal [Transonic T106/T206, T108/T208 Flowmeter Manual], thus for pulsatile flow profiles at frequencies of the order of 60bpm (1Hz), a 10Hz bandwidth should be examined such that the signal is accurately described. The flow loop simulator is optimized for a 72bpm cycle rate, which is greater than the 60bpm standardization above. However, the physiological flow profiles to be produced in the compliance tester are known to not comprise frequencies exceeding 10Hz. Thus all frequencies above 10Hz were considered to be noise, and the T108 onboard 10Hz bandpass filter was engaged at the flowmeter output.

The raw filtered data from the flowmeter is output as an analogue voltage from the rear (pulsatile) output port. This voltage is a scaled representation of the actual volume flowrate through the transducer. For the case of the 12mm collar transducer (Transonic Systems Inc., New York, USA) as used in the flow loop simulator, the scale option of 1L/min/V was chosen for optimal signal resolution. An analogue input was used on the DAQ for data capture with a sample rate of 1kHz to ensure a well described measurement profile.

Independent assessment of the unprocessed flow signal yielded the following:

Figure 30(a) displays signal noise amplitude of 0.13V. To determine the severity of the signal noise it was necessary to quantify the peak desired flow velocity, u_1, at the flow transducer location in terms of the volume flowrate, Q, as measured by the T108. For a planar flow velocity, u_2, within the graft of 100cm/s (see Table 1), and considering the piston and graft diameters of 1cm and 0.4cm respectively, the peak desired volume flowrate at the flow transducer location was calculated using the principle of continuity of flow as follows:

$$u_1 = \frac{A_2 u_2}{A_1} = \frac{\pi(0.2)^2 100}{\pi(0.5)^2} = 16 \text{ cm/s} \tag{21}$$

$$\therefore Q = \pi(0.5)^2 \times 16 = 12.566 \text{ cm}^3/\text{s} = 12.566 \text{ mL/s} = 0.754 \text{ L/min} \tag{22}$$

For a scale factor of 1L/min/V the associated peak voltage is 0.754V (≈0.8V), therefore the unfiltered noise amplitude of 0.13V, as established above, was expressed as

$$\frac{0.13}{0.8} = 16.25 \text{ \% of the peak voltage} \tag{23}$$

$$\rightarrow 100 \times 0.1625 = 16.25 \text{ cm/s peak to peak within the graft} \tag{24}$$

To reduce the error associated with signal noise, an averaging algorithm was once again implemented to yield a net sample rate of 100Hz. The noise amplitude was reduced further by 54% to 0.07V as shown in Figure 30(b). Thus after processing, the flow signal yielded noise amplitude of 8.75% of the peak voltage of 0.8V. This equated to an associated error of 8.75cm/s peak-to-peak within the graft, i.e. $\pm$4.375cm/s.

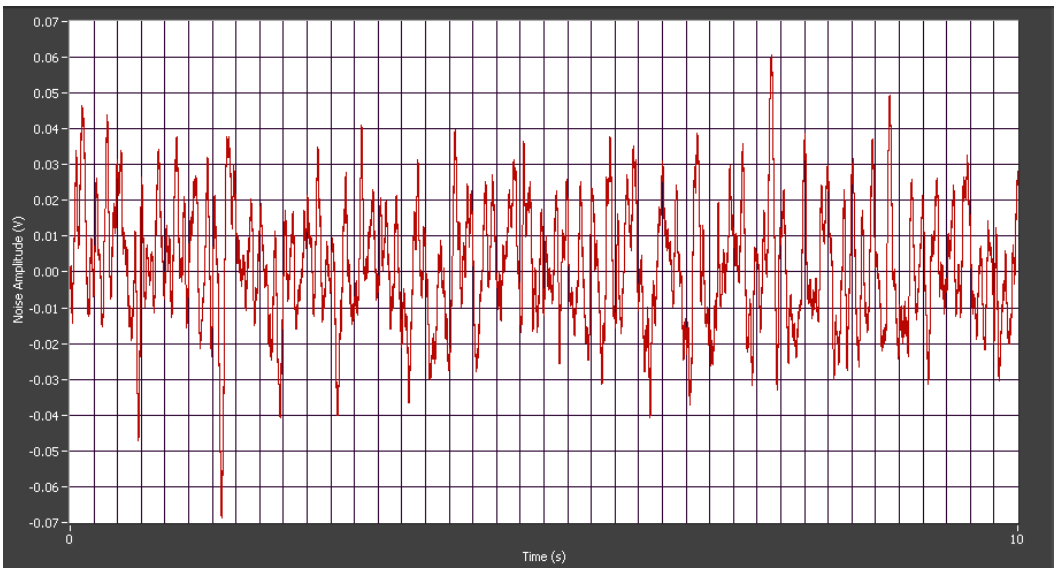

(a)

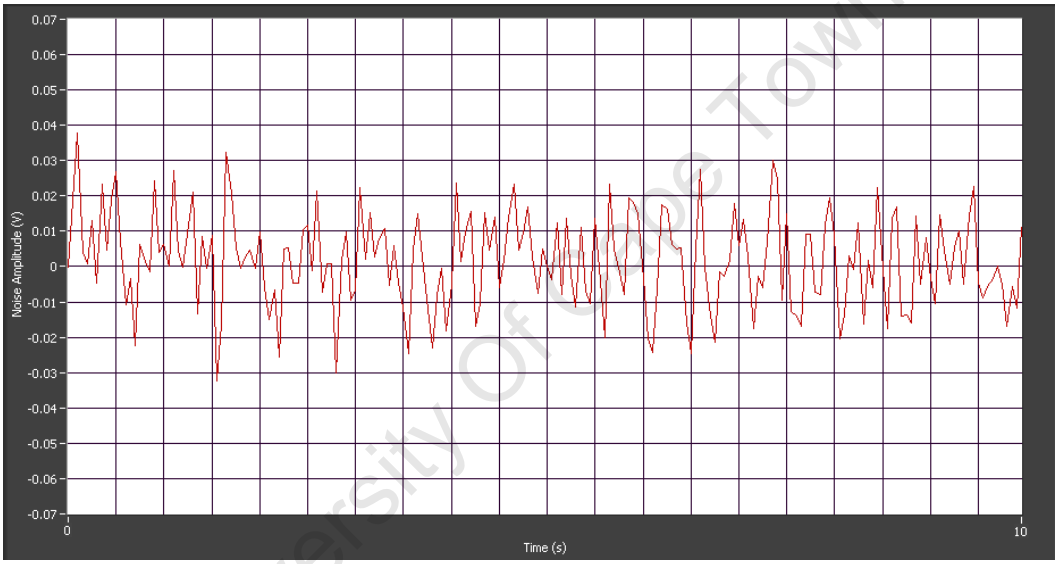

(b)

Figure 30: LabVIEW plot of the output signal noise from the T108 Volume Flowmeter (a) before averaging and (b) after averaging while disconnected from the flow loop system

To develop a relationship between the graft flow velocity and transducer output voltage, the volume flowrates at the location of the flow transducer were converted to fluid velocity, u_1, relative to the 10mm diameter flow path. The conversion was implemented as follows

$$u_1 = \frac{Q\,[\mathrm{L/min}]}{\pi(0.5)^2\,[\mathrm{cm^2}]} = \frac{1000}{60} \cdot \frac{Q\,[\mathrm{cm^3/s}]}{\pi(0.5)^2\,[\mathrm{cm^2}]} = 21.221\ Q\ \mathrm{cm/s} \tag{25}$$

Since the flowmeter output was scaled at 1L/min/V, it followed from Eqn. (25) that the flow velocity could be expressed relative to a voltage as 21.221cm/s/V. Referring this ratio to the flow velocity within the graft yielded

$$u_2 = \frac{A_1 u_1}{A_2} = \frac{\pi(0.5)^2 21.221}{\pi(0.2)^2} = 132.63\ \mathrm{cm/s/V} \tag{26}$$

Inverting yielded the voltage-flow gradient of 7.54mV/cm/s.

Similar to the DIPT pressure transducers, integrating the flow transducer into the flow system resulted in significant EMI from the drive stepper motor. However, the ultrasound probe used for flow measurement is extremely sensitive to ambient noise and was affected in a different manner to the DIPT transducers. With reference to Figure 27, the flow measurement noise was captured simultaneously, as shown in Figure 31(a). The flow signal exhibited similar behaviour to the DIPT transducers during initiation of the drive stepper motor. However at time t=11.5s, when the copper mesh cage was grounded, the transducer noise was amplified further rather than reduced.

The aforementioned averaging algorithm was implemented, but Figure 31(b) shows that the signal noise was not affected. Due to the magnitude of the noise it was not possible to incorporate the flow measurement in the system, as an accurate or qualitative output signal, by using the aforementioned noise reduction techniques.

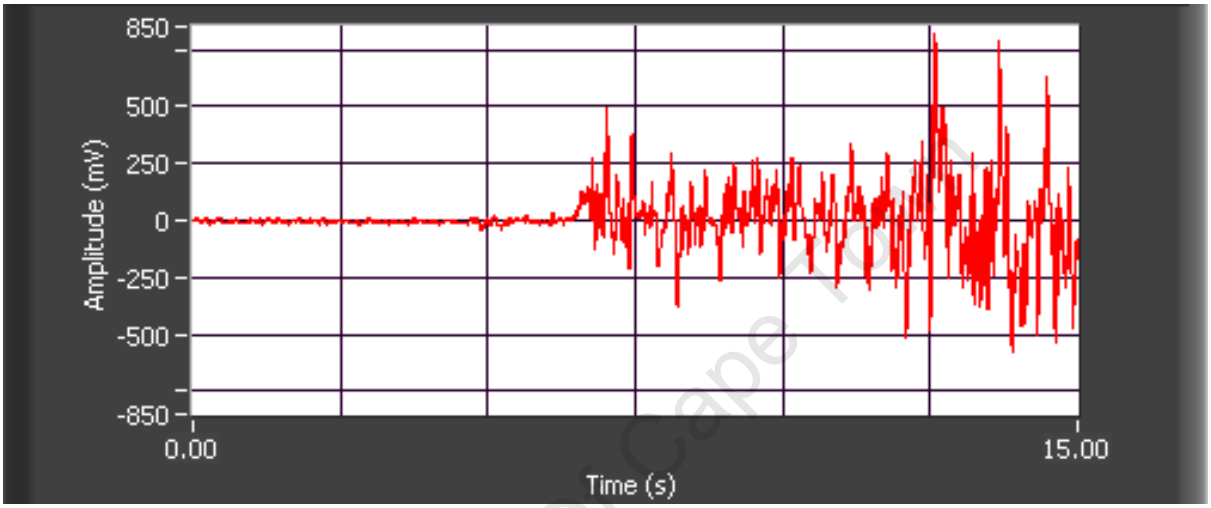

(a)

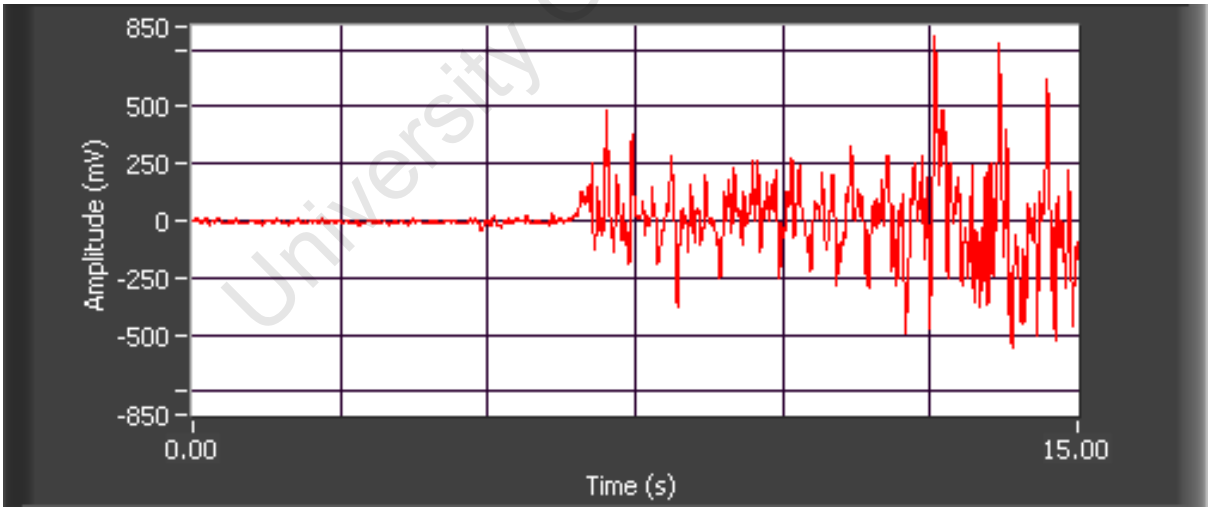

(b)

Figure 31: LabVIEW plot of the (a) raw and (b) averaged T108 flow signal, showing the effect of EMI on signal noise

Chapter 4: Design Outcomes

4.1 Mechanical Assembly Overview

Figure 32 shows the integrated mechanical assembly. The system structure is as designed in Chapter 3 with the exception of temporary modifications that were implemented due to time constraints. These temporary modifications served to assess the functionality of the design before completion of the construction. The constructed assembly, with temporary modifications, is described as follows:

Figure 32(a) shows the container that was used as the upper reservoir, elevated with a retort stand, with non-compliant tubing leading to the valve stage intake (a), from the valve stage bypass (b) and from the distal graft adapter (c). Manually operated tube clamps (d) were used at the bypass and distal flow lines in the place of the aforementioned needle valves. Figure 32(b) shows the lower level assembly with the drive (Block A) and flow (Block B) systems integrated as described in Section 3.4.1. As per the design, the flow loop comprises the piston cylinder (e), valve stage (f), flow probe mount (g), proximal graft adapter (h) and distal graft adapter (i). Block R shows the upper reservoir construction with integrated proximal (j) and distal (k) needle valves, heating element (l) and temperature probe (m). This reservoir assembly was constructed to be used as the upper reservoir but was instead used as the lower reservoir due to time constraints during diagnostic testing.

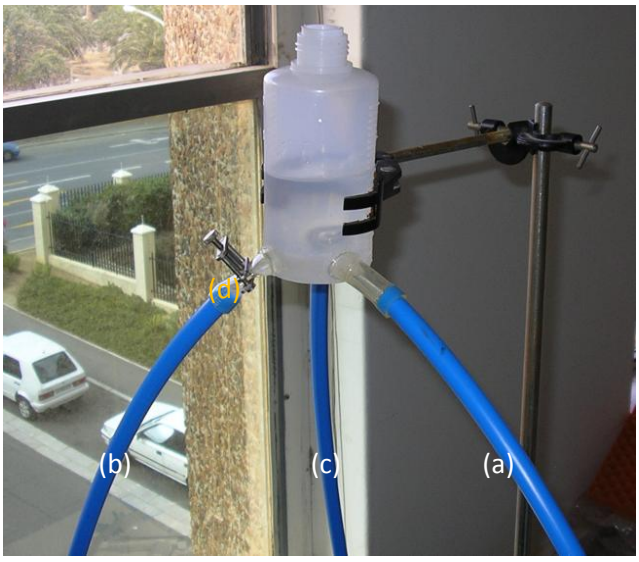

(a)

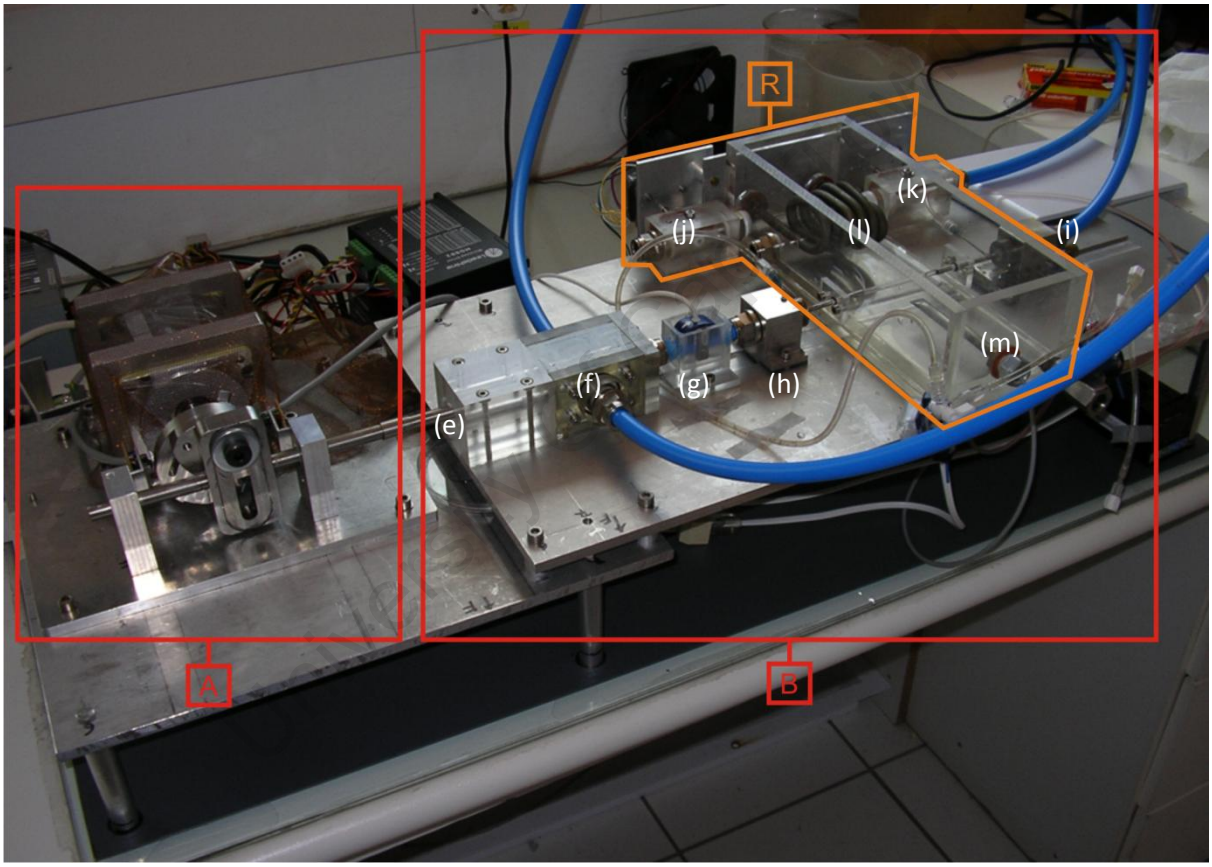

(b)

Figure 32: Overview of the integrated flow loop showing the (a) temporary upper reservoir and (b) lower level assembly with elements: (a) intake tube, (b) bypass tube, (c) distal ejection tube, (d) tube clamp, (e) piston cylinder, (f) valve stage, (g) flow probe mount, (h) proximal graft adapter, (i) distal graft adapter, (j) proximal needle valve, (k) distal needle valve, (l) heating element, (m) temperature probe

Figure 33 shows a detailed view of the pump assembly as built from the design in Figure 7. The large washers with Teflon discs (a) can be seen against the Scotch Yoke body (b), as well as the Teflon bushings (c) in the aluminium pillars (d). All Teflon components and the Scotch Yoke slot (e) were greased with Beckman grease (Palo Alto, California, USA) to reduce friction and wear. A major addition to the basic design included the aforementioned copper mesh cage (f) surrounding the drive stepper motor and grounded with a clip connection (g) to the motor power supply.

The optical sensors (a) can be seen in Figure 34 on either side of the Scotch Yoke assembly, comprising the crank disc (b), crank slider (c), Scotch Yoke body (d), linearization rod (e) and pushrod (f). The aluminium flag (g) attached to the crank disc passes through the optical sensors and breaks the infra-red beam to trigger a digital pulse at TDC and BDC.

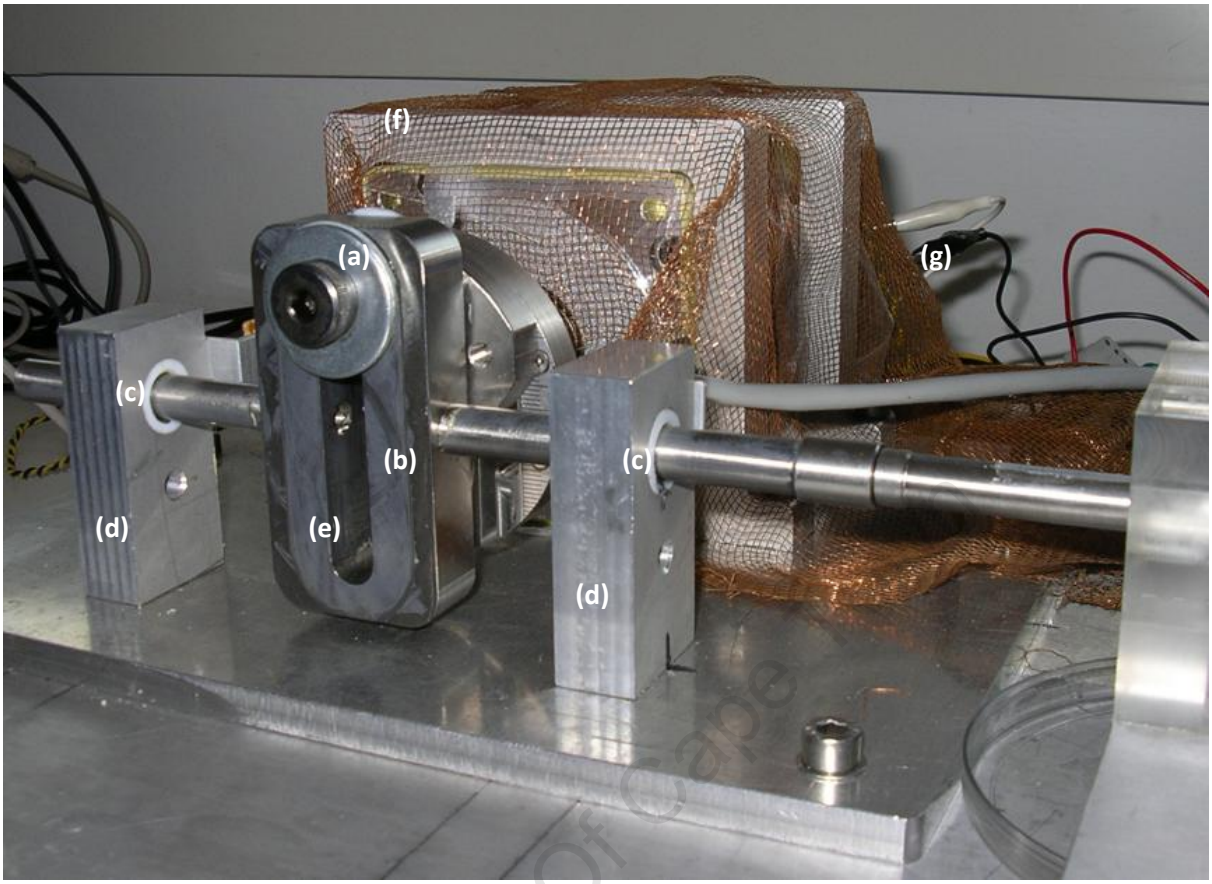

Figure 33: Final pump assembly including copper mesh shield: (a) Washer with Teflon disc, (b) Scotch Yoke body, (c) Teflon bushings, (d) aluminium support pillars, (e) Scotch Yoke slot, (f) copper mesh cage, (g) clip connection

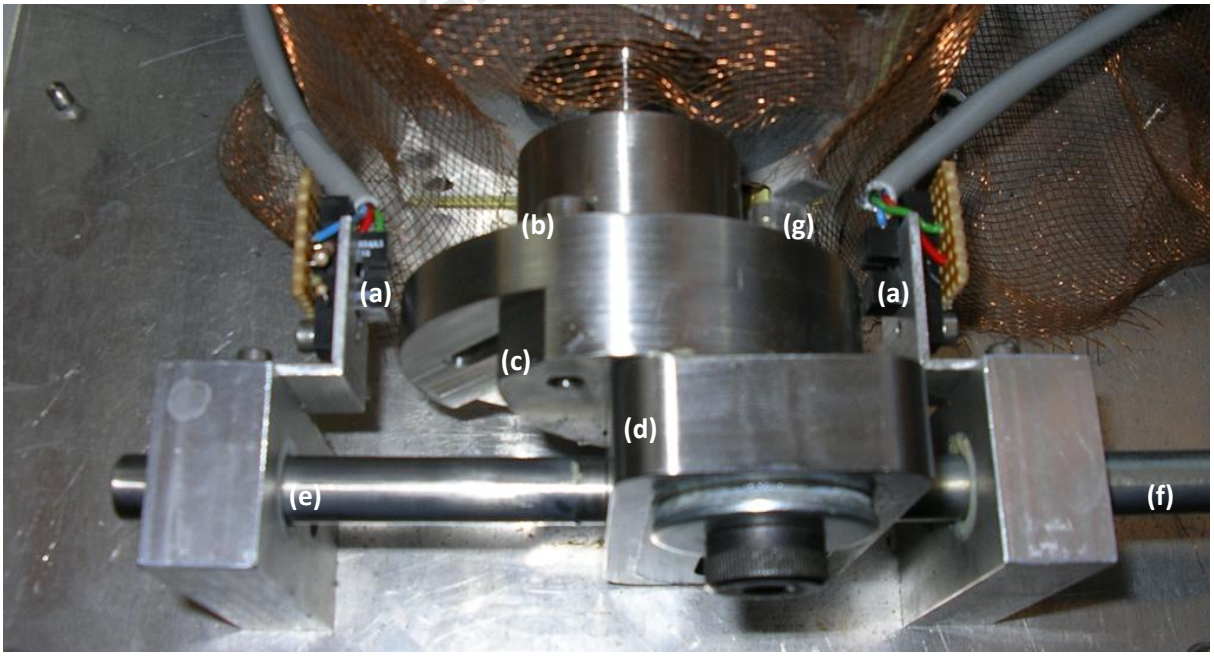

Figure 34: Scotch Yoke assembly with optical sensors: (a) optical sensors, (b) crank disc, (c) crank slider, (d) Scotch Yoke body, (e) linearization rod, (f) pushrod, (g) aluminium flag

The integrated Stainless Steel piston plunger (a) and Perspex cylinder (b) are shown in Figure 35. The Teflon disc (c) can be seen at the end of the plunger, as well as the four set screws (d) used to fix the cylinder to the aluminium base plate (e).

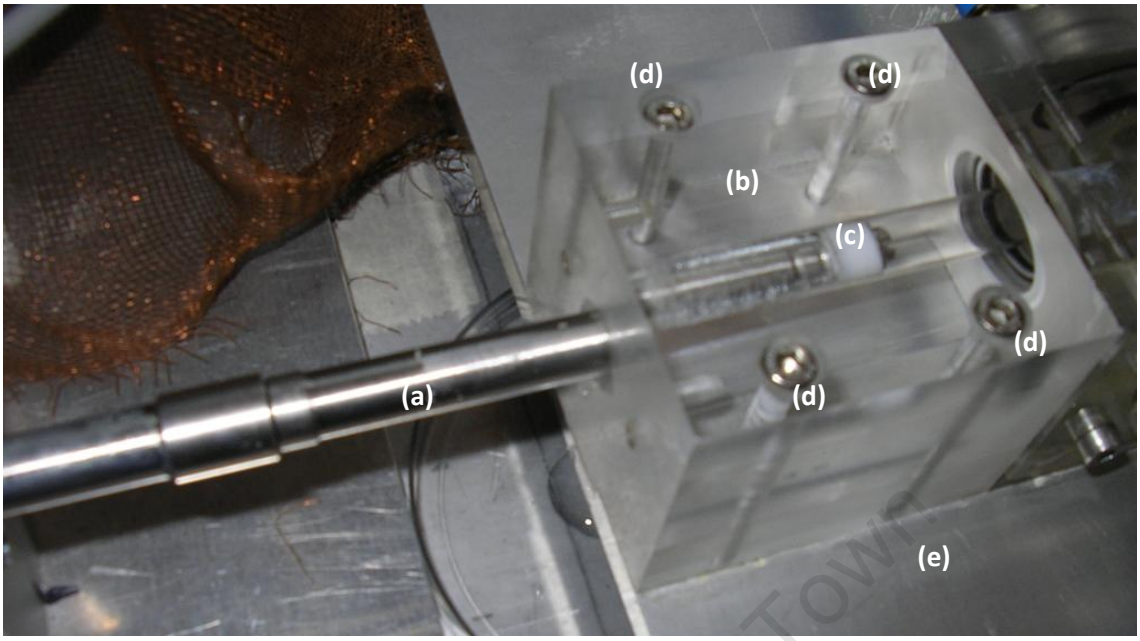

Figure 35: Integrated piston plunger and cylinder with Teflon seal: (a) piston plunger, (b) piston cylinder, (c) Teflon disc, (d) set screws, (e) aluminium base plate

Figure 36 shows the valve stage (a) coupled to the piston cylinder (b). The location of the intake (c), bypass (d) and ejection (e) check valves can be seen, as well as the flow probe mount (f) distal to the valve stage. All non-compliant tubing was coupled to the valve stage body using MA12 push-to-connect fittings (Gripper, Cape Town, South Africa) (g).

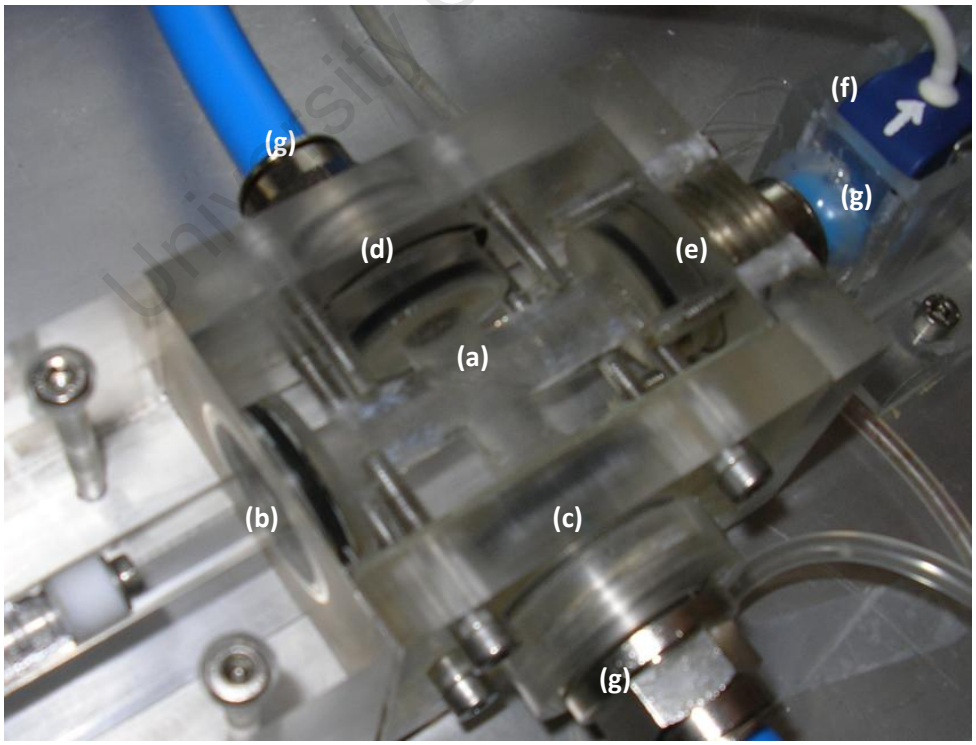

Figure 36: Integrated valve stage with the piston cylinder and Transonic flow probe mount: (a) valve stage, (b) piston cylinder, (c) intake check valve, (d) bypass check valve, (e) ejection check valve, (f) flow probe mount, (g) push-to-connect fittings

The disassembled valve stage is shown in Figure 37 and reveals the assembly of the latex membrane (a), wire mesh scaffold (b), tri-leaflet cut (c) of the valve opening and the surrounding O-ring seal (d) of the intake check valve. The valve stage body (e) is fixed to the base plate (f) with a pair of vertical screws (g), on either side of the valve stage body, that are concealed when the intake and bypass valves are attached.

Figure 38 shows the graft adapter as built from the design in Figure 14. The final component incorporates the hypodermic tube (a) and orthogonal Luer needle (b), as designed. Due to manufacturing technicalities, practical modification was made to the key that aligns the graft adapter in the proximal and distal mounts. Rather than machining the key as in Figure 14, a short Stainless Steel rod (c) was glued into a machined recess such that it fit into the required slot and could be secured with a grub screw.

Figure 39 shows the graft adapter mounted in the proximal position, with the grub screw (a) fastened against the aforementioned rod section, and a set screw (b) on either side of the adapter mount to fix it to the base plate. The hypodermic needle is secured by a flange (c) as it passes through the proximal wall of the lower reservoir. The hypodermic tube is sealed in the flange of Figure 39 by an O-ring (a) fastened between the flange (b) and the reservoir wall (c), as shown in Figure 40.

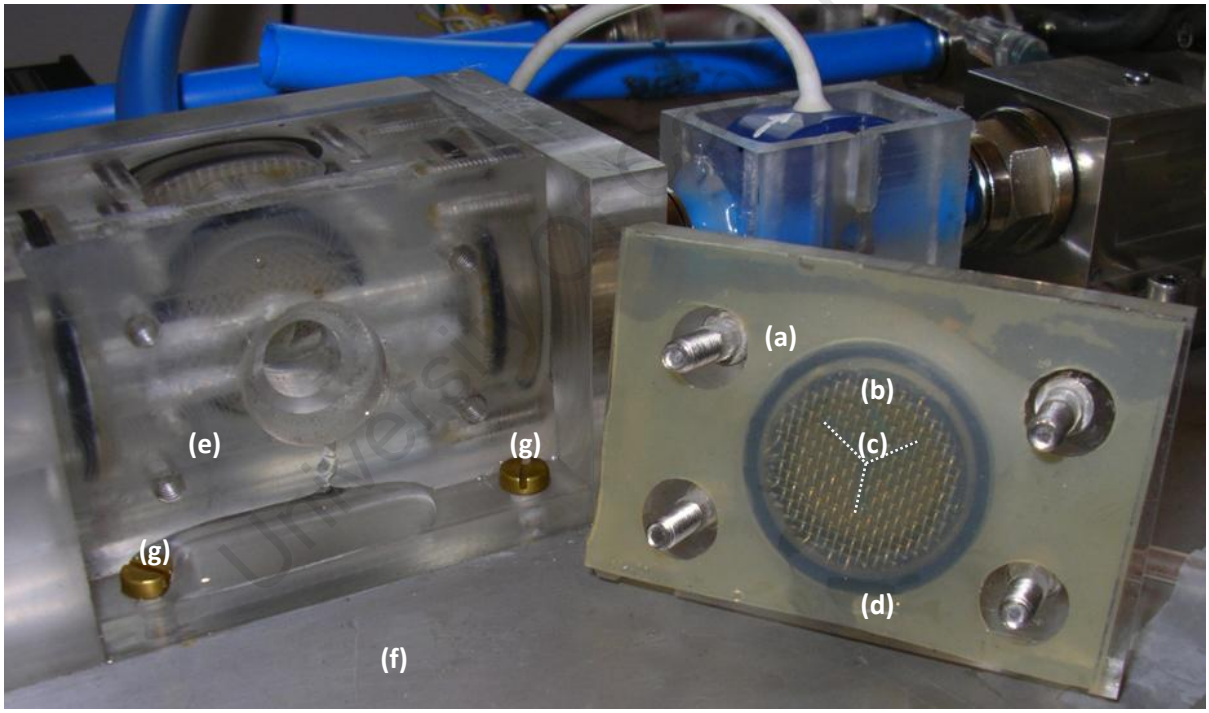

Figure 37: Disassembled intake check valve, showing the valve membrane and wire mesh scaffold: (a) latex membrane, (b) wire mesh scaffold, (c) tri-leaflet cut, (d) O-ring seal, (e) valve stage body, (f) aluminium base plate, (g) mounting screws

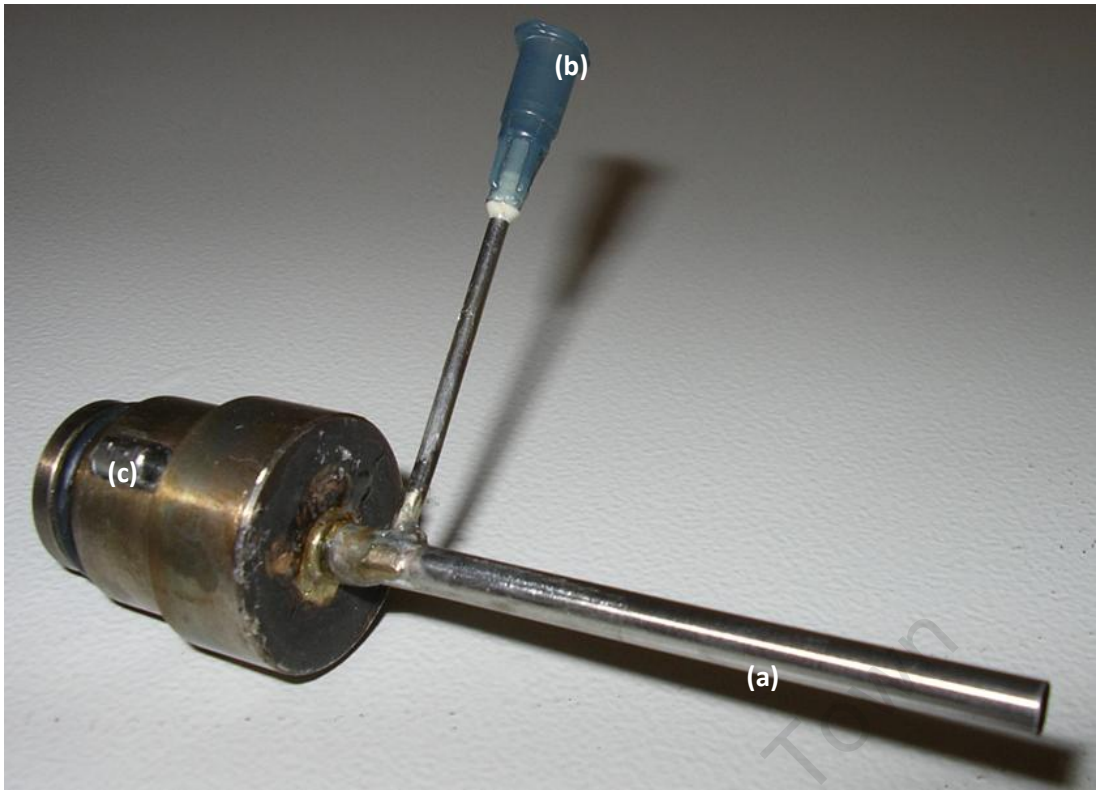

Figure 38: Graft adapter with orthogonal Luer needle for pressure measurement: (a) hypodermic tube, (b) Luer needle, (c) Stainless Steel key rod

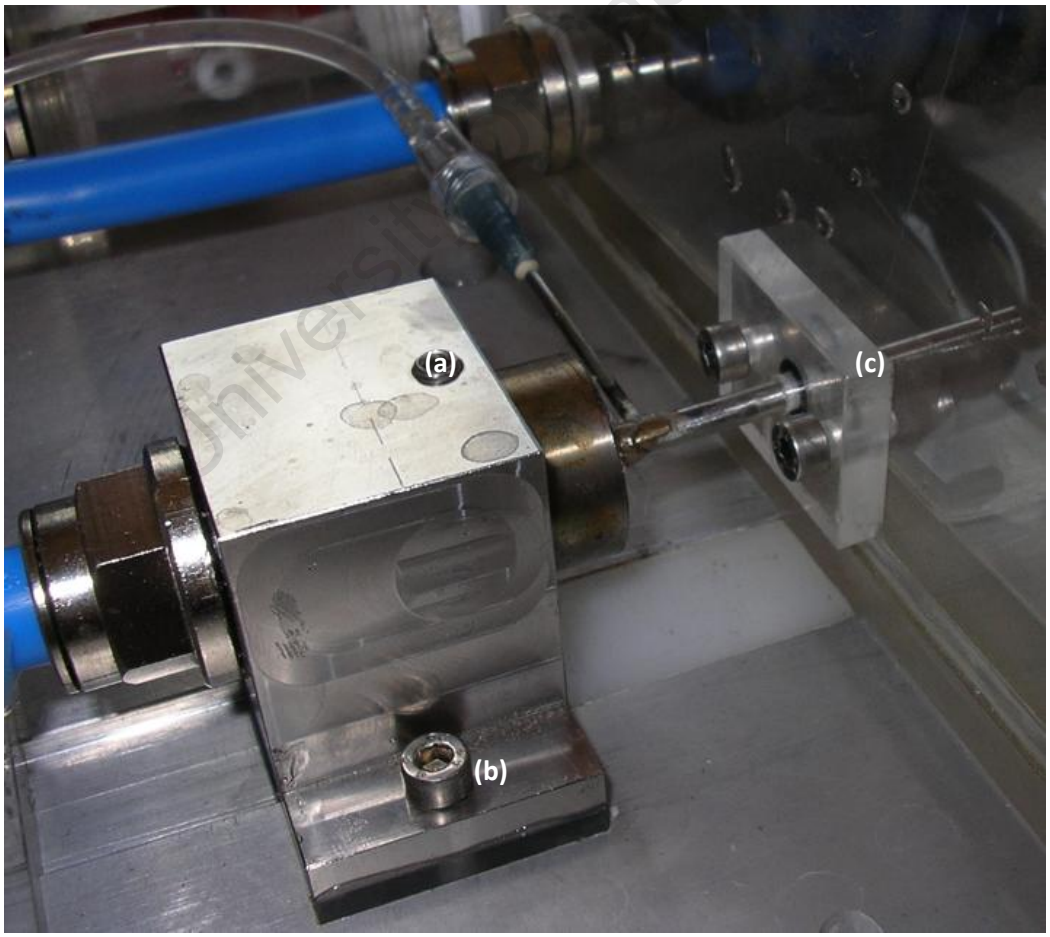

Figure 39: Proximal graft adapter secured in the mount and interfaced with the reservoir wall: (a) grub screw, (b) set screw, (c) reservoir flange

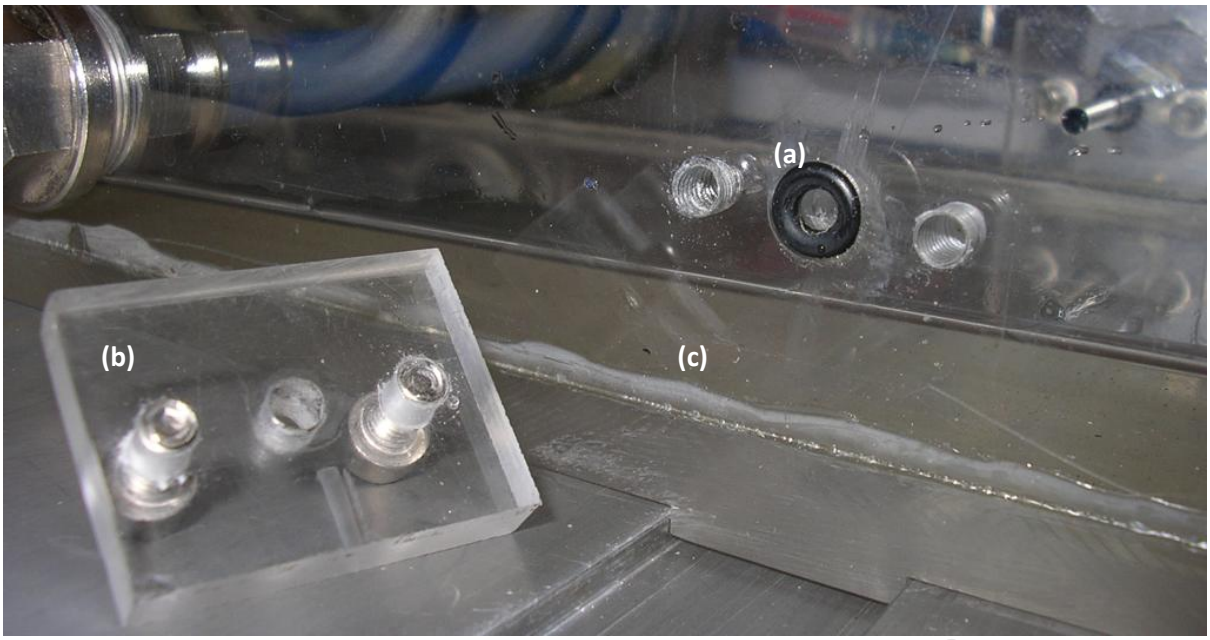

Figure 40: Disassembled reservoir flange showing the O-ring in the proximal wall of the lower reservoir: (a) O-ring seal, (b) reservoir flange, (c) proximal reservoir wall

Figure 41 shows a graft sample (a) mounted between the proximal (b) and distal (c) graft adapters in the lower reservoir. The location of the heating element (d) and temperature probe (e) can be seen in relation to the graft location.

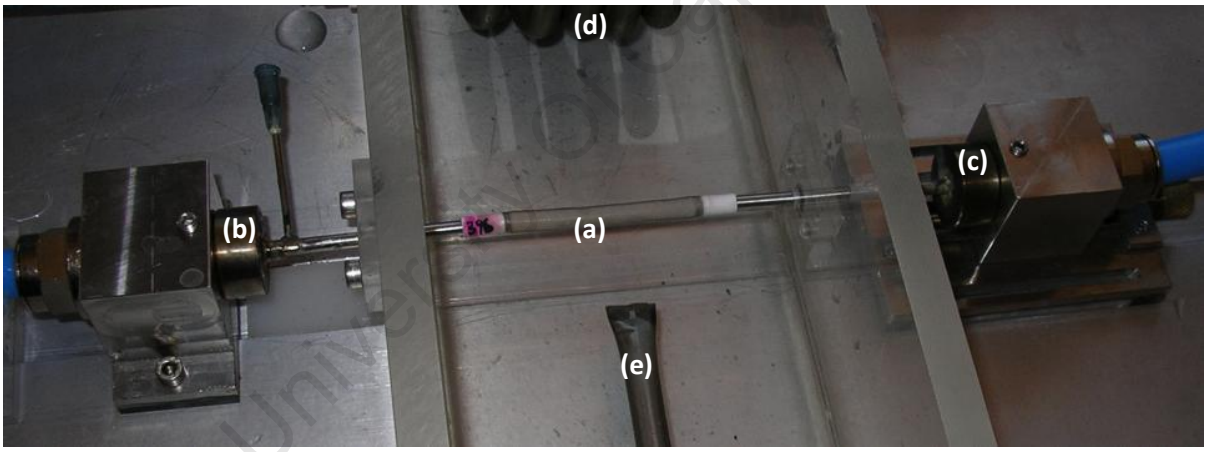

Figure 41: Graft mounted in the lower reservoir between the proximal and distal graft adapters: (a) graft sample, (b) proximal graft adapter, (c) distal graft adapter, (d) heating element, (e) temperature probe

Distal to the lower reservoir is the distal graft adapter (a) mounted on the pre-tension mount (b), as shown in Figure 42. A brass screw (c) was custom threaded to adjust the position of the distal graft adapter along its longitudinal axis, thus applying a strain to the graft sample. An MA12 fitting (d) was used to connect the non-compliant tubing from the distal graft adapter to the upper reservoir.

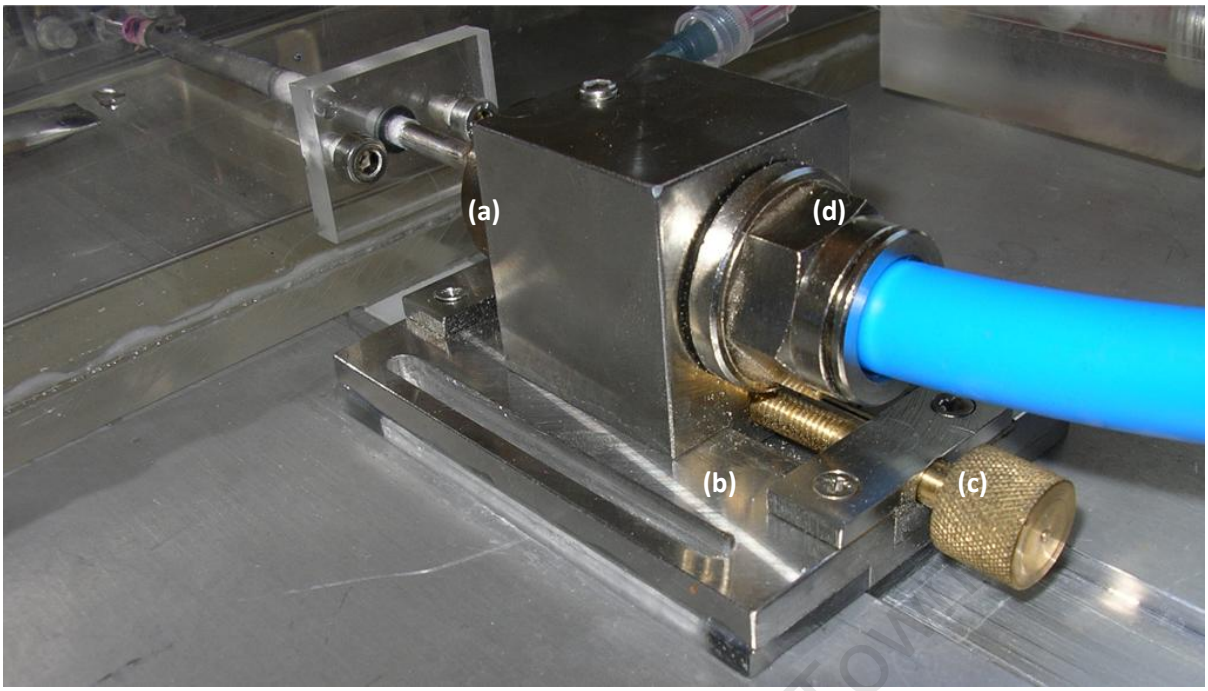

Figure 42: Distal graft adapter integrated with the pre-tension mount and longitudinal adjusting screw: (a) distal graft adapter, (b) pre-tension mount, (c) brass screw, (d) push-to-connect fitting

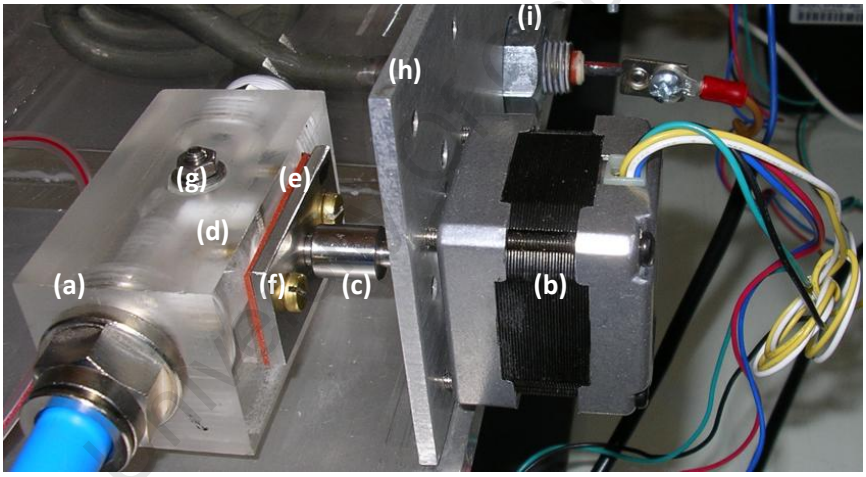

Figure 43: Distal needle valve interfaced with mini-stepper motor for digital control: (a) distal needle valve, (b) mini-stepper motor, (c) Stainless Steel shaft fitting, (d) needle valve gate, (e) rubber gasket, (f) Stainless Steel plate, (g) linearization pin, (h) aluminium mounting plate, (i) heating element mounting bolt

Figure 43 shows the integration of the distal needle valve (a) and mini-stepper motor (b), as designed for the upper reservoir assembly. A custom turned screw fitting (c) couples the motor shaft to the Teflon needle valve gate (d). The coupling is hydraulically sealed with a rubber gasket (e) fixed to the needle valve by a Stainless Steel plate (f). The linearization pin (g), as mentioned in Section 3.3.8, can be seen. The mini-stepper motor is rigidly mounted to an aluminium plate (h) that, in turn, is mounted against the back of the reservoir. The aluminium plate incorporates large holes to fit around the mounting bolts (i) of the heating element, such that the plate and mini-stepper assembly can be removed easily without decoupling the heating element from the reservoir. The proximal needle valve system is similarly assembled on the opposite side of the reservoir.

4.2 Integrated System Operation

4.2.1 System Preparation

The initial setup of the flow loop simulator requires priming of the hydraulic system components once the graft is attached to the adapters in the lower reservoir. This entails filling both reservoirs with the desired fluid solution and running the priming sequence, during which the drive stepper motor rotates at constant speed. The constant speed rotation, and consequent pumping action of the piston, forces air bubbles out of the tubing and flow loop components and into the upper reservoir where they are vented to atmosphere. This procedure is conducted with both needle valves fully open such that negligible pressure is produced within the graft sample.

Once the system is primed, the heating systems may be switched on to heat the fluid in both reservoirs. Note that for diagnostic testing of the current system configuration only the lower reservoir was equipped with a heating system. Also, since manually operated tube clamps were used temporarily in the place of the needle valves, all further references to the needle valves relate to the tube clamp configuration.

4.2.2 System Calibration

Before the system is initialized, the DIPT transducers should be calibrated. It was verified in Chapter 3 that the DIPT transducer output could be described as linear over the required operating range; therefore calibration is performed as follows:

With the upper reservoir lowered to the base plate level, the initial state of the proximal and distal DIPT output voltages are recorded. The output voltages are then offset by this initial value to establish a zero reference. The upper reservoir is then raised to the desired height in order to set the diastolic baseline pressure, and the resulting DIPT output voltages recorded. The height of water is converted to a pressure in terms of mmHg, and the linear voltage-pressure gradients are established. The offset values and DIPT output voltages are then scaled by this gradient to yield the calibrated pressure measurements in mmHg relative to the zero reference. The two DIPT signals are then averaged and plotted as a single graph. Figure 44 shows the resulting calibrated reference pressure and diastolic baseline pressure of 80mmHg as used for the diagnostic assessment of the current rig setup.

4.2.3 System Initialization

Having completed the system setup, the user can configure the desired flow profile as well as the piston and graft diameters in the GUI. The computed crank radius can then be set mechanically.

Once the above procedures are complete, the user may activate the “Initialize” sequence, as shown in Figure 22, to output the desired flow profile. The profile output speed may be changed in real-time to the desired frequency. Thereafter the user may adjust the proximal and distal needle valves to establish a pressure profile, superimposed on the diastolic baseline pressure, relative to the programmed flow profile. For diagnostic testing of the current setup, the proximal (bypass) tube clamp was fully closed (since the entire ejected volume was required for accurate pressure production), and the distal (ejection) tube clamp manually adjusted to set the systolic pressure profile amplitude. Thus, the system is considered to be setup and may be run for the desired duration of the graft test.

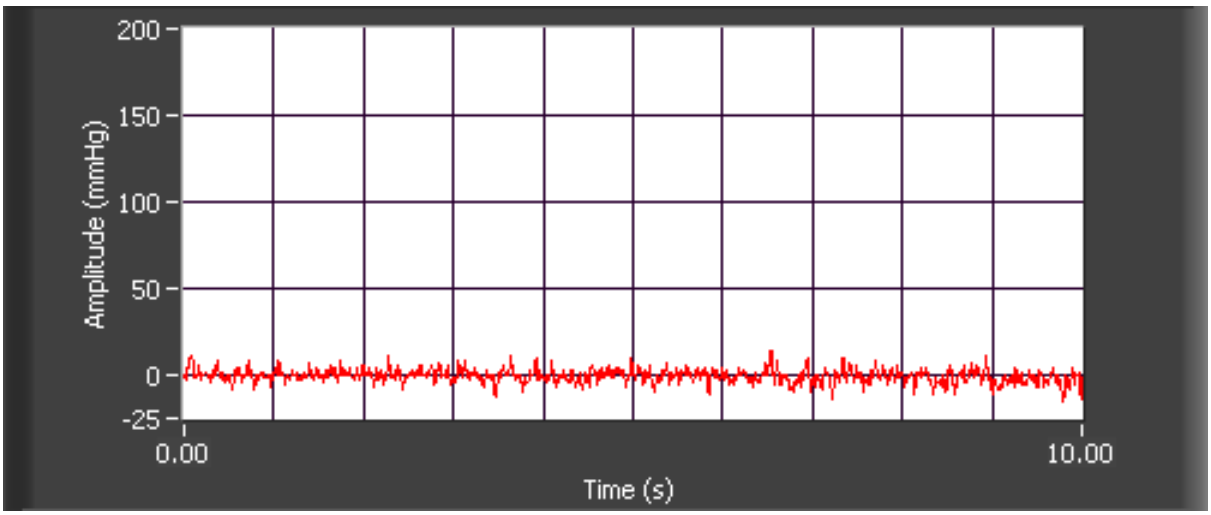

(a)

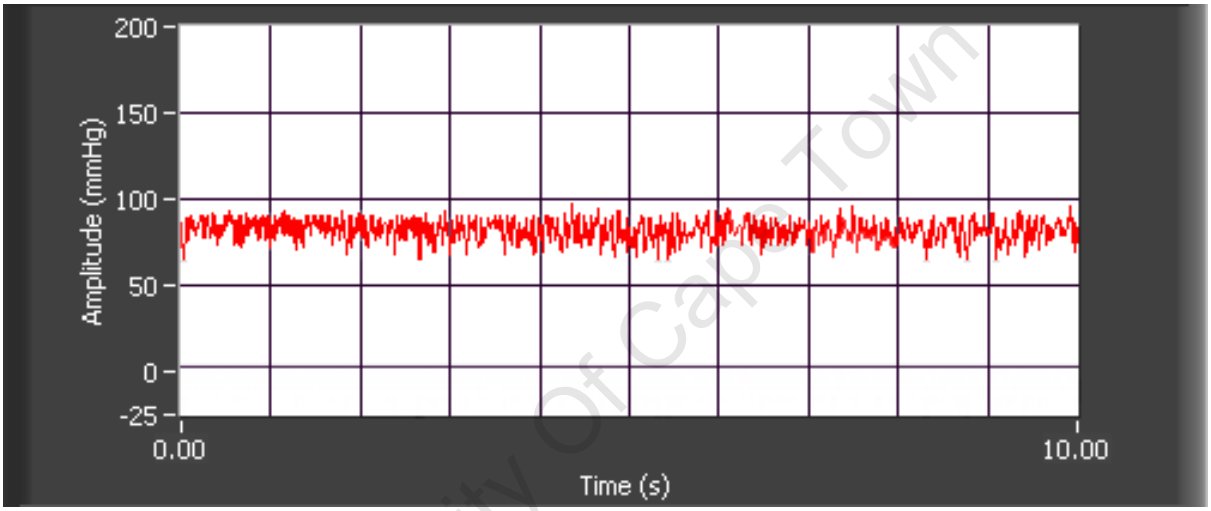

(b)

Figure 44: LabVIEW plots showing the (a) zero reference pressure and (b) calibrated diastolic baseline pressure

4.2.4 System Output

During testing, system output takes the form of a real-time plot of the pressure measurement, as well as numerical data comprising the pressure magnitude and time. The real-time plot serves as a qualitative output for user interpretation and monitoring, whereas the numerical data is intended for use with a correlated diameter measurement in order to compute the graft compliance.

4.3 Integrated System Performance

4.3.1 Heating System Performance

A single temperature control system, comprising a heating element, PT100 temperature probe and DTD controller, was used to heat the fluid in the lower reservoir. The auto-calibrate function on the DTD temperature controller was initialized to characterize the PID control variables required to heat the fluid in the reservoir.

The desired setpoint of 37°C was programmed as well as an alarm signal to trigger if the temperature exceeded 40°C. Figure 45 illustrates heating from the ambient temperature of 22°C to the setpoint. The total time taken to reach the setpoint was 8 minutes, without overshoot; thereafter the setpoint temperature was maintained to within 1°C.

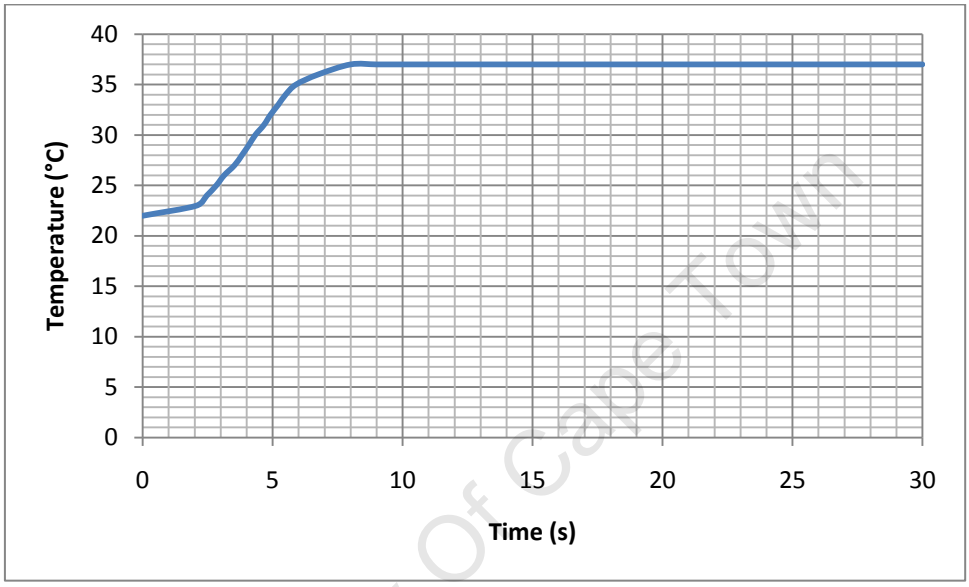

Figure 45: Graph of temperature vs time to illustrate heating and temperature control of the fluid in the lower reservoir

4.3.2 Pressure Profile Production

The flow profile configured in the GUI is actuated during the piston ejection phase, from 0° to 180°. The piston intake phase, from 180° to 360°, serves to draw a volume of fluid from the upper reservoir, required for the next ejection phase, and is therefore not considered as part of the profile actuation. Henceforth, the region of interest with regards to profile production is the piston ejection phase, and the system was assessed on this basis by programming the profile to execute to completion before intake of the subsequent volume of fluid.

Figure 46 shows the flow profile as programmed for diagnostic testing of the current rig setup. The profile has a random structure, but comprises explicit programming of the significant elements of a pressure profile, namely the initial pressure peak (a) and dicrotic wave (b). The minor third peak (c) was programmed to illustrate the versatility of the profile production, as well as the degree of subtlety within the profile that the mechanical components could accurately represent. As it was mentioned, the pressure decay (d) was also explicitly programmed. The profile also assumes minimizing the duration of the intake phase such that the ejection phases are actuated as close together as possible.

As previously described, the distal needle valve may be set by the user to configure a pressure profile of the desired amplitude, based on the flow profile set in the GUI.

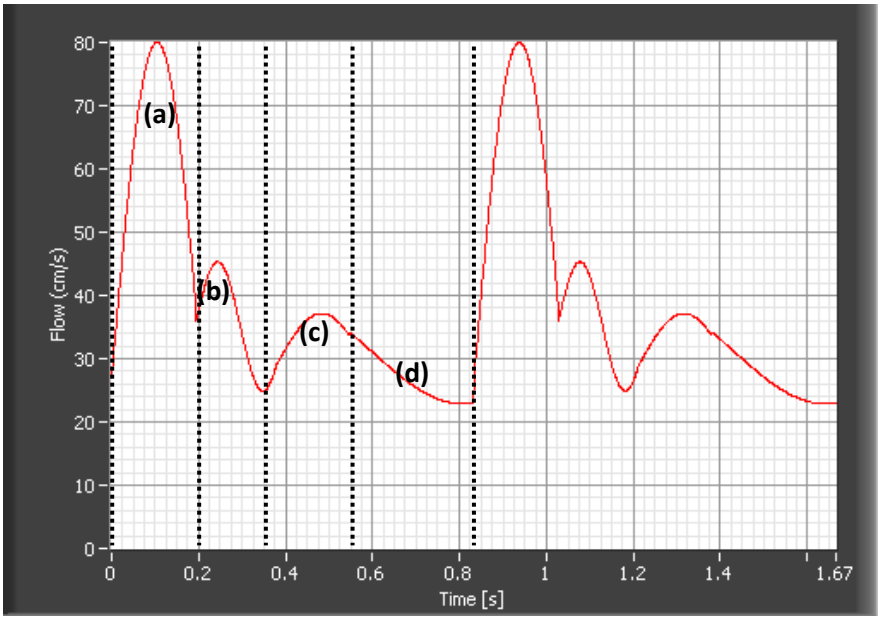

Figure 46: Desired flow profile as programmed in the GUI for qualitative pressure production, showing the (a) initial pressure peak, (b) dicrotic wave, (c) minor third peak, (d) decay

Figure 47 shows the dynamic pressure produced through a single 360° rotation of the drive stepper motor shaft. Compared qualitatively to the profile in Figure 46, Figure 47 exhibits a well-described ejection phase with accurate production of the initial pressure peak (a) and dicrotic wave (b), followed by the minor third peak (c) and the programmed pressure decay (d). The ejection phase in Figure 47 was set to execute with a period of 0.83s, thus replicating profile behaviour at a heart rate of 72bpm. During the intake phase (e), the applied negative pressure required for closure of the ejection check valve manifested as a large pressure drop until the valve was closed. Thereafter the fluid momentum produced a reflected wave (f), thus momentarily increasing the pressure as the wave abutted the closed check valve. A pause due to internal LabVIEW code execution manifested as a dead-time (g) comprising only the diastolic baseline pressure and random signal noise.

Figure 48 shows five such pressure cycles actuated continuously, and the effect of various needle valve positions on a pressure profile produced upon a diastolic baseline pressure of 80mmHg. Figure 48(a) is a plot of the pressure profile produced at very high amplitude, with a systolic peak of 280mmHg.

Figure 48(a) shows that the aforementioned elements of Figure 47 were all reproducible, with errors in magnitude attributable primarily to the DIPT signal noise. Additionally, it is worth noting that the only element of the profile that showed notable irreproducibility occurred during the dead-time (g), when the pressure signal comprised only the random noise superimposed on the constant diastolic baseline pressure.

Figure 48(b) shows the same pressure profile actuated with the distal needle valve at a more open setting, and the resulting systolic peak at a lower amplitude of 210mmHg. The profile elements were once-again reproducible, with minimal loss of clarity due to the DIPT signal noise, and only the dead-time section exhibiting significant irreproducibility.

Figure 48(c) shows more prominent interference of the DIPT signal noise when the distal needle valve was set to produce a yet lower peak systolic pressure of 160mmHg. The profile elements could be identified, relative to the aforementioned plots, as similarly reproducible. However, the profile contours were no longer accurately represented in the measurement signal, and the signal noise contributed significant inaccuracy to the systolic pressure peak measurement.

The distal needle valve setting was adjusted a final time to assess the measurement inaccuracy with respect to a systolic pressure peak of 120mmHg. As can be seen in Figure 48(d), almost the entire profile was encompassed by the DIPT signal noise. However, the systolic pressure peaks, and reflected pressure waves due to check valve closure, could be made out as spikes in the profile measurement thus confirming that the profile still maintained the desired period.

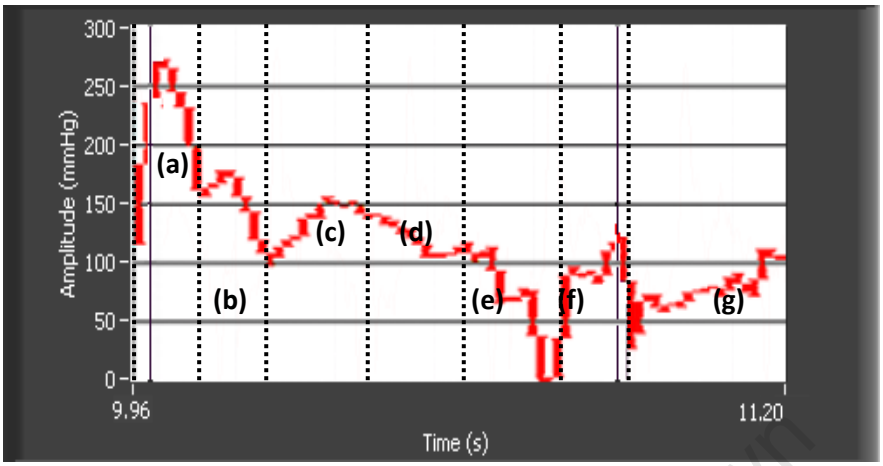

Figure 47: Zoomed view of a single pressure profile measurement through ejection and intake phases, showing the (a) initial pressure peak, (b) dicrotic wave, (c) minor third peak, (d) decay, (e) valve closure, (f) reflected wave, (g) delay

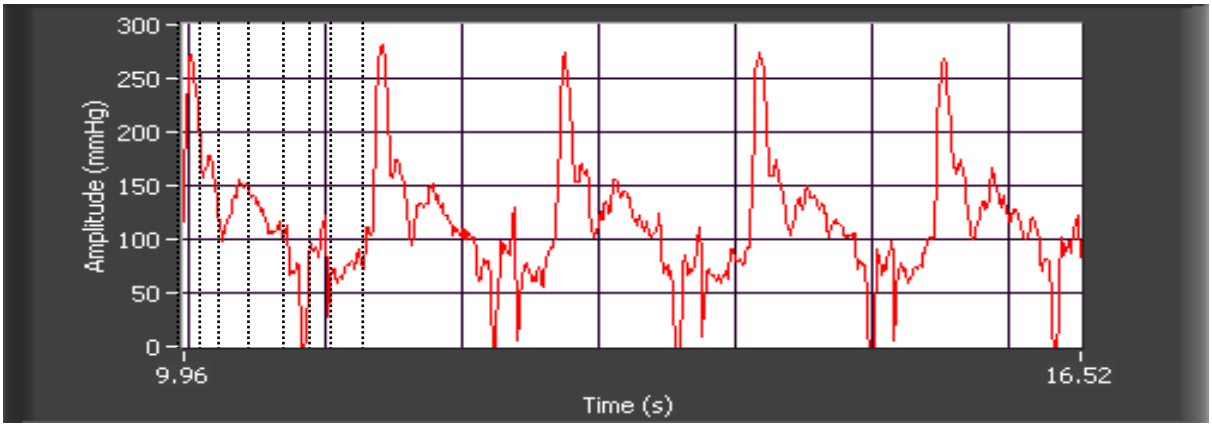

(a)

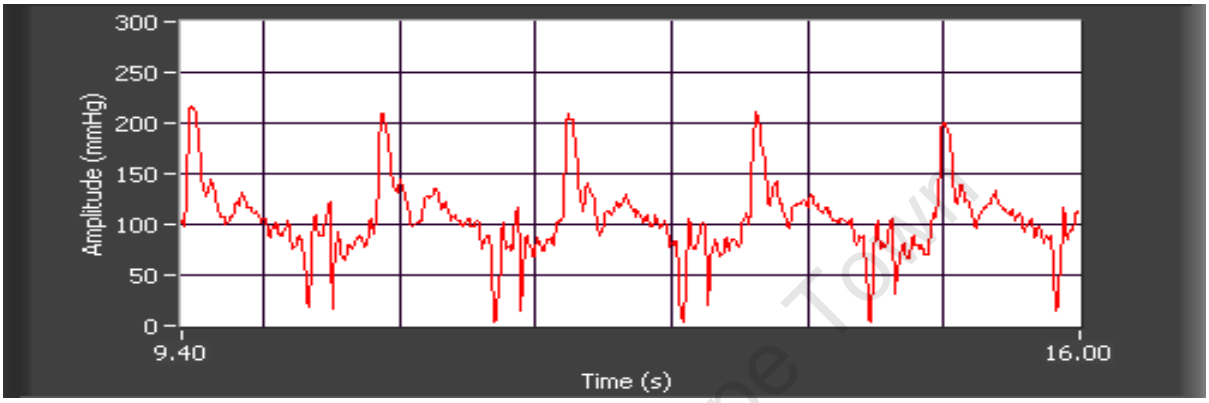

(b)

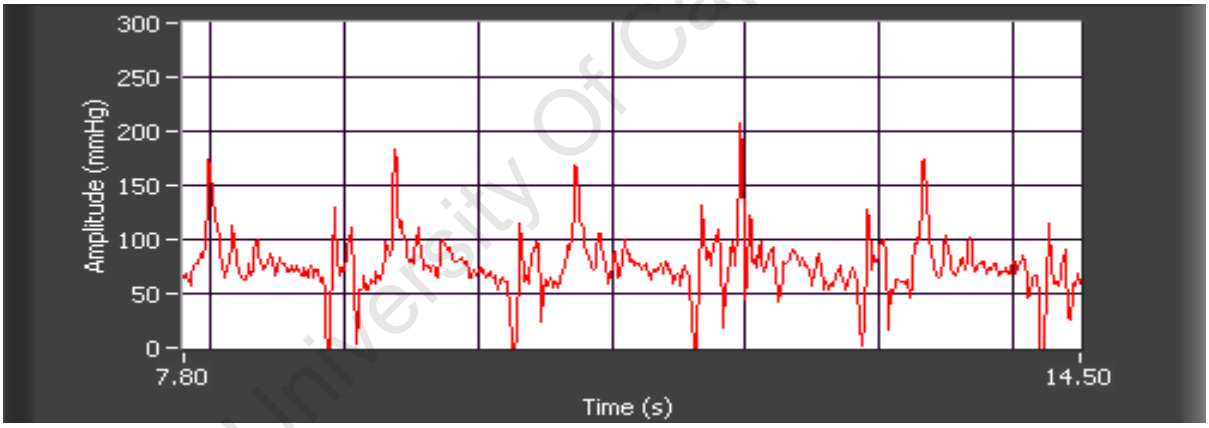

(c)

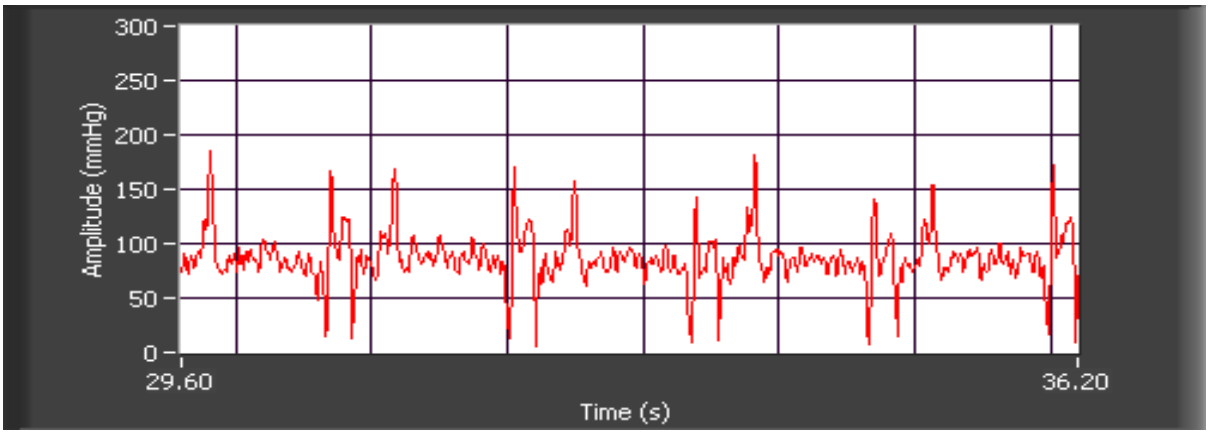

(d)

Figure 48: LabVIEW plots of the pressure profiles produced with different distal needle valve settings for pressure amplitudes between 80mmHg and (a) 280mmHg, (b) 210mmHg, (c) 160mmHg and (d) 120mmHg

Chapter 5: Discussion of Design Outcomes

5.1 Mechanical System

As described in Section 4.3.2, the mechanical components, including temporary modifications, performed their desired functions. A critical assessment of the component performance was carried out and noteworthy considerations are outlined below.

The temporary upper reservoir and retort stand confirmed that elevating the reservoir produced an effective diastolic baseline pressure, controllable by virtue of the reservoir height. The proximal tube clamp on the bypass line exhibited that fully closing the proximal clamp redirected all fluid through the distal flow path during pumping. The distal tube clamp on the ejection line showed that the amplitude of the pressure profile could indeed be controlled, as described in Section 3.3.8, by varying the tube cross-sectional area. Thus the tube clamps were a good indication of the level of control proposed in the needle valve design, albeit without quantifying the change in cross-sectional

area. The needle valves, however, would afford this quantification. Thus the tube clamp performance suggests that the needle valves may indeed be automated to serve their desired function, and do so with a higher level of control than the tube clamp configuration.

The heating of the lower reservoir was conducted efficiently by the Delta DTD temperature controller. In terms of heating, a compromise exists between the power of the heating element, the rate of heating and the longevity of the temperature controller. A more powerful element would increase the heating rate, thereby shortening the time taken to reach the setpoint for a given fluid volume. However, the element would require more rapid switching to maintain the setpoint temperature and minimize overshoot. This rapid switching would fatigue the internal controller relay more quickly and shorten the controller lifespan. A lower power element would, conversely, decrease the heating rate, increase the heating duration and reduce wear on the internal controller relay; the chief sacrifice being the longer heating duration. In the current setup, the short heating time, accurate control at the setpoint and minimal controller switching confirmed that the heating element design was satisfactory for the volume of fluid to be heated. Thus, similar integration of a heating system in the upper reservoir would, in all likelihood, control the temperature of the circulating fluid at the same level of efficiency. This is a reasonable prediction, since the temperature controller can be calibrated while the system is running to account for the temperature changes due to the circulating fluid.

As illustrated in Figure 27, the effect of the copper mesh cage around the drive stepper motor was significant. It is believed that the caging method could be optimized further, to improve the EMI-reduction, in terms of the cage material, mesh density, selected grounding point and motor decoupling method. The motor optical sensors exhibited decreased efficiency as the motor speed was increased. The ability of the optical sensors, as shown in Figure 34, to detect the passing flag was diminished at higher motor speeds. Whilst the motor is capable of rotating at higher speeds, the intake speed was optimized such that the optical sensors, particularly the BDC sensor, were able to detect the motor position. Thus the optical sensors contributed to restrictions placed on the motor rotation profiles.

With regards to the graft adapter design, the current orthogonal Luer needles used for the pressure measurement have plastic heads. Due to the heat required to solder the Luer needles into the hypodermic tubing, it was necessary to leave the Luer needles long, to prevent melting of the plastic heads. The longer needles cause slight obstruction during setup, despite angling them out of the way of a passing hand. Additionally, the length creates a longer lever arm such that, if knocked, the produced torque could bend the needle free from its solder point.

Introducing the graft adapters into the lower reservoir currently entails disassembly of the flange and O-ring seal, as shown in Figure 40. This is because of the thin walls of the hypodermic tubing, and the resulting sharp edge at the circumference. Thus, simply pushing the tubing through the O-ring seal, whilst mounted in the flange, would cut into the O-ring seal and compromise its effectiveness.

5.2 Heating System Operation

Use of the Delta DTD temperature controller, with the heating element and PT100 temperature probe, enabled closed loop temperature control that was completely independent of the DAQ interface. This allowed for more efficient computer resource distribution amongst the more CPU-intensive tasks of drive stepper motor actuation and simultaneous pressure measurement. Additionally, outsourcing the temperature control device ensured accurate and repeatable control.

5.3 Pressure Profile Production

It was shown that a constant diastolic baseline pressure could be established, and a dynamic pressure profile superimposed upon the baseline pressure. At large systolic amplitudes it was shown that the pressure profile could be accurately produced as per the desired profile set in the GUI. Reducing the amplitude showed reduced measurement clarity due to significant DIPT transducer noise. The iterative reduction of the profile amplitude showed that the pressure profile retained its structure, but the signal-to-noise ratio became increasingly unfavourable. The pressure measurement eventually became an inconclusive indication of the pressure profile at physiological systolic-diastolic pressure ratios. This result was not surprising since, with reference to Section 3.5.3.1, it was shown that the DIPT transducer error was $\pm$11mmHg. This error was significant compared to the manufacturer-quoted error of $\pm$1mmHg; and for a systolic-diastolic pressure difference of 40mmHg, as in the common physiological occurrence, this error would be expected to encompass any and all undulations in the pressure profile. That said it does not negate that the actual pressure profile is in fact produced, but rather confirms that it cannot be measured accurately with the current signal noise levels present in the system.

With regards to the period of the produced pressure profile, it was chosen to assess the system performance with the ejection phase executed in 0.83s from initial peak to decay. This ejection period corresponds to the specified heart rate of 72bpm. In the current setup the intake phase was actuated between ejection phases and was considered not to be a part of the active profile production. For this reason, the delay between ejection periods was defined as the sum of the intake phase period and the duration of the internal LabVIEW code execution at the end of each cycle. Whilst the ejection profile was an accurate representation of the arterial pressure profile, the period of an entire cycle thus included the delay between ejection phases. This delay accounted for a 50% increase in the overall cycle frequency, thus reducing the overall frequency to 48bpm. It was decided that for diagnostic assessment of the current setup, it was a priority to ensure accurate pressure profile production, in the desired period of that profile, during the piston ejection phase; and that improvements to the overall period would constitute improvement of the intake phase actuation and optimization of the LabVIEW code execution.

As shown in Figure 48, the effect of the ejection check valve on the pressure profile was profound. The large pressure drop during valve closure and the resulting pressure wave reflection just after closure indicates that the check valve construction and behavior are candidates for improvement.

5.4 Flow Profile Production

Further impact of the system noise manifested as the inability to use the ultrasound flow transducer for dynamic flow measurement. Despite flow production being essential to produce the dynamic pressure profile, it was not required to characterize this flow other than to minimize reverse-flow in the system. Due to the sensitivity of the ultrasound transducer and the magnitude of the drive stepper motor EMI, the methods implemented to remove DIPT transducer noise were unsuccessful with regards to the flow transducer. Thus in order to quantify the flow profile as produced in the graft it is essential to reduce dramatically the flow transducer signal noise.

5.5 Validation of the System Design

The system specifications were established by the CVRU using the standards outlined by the Association for the Advancement of Medical Instrumentation (AAMI, 1994) as a guide. The AAMI standards stipulate the following specifications with respect to dynamic compliance testing:

- A reproducible dynamic pressure should be applied to the inside of a prosthesis
- The test sample and circulating fluid should be maintained at 37 ± 2°C
- Pressure measuring devices should be capable of measuring dynamic pressures up to 200mmHg with an accuracy of $\pm$ 2mmHg
- The test fluid should be distilled water, unless otherwise specified and justified
- The graft sample should be assessed under constant tension or at a fixed length

The developed flow loop simulator was shown to be capable of producing a reproducible dynamic pressure within a graft sample, and maintaining the fluid temperature with greater accuracy than required. Diagnostic testing of the system only considered heating of the graft sample, but it was shown that applying the same heating system to the upper reservoir would likewise maintain the circulating fluid temperature to within specification. The DIPT transducers exhibited a larger measurement range than required (300mmHg), and the manufacturer-quoted error/accuracy was deemed acceptable. However in the presence of EMI the accuracy fell short of the AAMI specifications with respect to providing a numerical output of the instantaneous pressure. The CVRU specified that the circulating fluid be phosphate buffered saline (PBS) and that the testing system also be capable of circulating glycerine solution. These requirements are specific to the CVRU and supersede the AAMI specifications in terms of more accurately replicating the mechanical properties of blood for more accurate testing of the graft samples. The developed flow loop simulator duly complies with these specifications and capabilities. The CVRU selected to test the graft samples at a fixed length with an applied strain. Adjustment of the graft pre-strain mount to a percentage of the graft length will apply the desired strain to the graft sample before testing and maintain the strain throughout the testing duration.

Chapter 6: Conclusions and Recommendations for Future Work

The desired outcome of the flow loop simulator project was to design and develop the rig to such a point where a synthetic vascular graft could be mounted and subjected to repeatable dynamic internal pressure profiles simulating the physiological pressure conditions in the arterial circulation. This objective has been achieved. Using the drive stepper motor and the developed LabVIEW algorithms, a digital pulse duplicator was developed whereby a wide range of customizable flow profiles can be produced in the flow loop. The software user interface enables simple redefinition of the desired profiles with mechanical adjustment of only the variable crank position, and without any mechanical redesign or manufacturing. This allows for configuration of a site-specific flow profile to replicate a physiological profile from any desired location throughout the arterial tree.

By adjusting the distal needle valve it was possible to set the graft internal pressure profile, corresponding to the flow profile contour, and manage the pressure amplitude with the needle valve setting. It was confirmed that decreasing the cross-sectional area of the flow path increased the pressure profile amplitude, thus laying the foundation for automated control of the needle valve systems. The motor actuation and resulting pressure profiles were shown to be repeatable.

The mechanical system was designed as modular to facilitate diagnostic testing throughout the design procedure, and to simplify any replacement or future modifications of the modular components. Additionally, the ergonomic design provides easy access to all user-adjustable mechanical components, with all other user input controlled from the GUI.

While the current setup is capable of producing the desired graft behaviour, some future work is required to improve the system and thus optimize it towards the final compliance measurement.

Currently only the fluid surrounding the graft is heated to 37°C. In order to also maintain the circulating fluid at the required temperature it is recommended that a second set of the heating apparatus is interfaced with the upper reservoir. This will facilitate full AAMI compliance with regards to temperature control of the graft as well as the circulating fluid.

Having shown that elevating a reservoir performs as desired with regards to the production of the diastolic baseline pressure, the manufactured upper reservoir assembly can be located as designed in Figure 8. A lower reservoir can then be manufactured to take its place on the lower level of the rig. Elevating the upper reservoir assembly would also allow for integration of the needle valves and remove the tube clamp configuration. The current setup involves manual adjustment of tube clamps instead of the intended digital control of the needle valves. Interfacing the needle valves with LabVIEW to provide digital control of the proximal and distal gate positions would enable the user to control the entire rig from the computer, with the exception of adjusting the crank radius. Further work could employ the characteristic curves, established to control the obstructed tube cross-sectional area by changing the needle valve gate position, in order to implement a higher level of computer control by automating the selection of the optimal gate positions for the desired pressure profile.

It is evident from previous discussion that EMI-related noise was the dominant cause of the measurement system inaccuracy. A strong recommendation would be to further curtail the EMI with hardware before attempting any software filtering or transducer replacement. While it is not a trivial task, sufficient removal of the EMI would dramatically increase the pressure transducer accuracy and provide a more useable numerical output for use with the future graft diameter measurement system. Additionally, EMI removal would possibly allow for the flow measurement system to be incorporated into the user interface for higher level diagnostics on graft behaviour during testing.

Secondary recommendations to improve the measurement accuracy would be to consider using industrial pressure sensors that have well-described performance. At this time it is not possible to comment on the level of EMI rejection of industrial pressure transducers, and the cost may well be prohibitive depending on the project budget.

Improvements can indeed be made to the system operation in order to more accurately represent a physiological pressure profile. Primarily, this concerns minimizing the delay between the profile ejection phases. This could be achieved by optimizing the LabVIEW code to minimize the computational delays, or using a more powerful computer to execute the existing code more quickly. Furthermore, the existing profile structure could be modified to incorporate the intake

phase during what is currently the decay phase of the ejection profile. This would have an impact on the pressure profile integrity, but would serve to remove the delay required for intake of fluid for subsequent ejection phases and hence iterate ejection phases in quicker succession.

Without modifying the current ejection and intake behaviour, the produced pressure profiles may be improved by optimising the design of the check valves in the valve stage. Considering the complexity of the physiological tricuspid valve, and the approximation thereof that was used in the valve stage, it is clear that there is room for improvement of the check valves. Areas of focus would be to reduce the cracking pressure and time required to close the valves, as well as to optimize the valve leaflet design in order to prevent small reverse flow when closed.

Additional mechanical improvements may be incorporated in the manufacture of subsequent graft adapters by incorporating a metal-head Luer needle as opposed to the plastic-head needle used in the current design for pressure measurements. This would significantly improve the robustness of the connection at the attachment point of the pressure tubing. Improved rigidity would also be an effect of the modification as it would allow for soldering of the needle closer to the head, thus producing a shorter member with smaller lever action and reducing the risk of bending due to careless operation.

The mounting procedure of the graft adapters could be made more ergonomic by removing the need to disassemble the O-ring flanges in the lower reservoir walls for each mounting. This could be achieved by rounding the circumference of the hypodermic tubing, to yield a smoother edge that is less likely to cut into the O-ring seals. Additionally, a mounting tool could be manufactured such that it expands the O-ring seal, while mounted in the reservoir flange, beyond the outer diameter of the hypodermic tubing, thus reducing contact as the hypodermic tubing is passed through the O-ring seal.

To extend the ergonomics of the GUI, a selection of profiles at various positions of the arterial tree could be introduced as a group of presets. Thus the user would not be required to programme a custom profile for each graft test, but would instead be able to select easily a profile from the preset group.

By implementing the above recommendations it is believed that the system performance will be improved to a sufficient level whereby a suitable dynamic pressure profile and numerical output may be obtained from the existing system. Interfacing the resulting system with a diameter measurement system of suitable specification would in all likelihood provide sufficient data for accurate and reproducible compliance measurement.

References

Binu, S., V. P. Mahadevan Pillai, et al. (2007). "Fibre Optic Displacement Sensor for the Measurement of Amplitude and Frequency of Vibration." Optics and Laser Technology **39**(8): 1537-1543.

Brant, A. M., J. F. Chmielewski, et al. (1986). "Simulation in vitro of Pulsatile Vascular Hemodynamics Using a CAD/CAM-designed Cam Disc and Roller Follower." Artificial Organs **10**(5): 419-421.

Charara, J., J. Ruel, et al. (1999). "Development of a Flow Simulator to Study Haemodynamic Behaviour of Natural and Artificial Blood Vessels Under Physiologic Flow Conditions." Journal of Medical Engineering & Technology **23**(3): 83 - 95.

Chuong, C. J. and Y. C. Fung (1983). "Three-Dimensional Stress Distribution in Arteries." Journal of Biomechanical Engineering **105**(3): 268-274.

Cinthio, M., A. R. Ahlgren, et al. (2005). "Evaluation of an Ultrasonic Echo-tracking Method for Measurements of Arterial Wall Movements in Two Dimensions." Ultrasonics, Ferroelectrics and Frequency Control, IEEE Transactions on **52**(8): 1300-1311.

Conti, J. C. (1990). Dynamic Vascular Compliance Tester, Dynatek Laboratories, Inc.

Conti, J. C. and E. R. Strope (2002). "Radial Compliance of Natural and Mock Arteries: How this Property Defines the Cyclic Loading of Deployed Vascular Stents." Biomed Sci Instrum **38**: 163-72.

Conti, J. C., E. R. Strope, et al. (1998). "Sources of Error in Monitoring High Speed Testing of Vascular Grafts." Biomedical Sciences Instrumentation **24**: 240-245.

Conti, J. C., E. R. Strope, et al. (1997). "Frequency Dependant Radial Compliance of Latex Tubing." Biomedical Science Instrumentation **33**: 524-529.

Dynatek MP3 Pulse Duplicator. http://www.dynatekdalta.com/products.htm, Dynatek Dalta.

Dynatek PVAD: Pulsatile Ventricular Assist Device. http://www.dynatekdalta.com/products.htm, Dynatek Dalta.

Elcam (2008). "DIPT: Disposable Integrated Pressure Transducer." **1**(1): 2.

Fung, E. b. C., Ed. (1966). Biomechanics, Proceedings of a Symposium sponsored by the Applied Mechanics Division of the ASME, at the Annual Meeting.

Greisler, H. P., K. A. Joyce, et al. (1992). "Spatial and Temporal Changes in Compliance Following Implantation of Bioresorbable Vascular Grafts." Journal of Biomedical Materials Research **26**(11): 1449-1461.

Holdsworth, D. W., D. W. Rickey, et al. (1991). "Computer-controlled Positive Displacement Pump for Physiological Flow Simulation." Medical and Biological Engineering and Computing **29**(6): 565-570.

Kok, D. J., K. P. Wolffenbuttel, et al. (2000). "Changes in Bladder Contractility and Compliance due to Urethral Obstruction: A Longitudinal Followup of Guinea Pigs." The Journal of Urology **164**(3P2): 1021-1025.

Law, Y., R. Cobbold, et al. (1987). "Computer-controlled Pulsatile Pump System for Physiological Flow Simulation." Medical and Biological Engineering and Computing **25**(5): 590-595.

Learoyd, B. M. and M. G. Taylor (1966). "Alterations with Age in the Viscoelastic Properties of Human Arterial Walls." Circulation Research **18**(3): 278-292.

Li, S., W. N. McDicken, et al. (1993). "Blood Vessel Diameter Measurement by Ultrasound." Physiological Measurement **14**: 291-297.

Meister, J.-J., Y. Tardy, et al. (1992). "Non-invasive Method for the Assessment of Non-linear Elastic Properties and Stress of Forearm Arteries in vivo." Journal of Hypertension **10**(6): S23-S26.

Mills, C. J., I. T. Gabe, et al. (1970). "Pressure-flow Relationships and Vascular Impedance in Man." Cardiovascular Res., 4:405-417.

Murgo, J. P., R. H. Cox, et al. (1971). "Cantilever Transducer for Continuous Measurement of Arterial Diameter in vivo." Journal of Applied Physiology **31**(6): 948-953.

National (2009). High-speed M Series Multifuntional DAQ for USB.

Normann, N. A. (1977). Balloon Activated Blood Pump, Baylor College of Medicine, Houston, Texas.

Omega. (2009). "Introduction to Ultrasonic Doppler Flow Meters." from http://www.omega.com/prodinfo/ultrasonicflowmeters.html.

Pampel, M., G. Pampel, et al. (2007). Dynamic Thickness Correction, Aluminium Norf GmbH, Neuss(DE).

Peterson, R. C., R. Tu, et al. (1990). "Dynamic Internal Compliance Measurements of Fresh and Fixed Artery." ASAIO Trans **36**(3): M766-9.

Qian, K. X. (1996). "Pulsatile Impeller Heart: A Viable Alternative to a Problematic Diaphragm Heart." Medical Engineering and Physics **18**(1): 57-66.

Rosenson, R. S., S. Shott, et al. (2002). "Hypertriglyceridemia is associated with an elevated blood viscosity Rosenson: triglycerides and blood viscosity." Atherosclerosis **161**(2): 433-439.

Runge, T. M. (1994). Blood Conduit for Pulsatile Cardiopulmonary Bypass Pump.

Seifalian, A. M., A. Giudiceandrea, et al. (1999). Noncompliance: The silent acceptance of a villain, In: Tissue Engineering of Vascular Grafts. P. Zilla and H. P. Greisler. Austin, Texas, Landes Co.**:** 47-58.

Tardy, Y., J. J. Meister, et al. (1991). "Non-invasive Estimate of the Mechanical Properties of Peripheral Arteries from Ultrasonic and Photoplethysmographic Measurements." Clin Phys Physiol Meas **12**(1): 39-54.

Werneck, M. M., N. B. Jones, et al. (1984). "Flexible Hydraulic Simulator for Cardiovascular Studies." Medical & Biological Engineering & Computing **22**(1): 86-89.

West, J. E. (1996). Infinitely Variable Pneumatic Pulsatile Pump.

White, R. A., S. R. Klein, et al. (1986). "Maintenance of Compliance in a Small Diameter Arterial Prosthesis." Transactions - American Society for Artificial Internal Organs **32**.

Wright, G. (1997). "Mechanical Simulation of Cardiac Function by Means of Pulsatile Blood Pumps." Journal of Cardiothoracic Vascular Anesthesia **11**(3): 299-309.

Yeoman, M. S. (2004). The Design and Optimisation of Fabric Reinforced Porous Prosthetic Grafts Using Finite Element Methods and Genetic Algorithms. Mechanical Engineering. Cape Town, University of Cape Town. **Doctor of Philosophy (Mechanical Engineering):** 200.

Appendix A: Code Segments

Profile Generator Graphical User Interface:

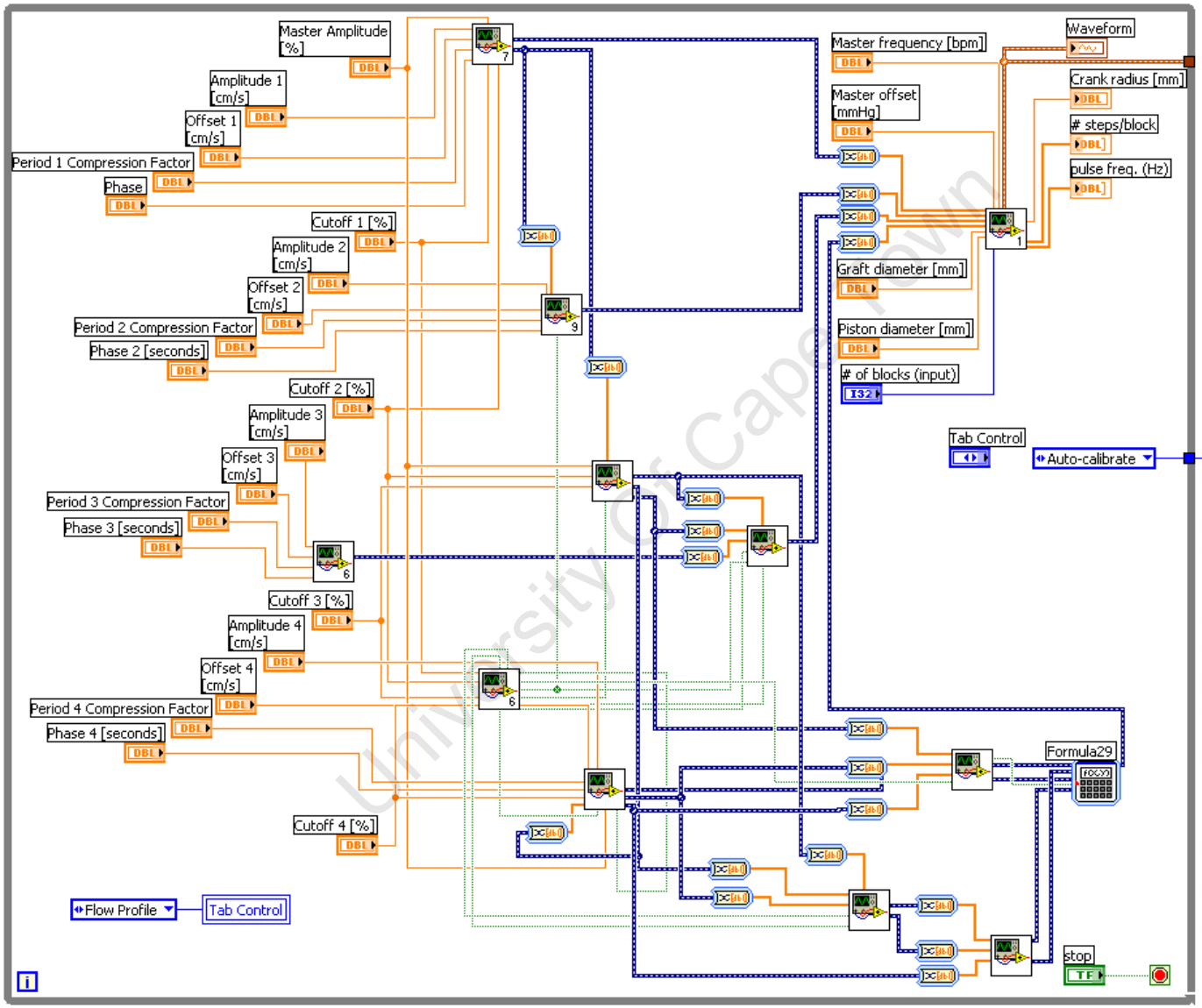

Profile Conversion Algorithm:

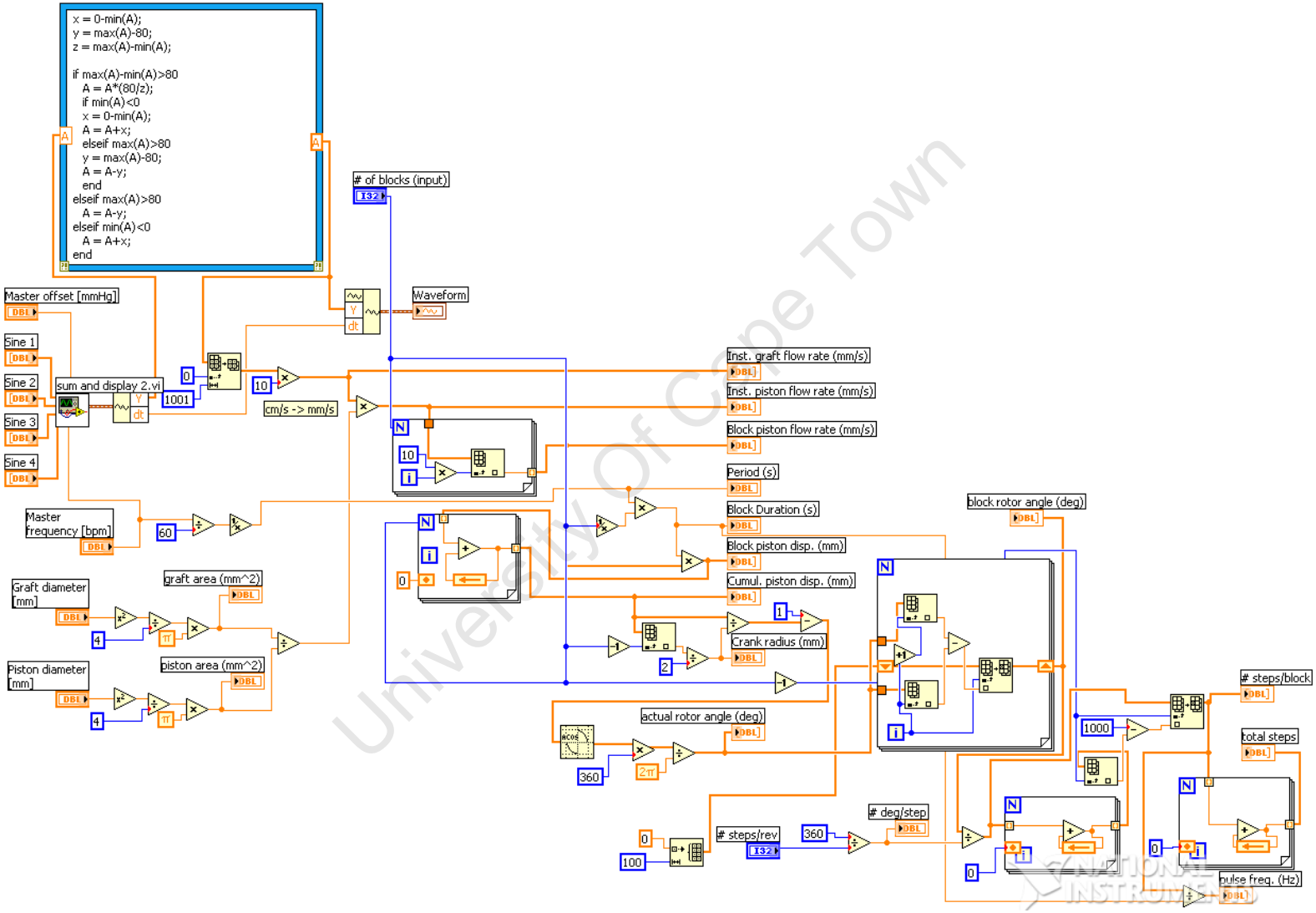

Profile Output Sequence:

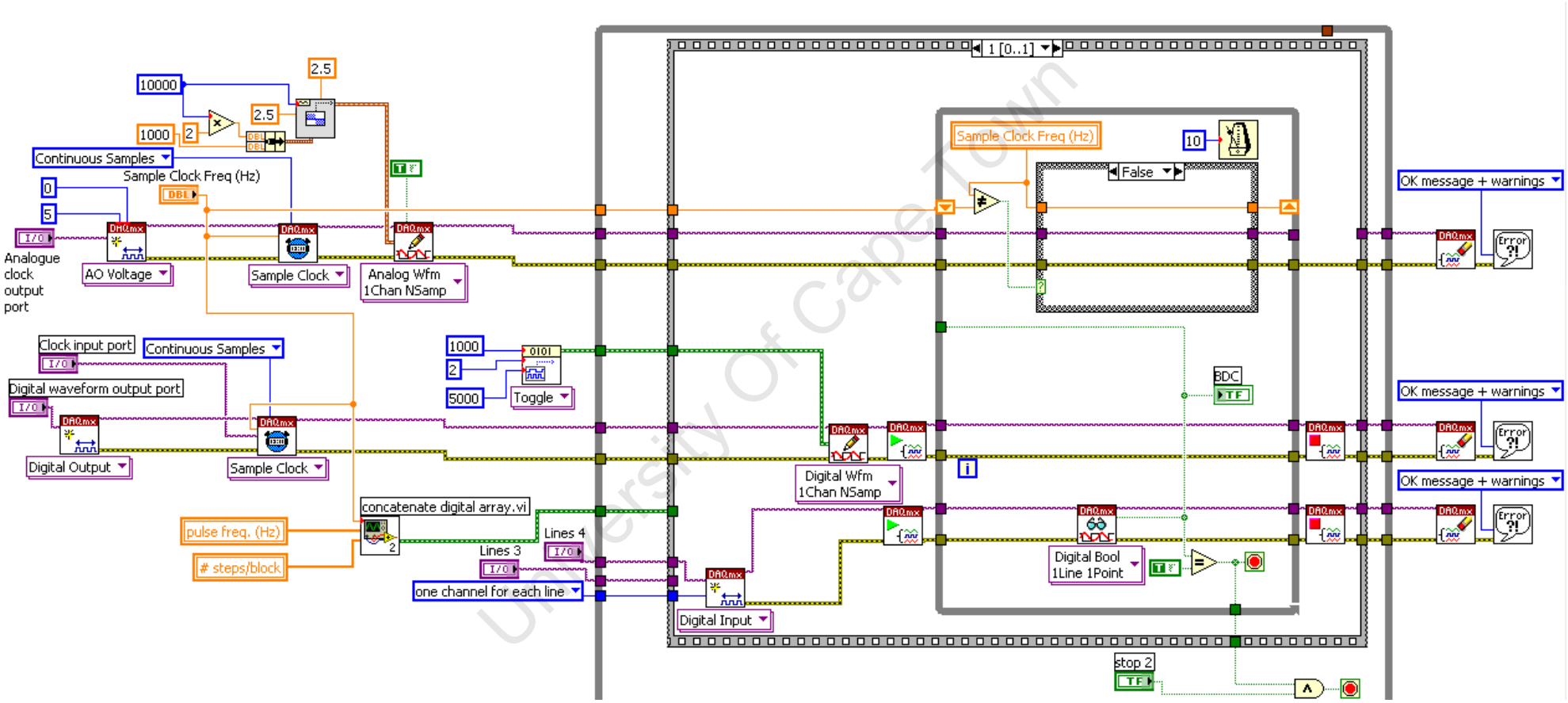

Appendix B: Parts Drawings

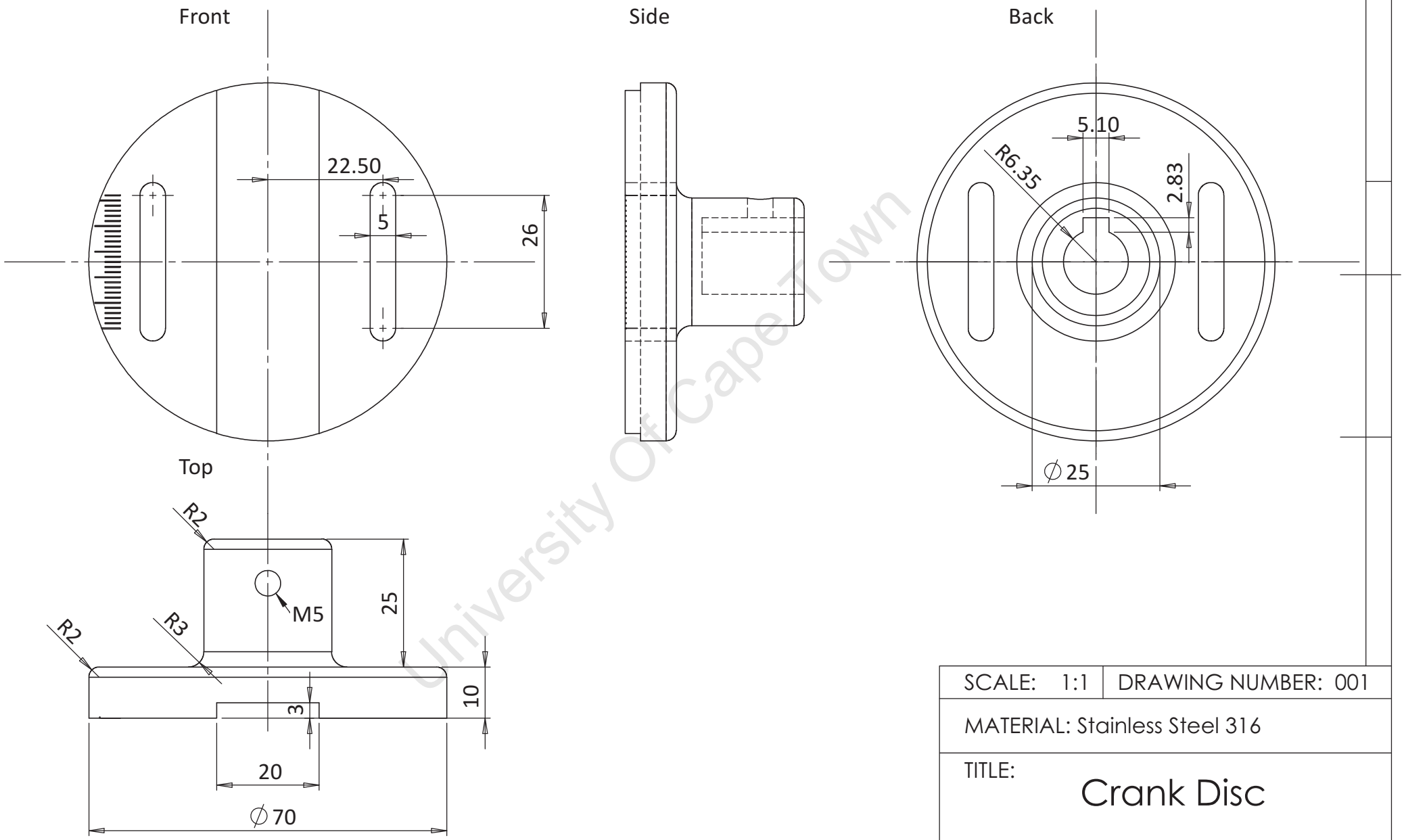

SCALE: 1:1	DRAWING NUMBER: 001
MATERIAL: Stainless Steel 316	
TITLE: Crank Disc	
AUTHOR: Jordi Reddy	
DATE:	June 2009

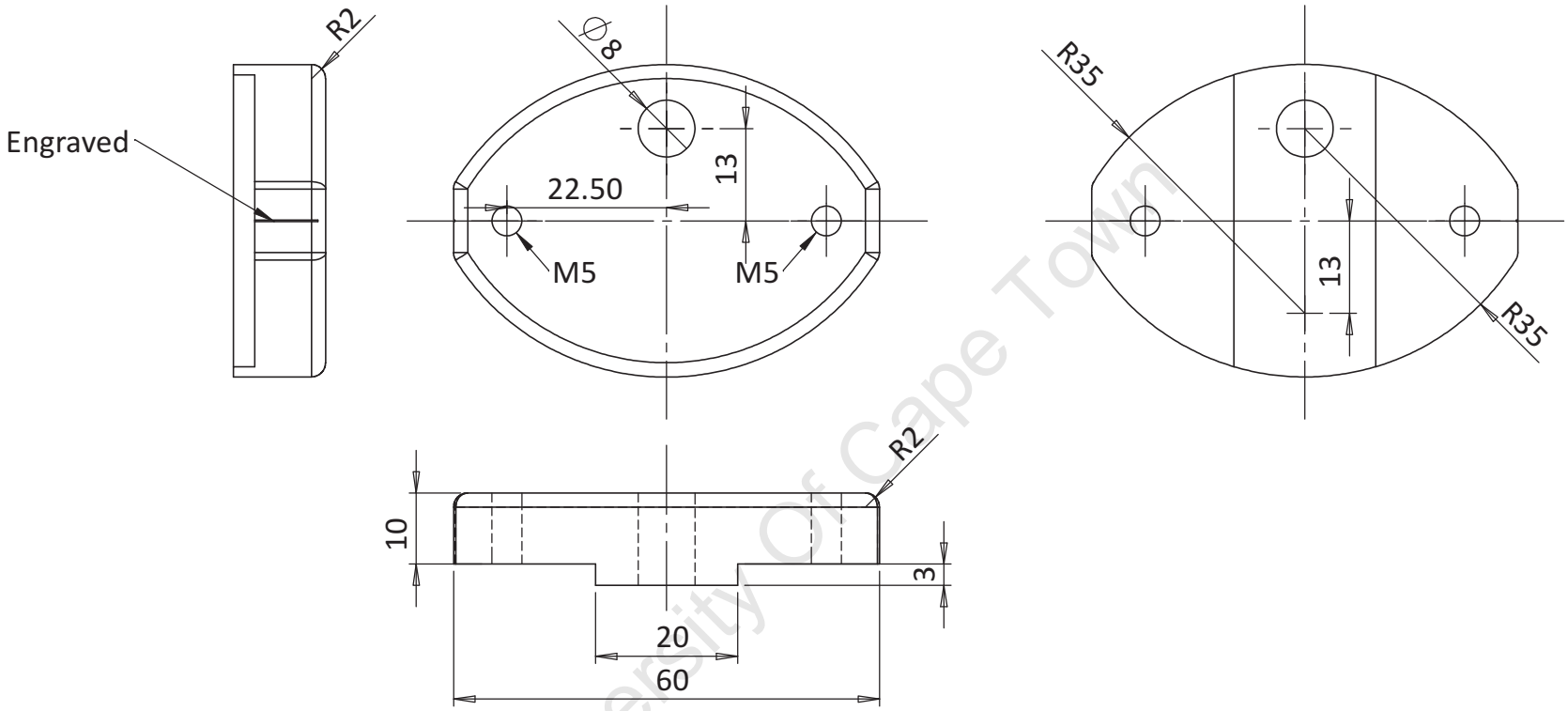

SCALE: 1:1	DRAWING NUMBER: 002
MATERIAL: Stainless Steel 316	
TITLE: Crank Slider	
AUTHOR: Jordi Reddy	
DATE:	June 2009

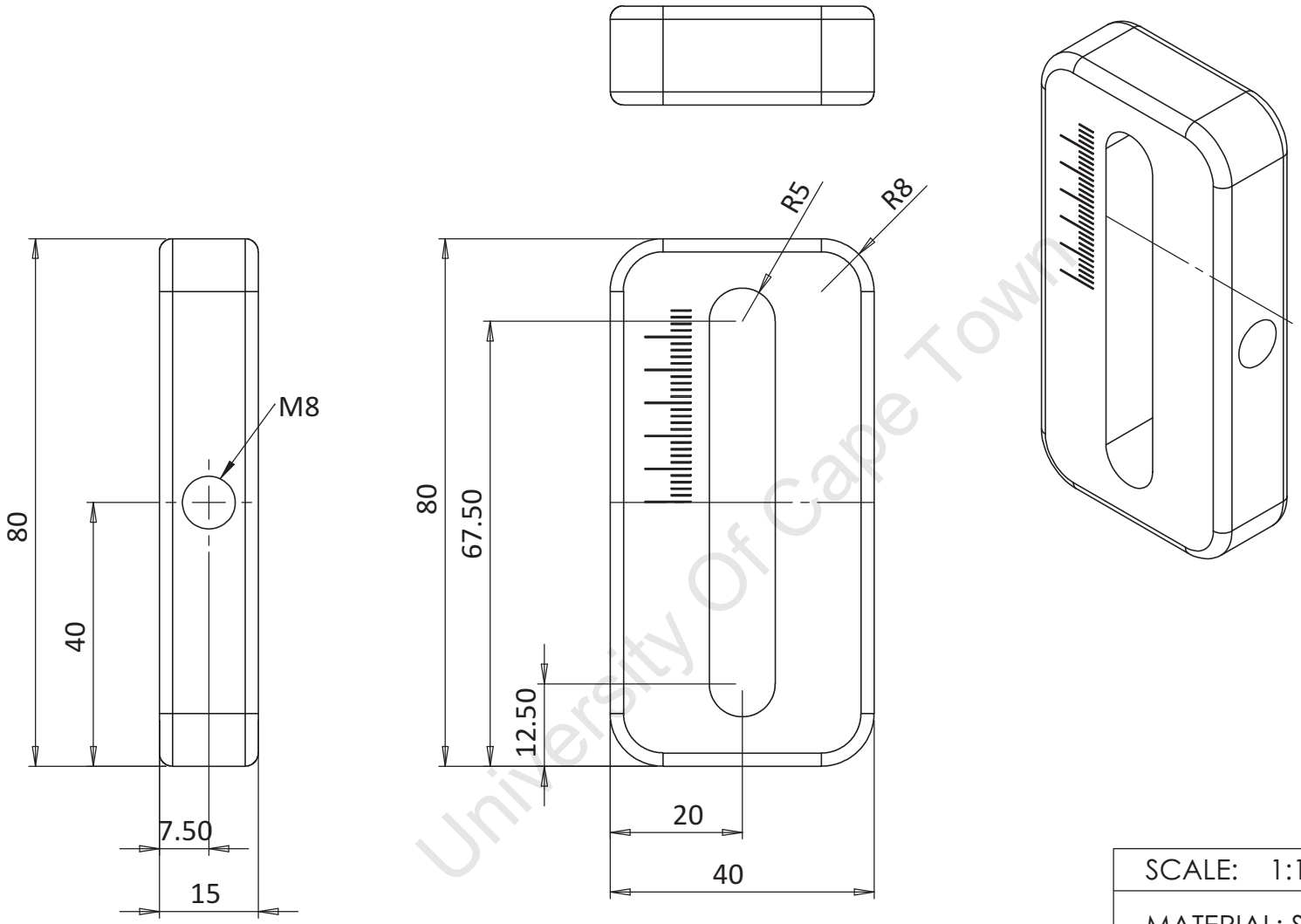

SCALE: 1:1	DRAWING NUMBER: 003
MATERIAL: Stainless Steel 316	
TITLE: Scotch Yoke Body	
AUTHOR: Jordi Reddy	
DATE:	June 2009

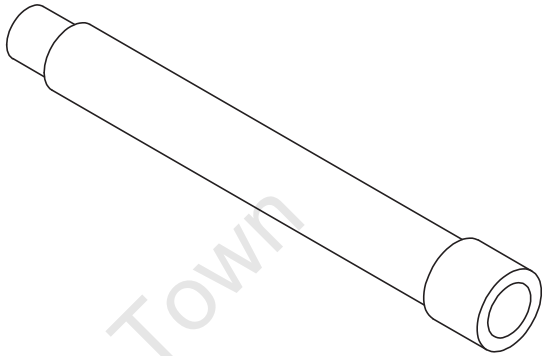

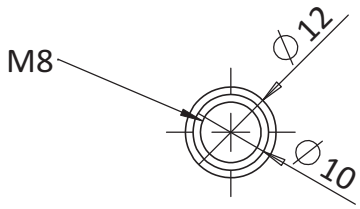

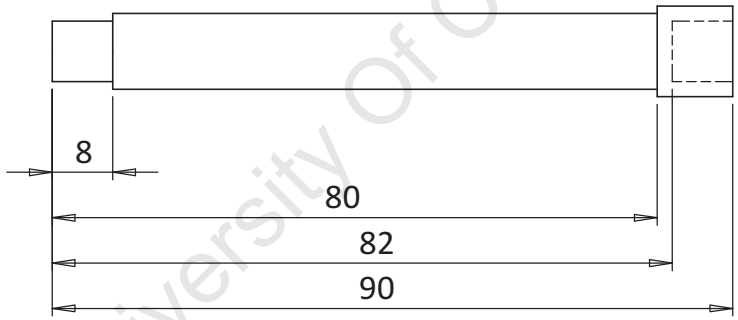

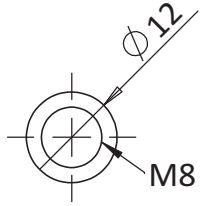

SCALE: 1:1	DRAWING NUMBER: 004
MATERIAL: Stainless Steel 316	
TITLE: Scotch Yoke Pushrod	
AUTHOR: Jordi Reddy	
DATE:	June 2009

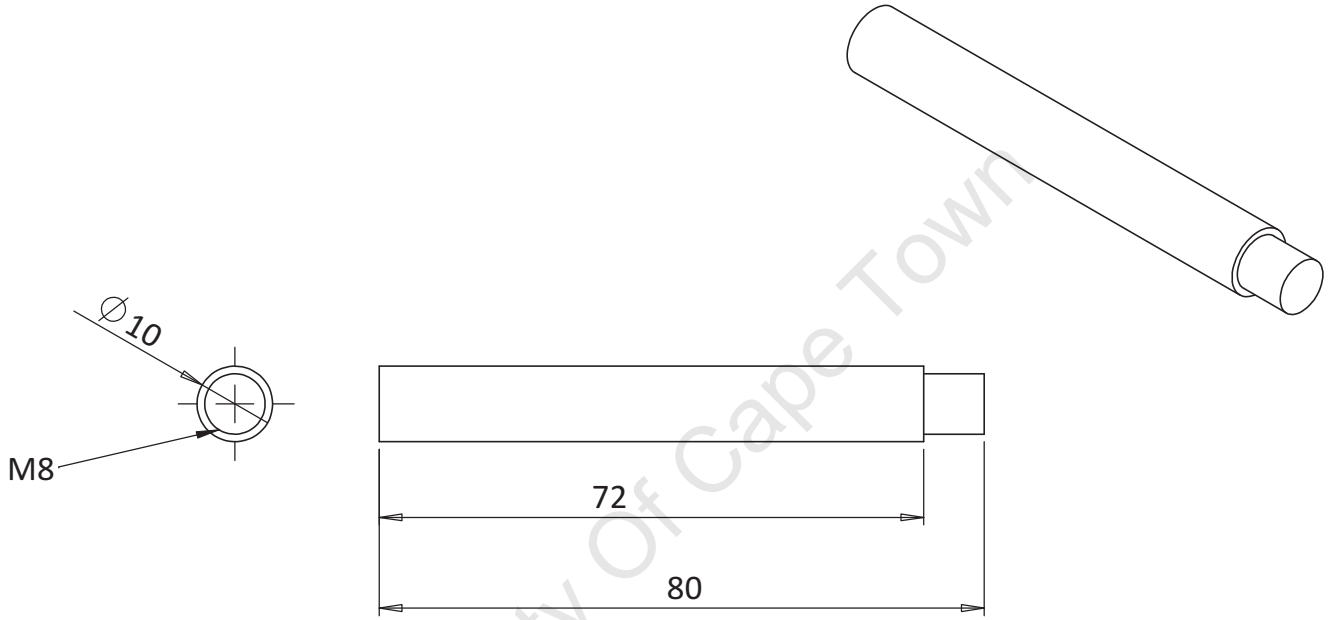

SCALE: 1:1	DRAWING NUMBER: 005
MATERIAL: Stainless Steel 316	
TITLE: Scotch Yoke Stabilizer	
AUTHOR: Jordi Reddy	
DATE:	June 2009

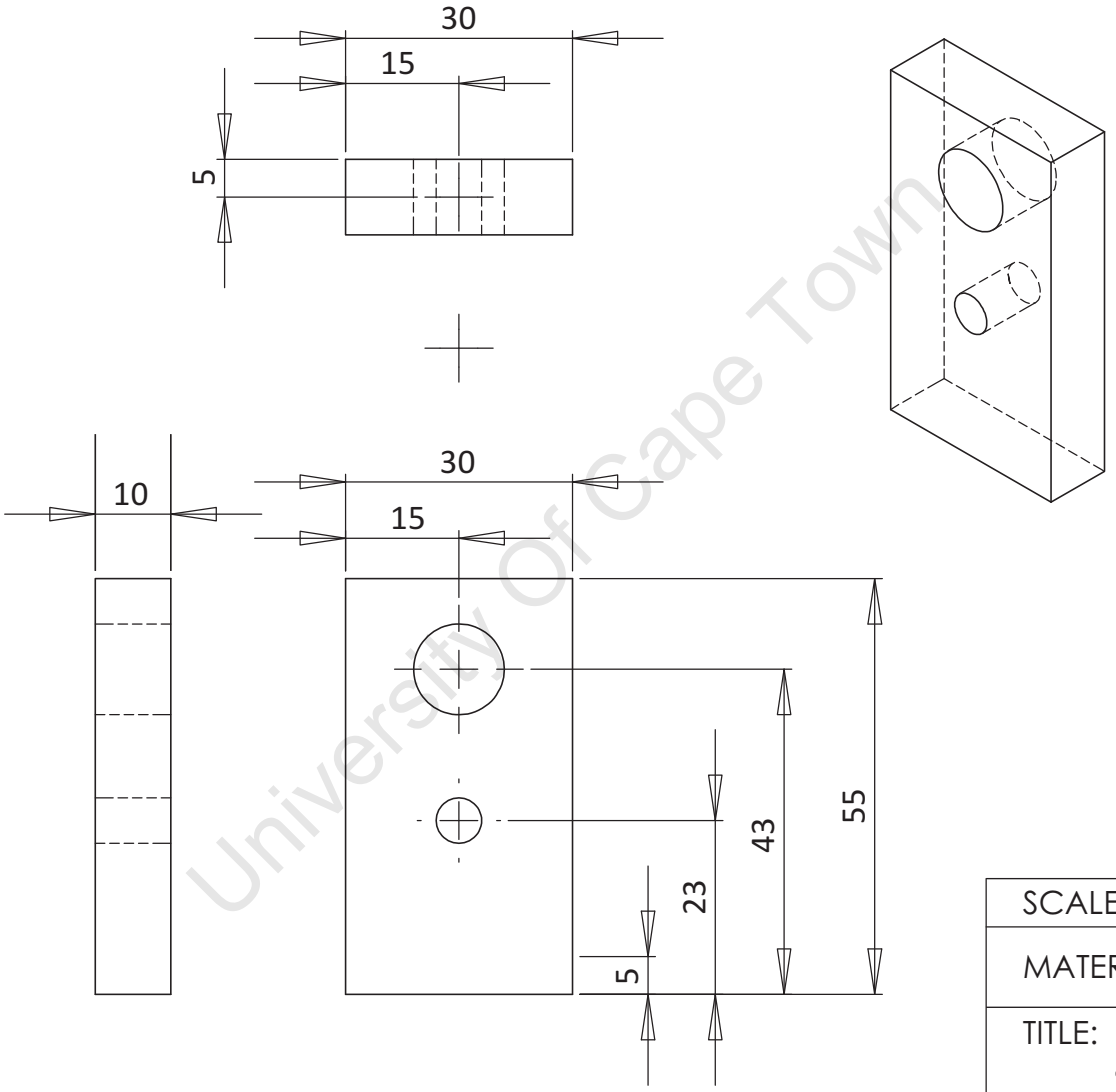

SCALE: 1:1	DRAWING NUMBER: 006
MATERIAL: Aluminium	
TITLE: Scotch Yoke Mount	
AUTHOR: Jordi Reddy	
DATE:	June 2009

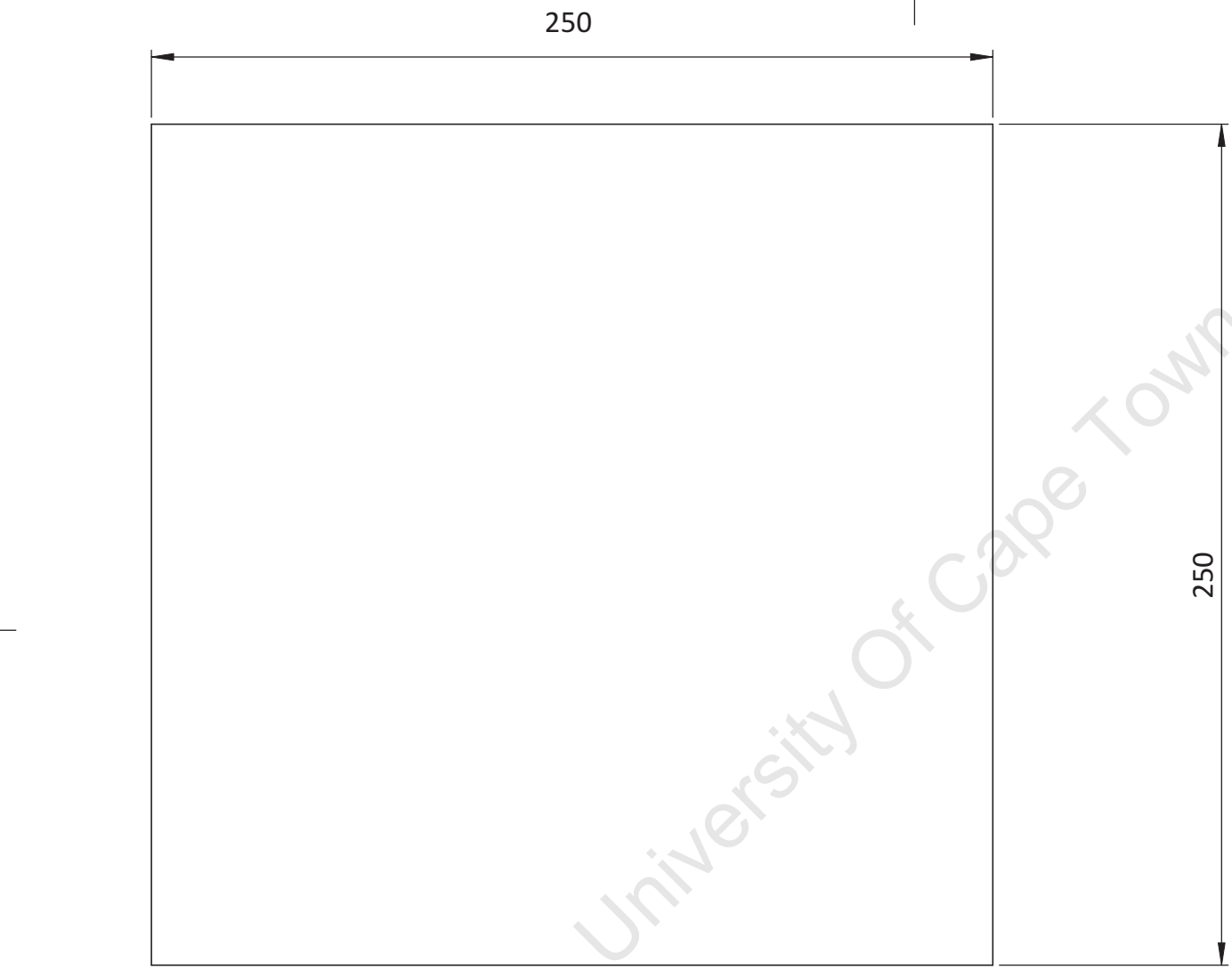

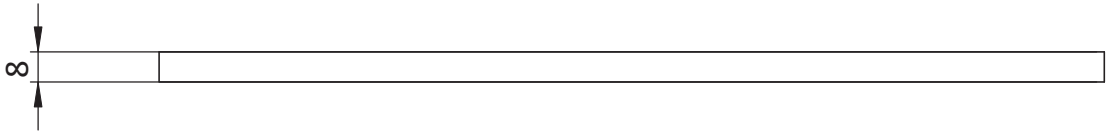

SCALE: 1:2	DRAWING NUMBER: 007
MATERIAL: Aluminium	
TITLE: Pump Base Plate	
AUTHOR: Jordi Reddy	
DATE:	June 2009

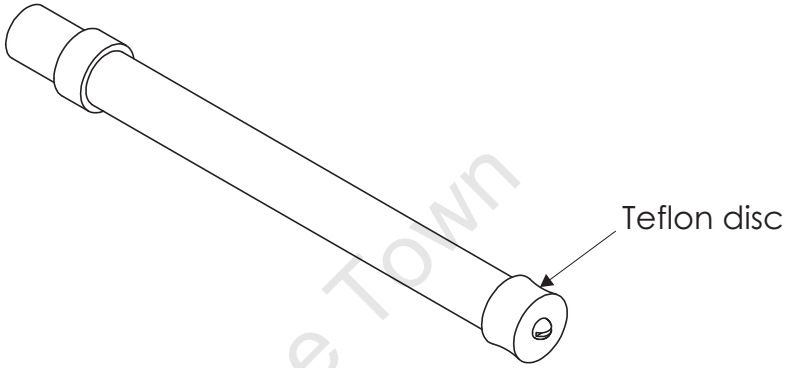

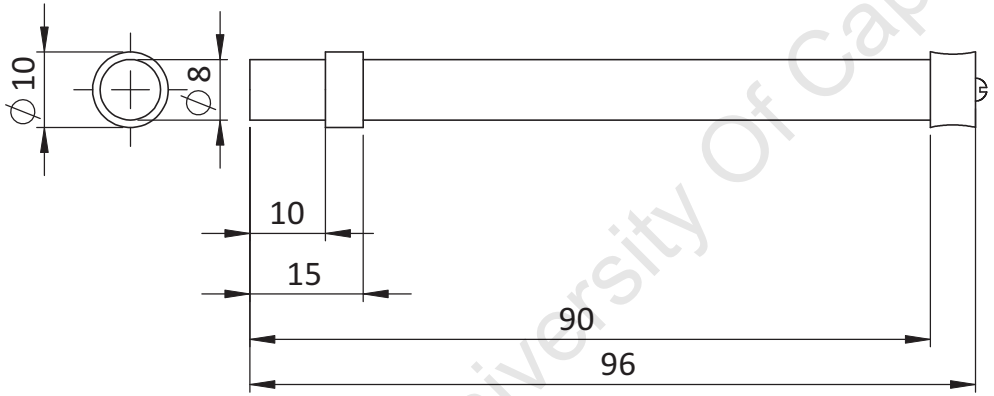

SCALE: 1:1	DRAWING NUMBER: 008
MATERIAL: Stainless Steel 316	
TITLE: Piston Plunger	
AUTHOR: Jordi Reddy	
DATE:	June 2009

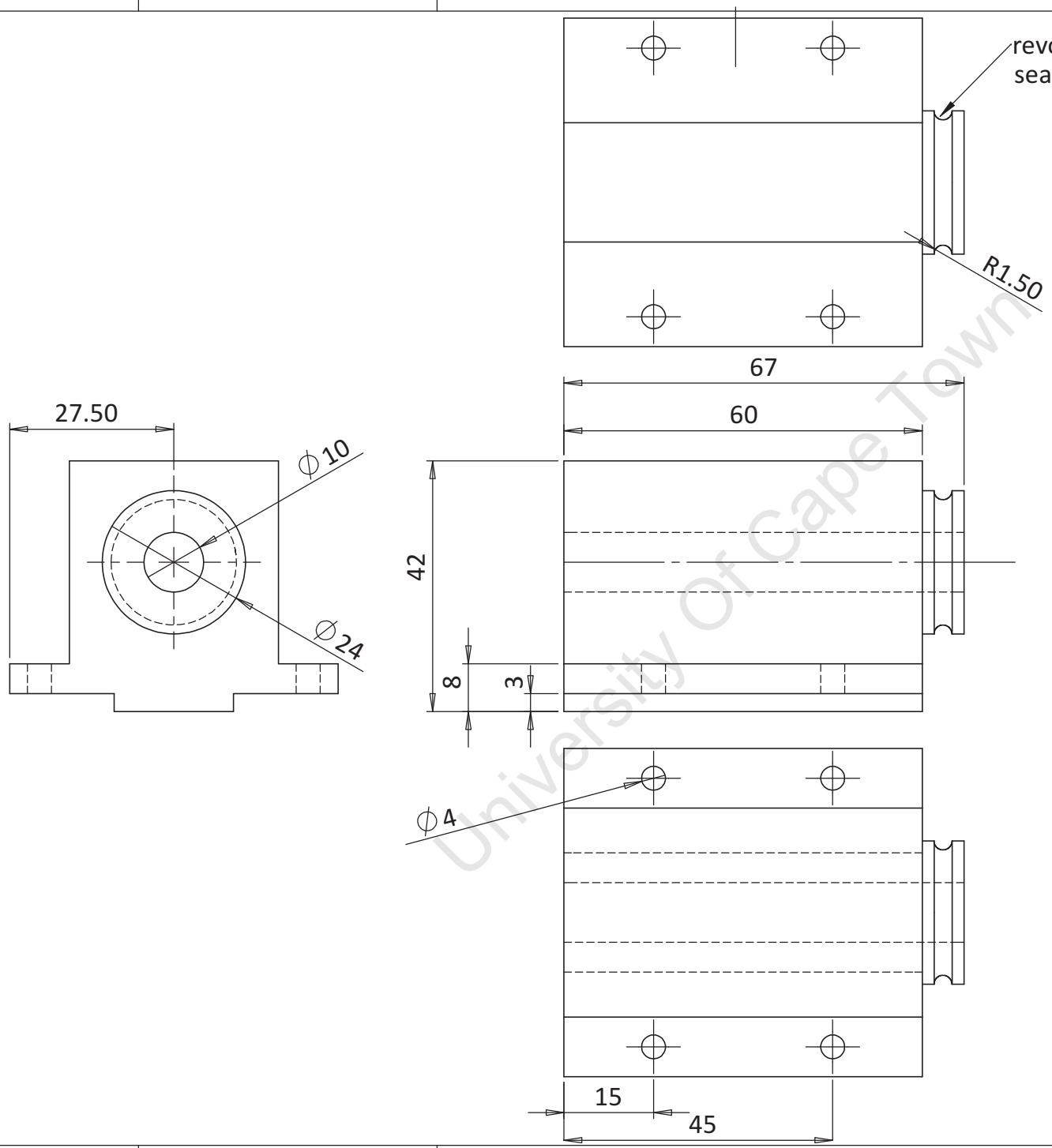

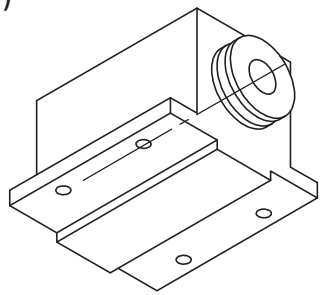

SCALE: 1:1	DRAWING NUMBER: 009
MATERIAL: Perspex	
TITLE: Piston Cylinder	
AUTHOR: Jordi Reddy	
DATE:	June 2009

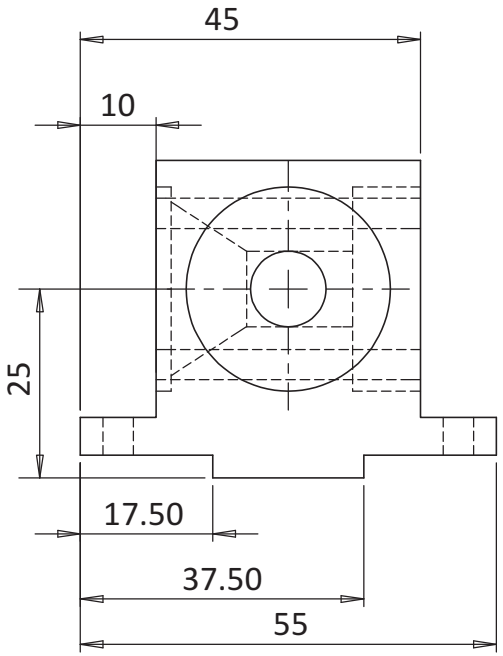

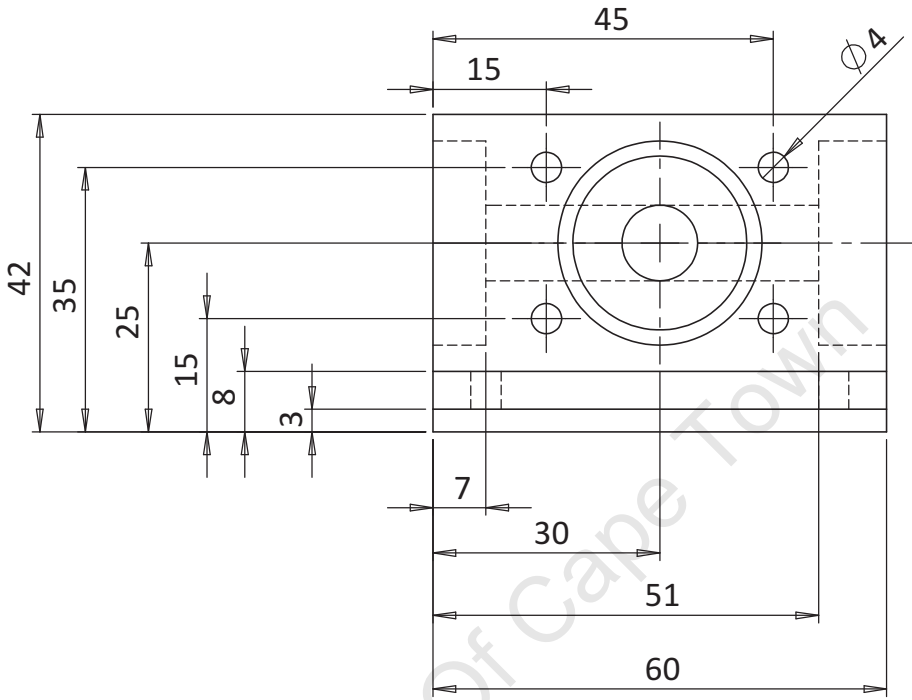

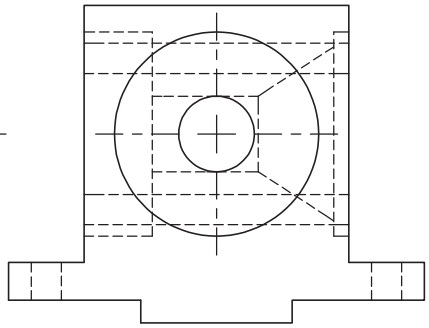

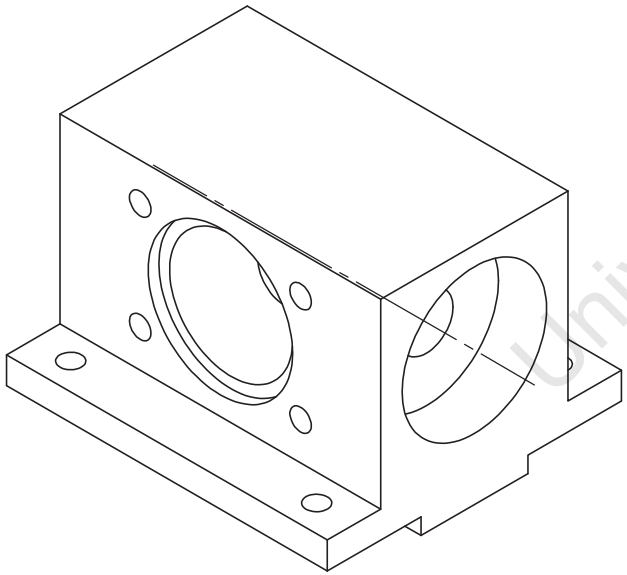

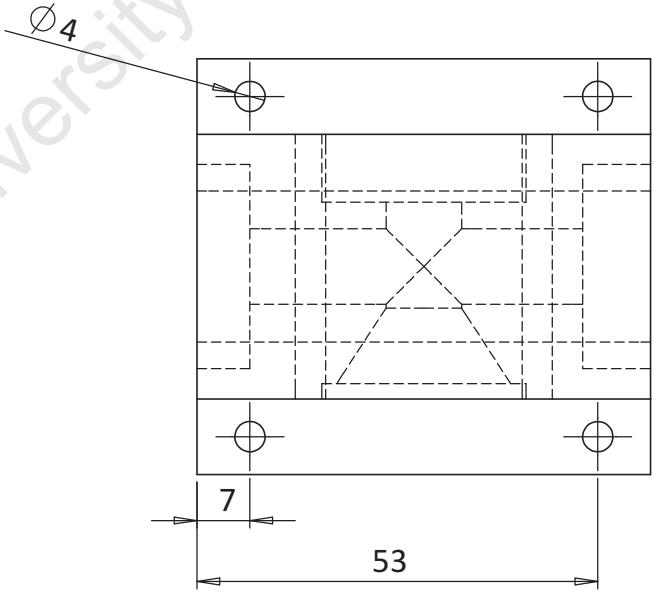

SCALE: 1:1	DRAWING NUMBER: 010
MATERIAL: Perspex	
TITLE: Valve Stage Body	
AUTHOR: Jordi Reddy	
DATE:	June 2009

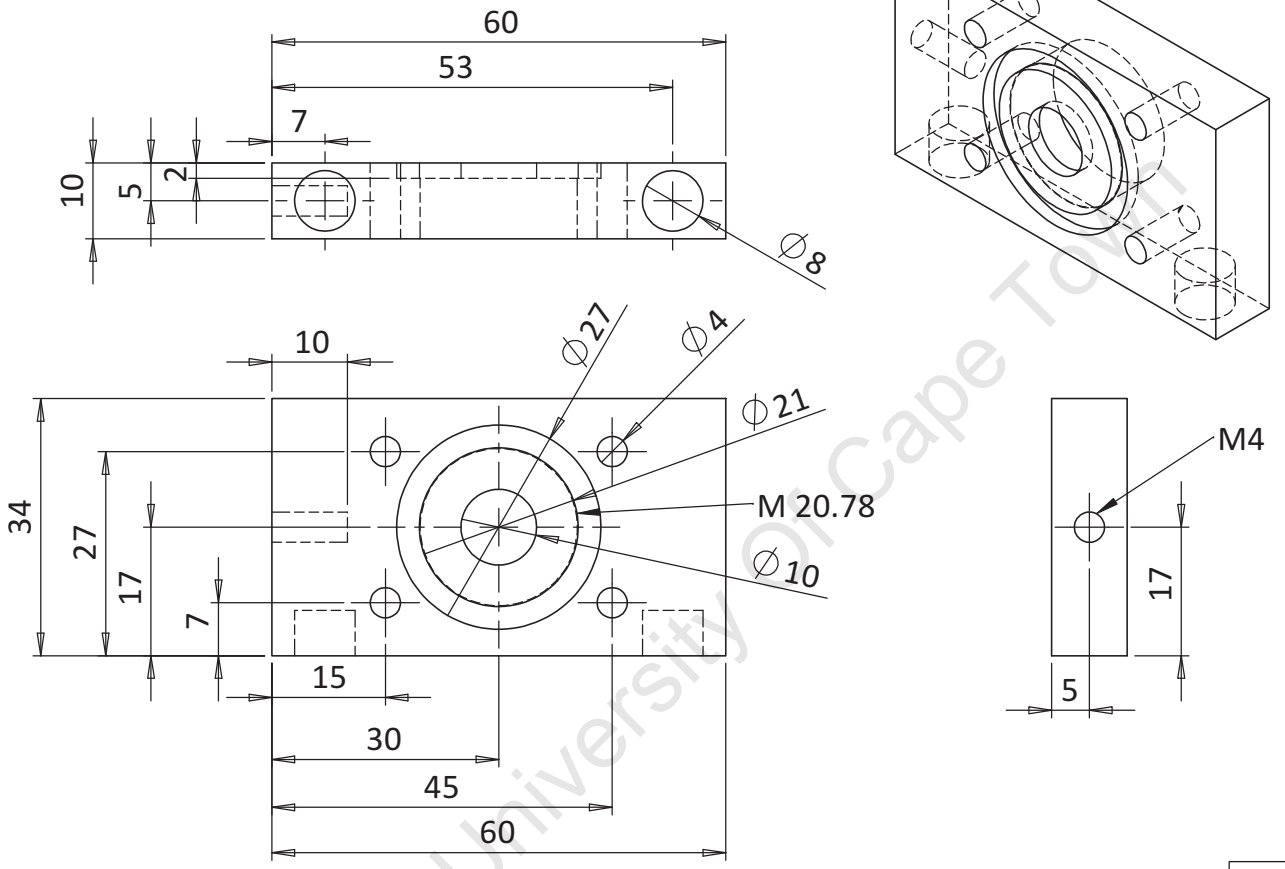

SCALE: 1:1	DRAWING NUMBER: 011
MATERIAL: Perspex	
TITLE: Valve Stage Intake	
AUTHOR: Jordi Reddy	
DATE:	June 2009

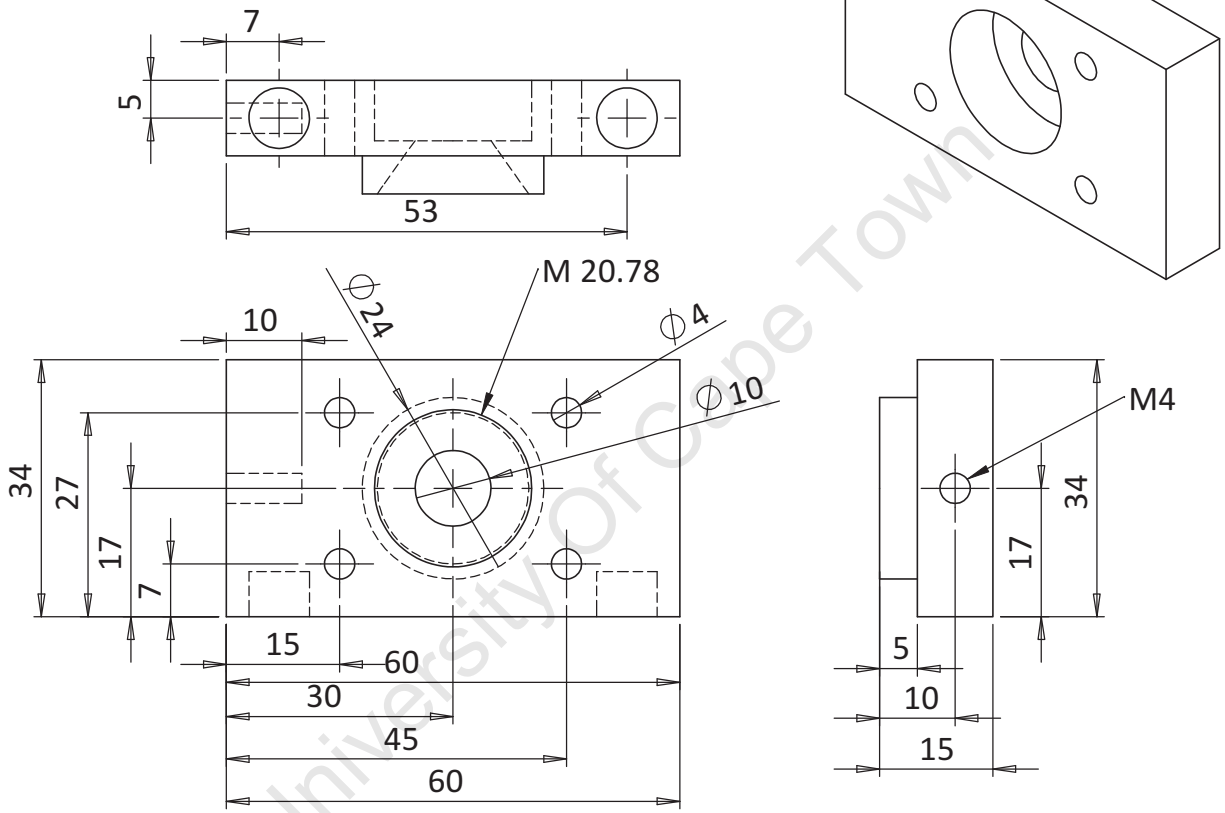

SCALE: 1:1	DRAWING NUMBER: 012
MATERIAL: Perspex	
TITLE: Valve Stage Bypass	
AUTHOR: Jordi Reddy	
DATE:	June 2009

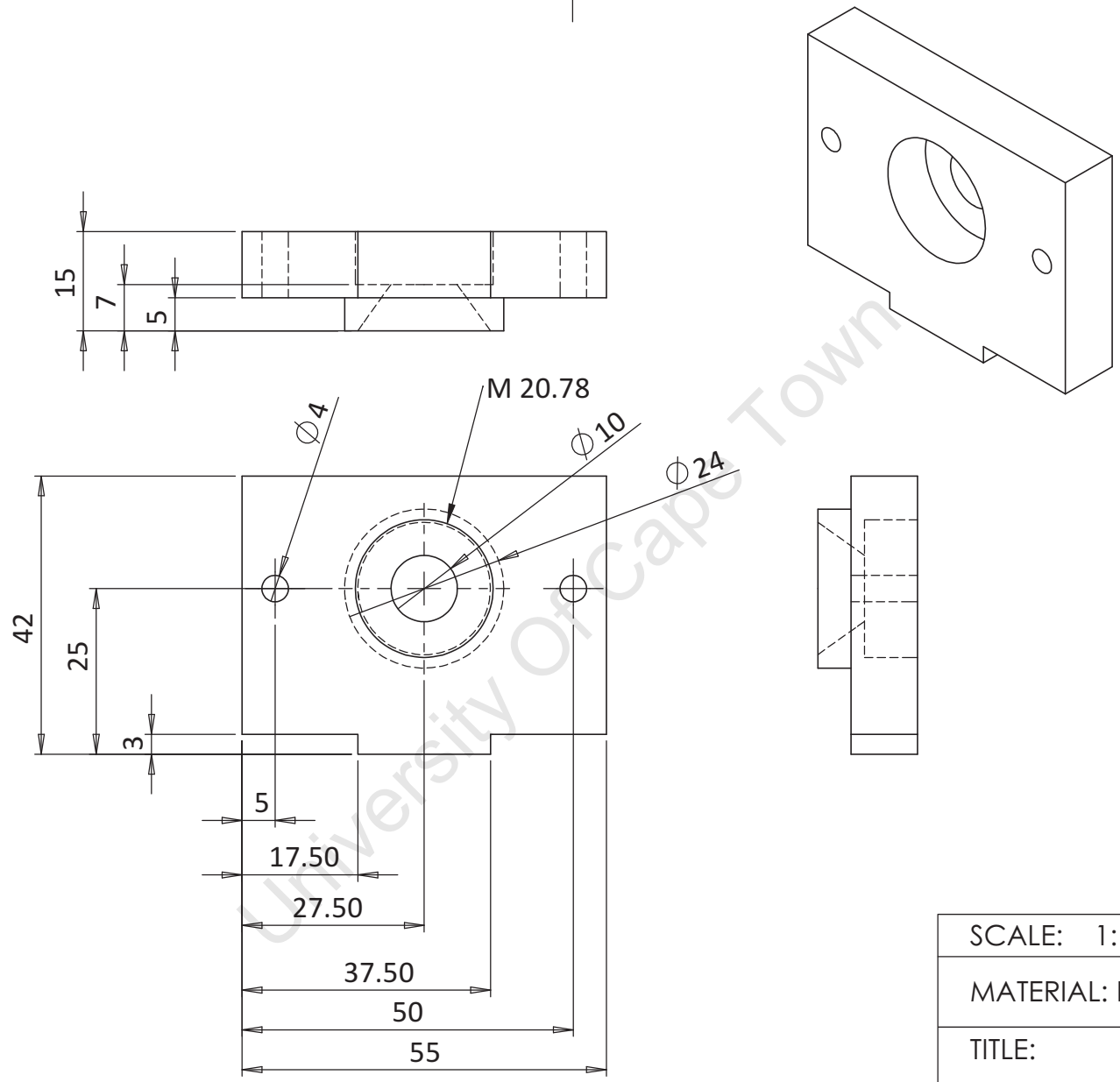

SCALE: 1:1	DRAWING NUMBER: 013
MATERIAL: Perspex	
TITLE: Valve Stage Eject	
AUTHOR: Jordi Reddy	
DATE:	June 2009

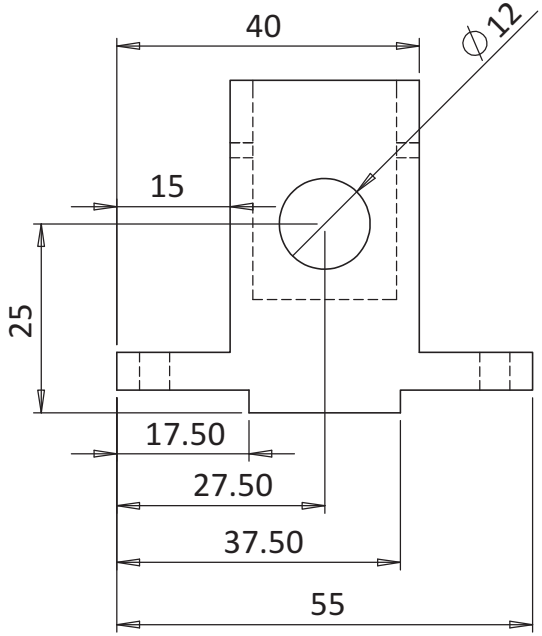

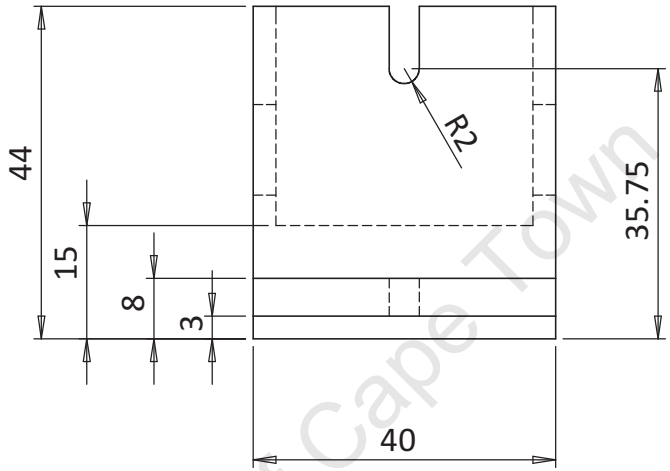

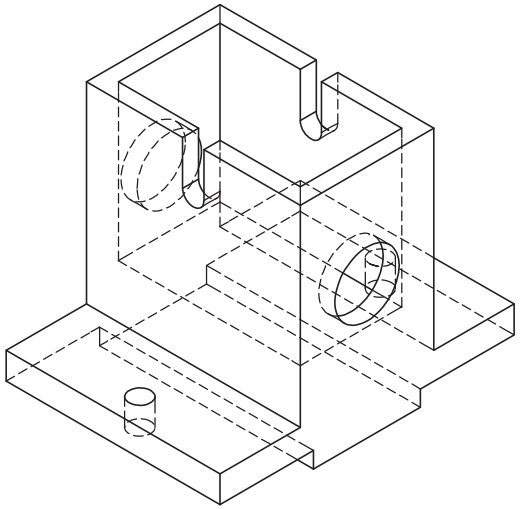

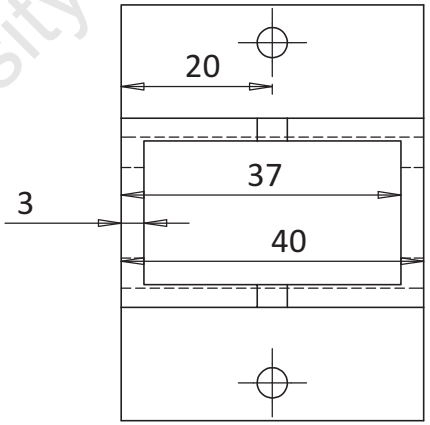

SCALE: 1:1	DRAWING NUMBER: 014
MATERIAL: Perspex	
TITLE: Flow Probe Mount	
AUTHOR: Jordi Reddy	
DATE:	June 2009

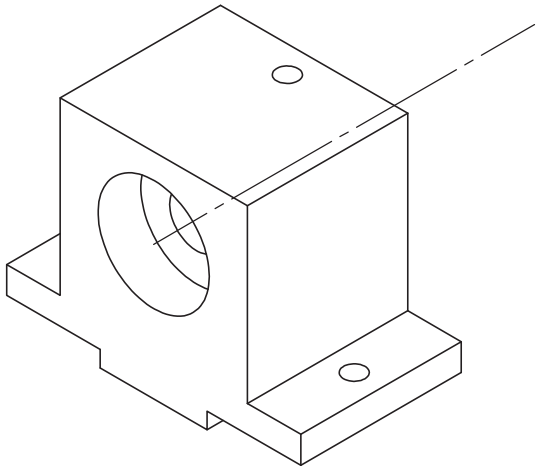

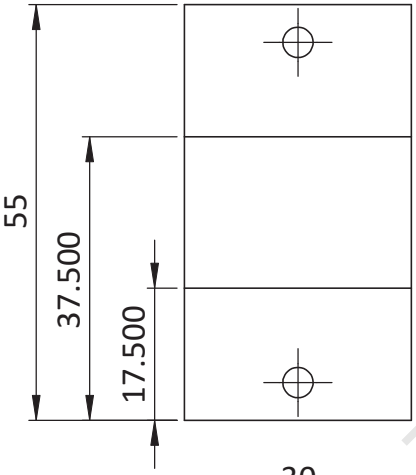

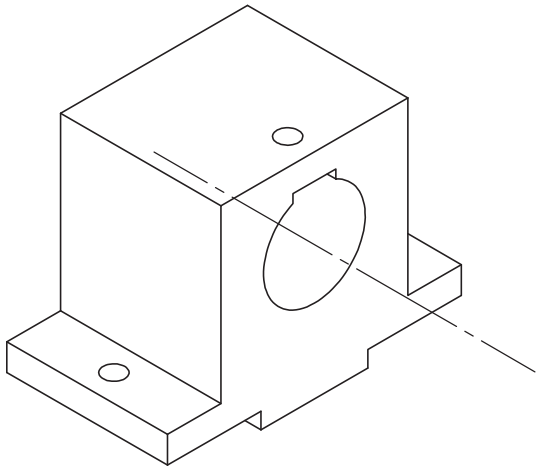

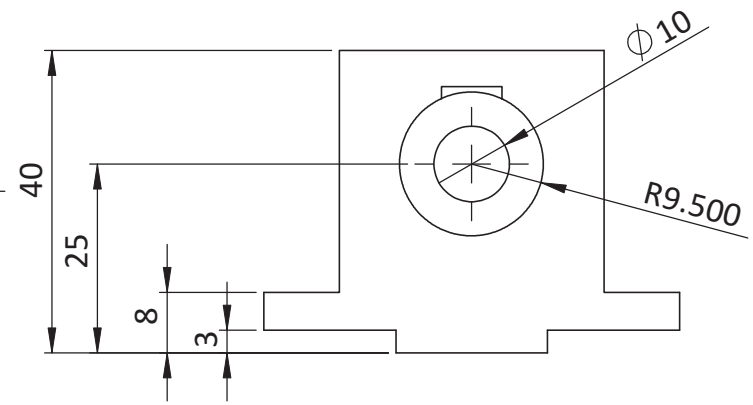

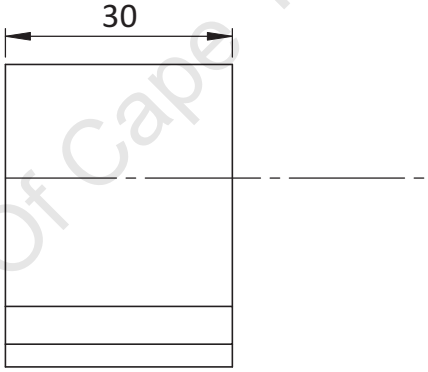

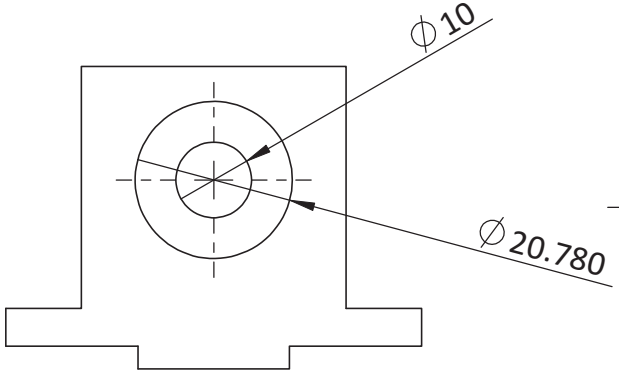

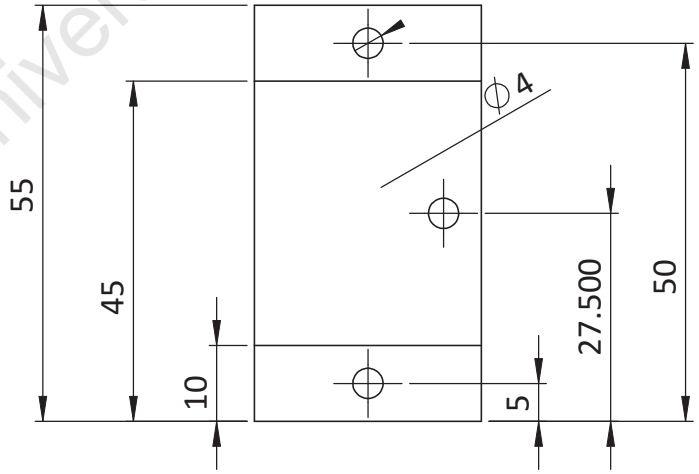

SCALE: 1:1	DRAWING NUMBER: 015
MATERIAL: Stainless Steel 316	
TITLE: Proximal Graft Adapter Mount	
AUTHOR: Jordi Reddy	
DATE:	June 2009

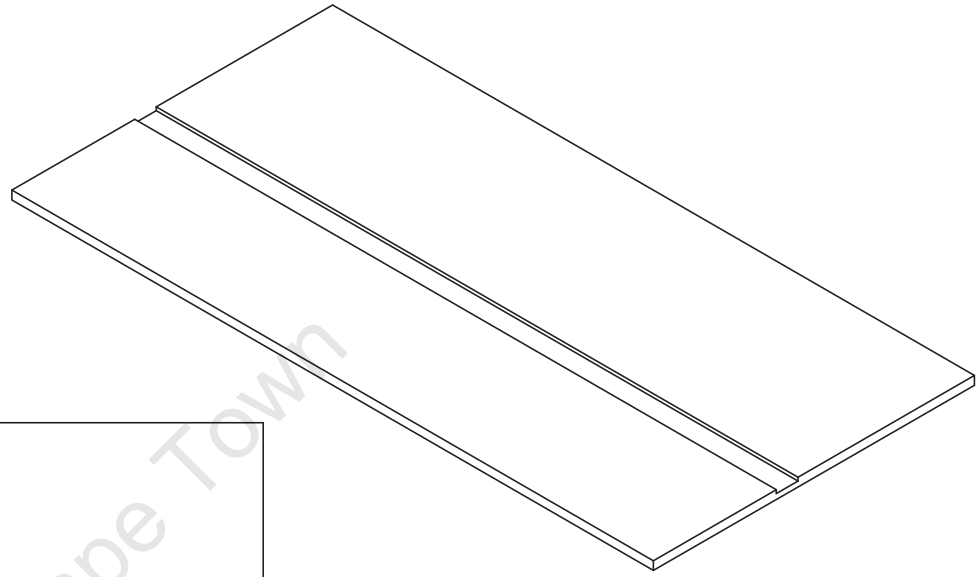

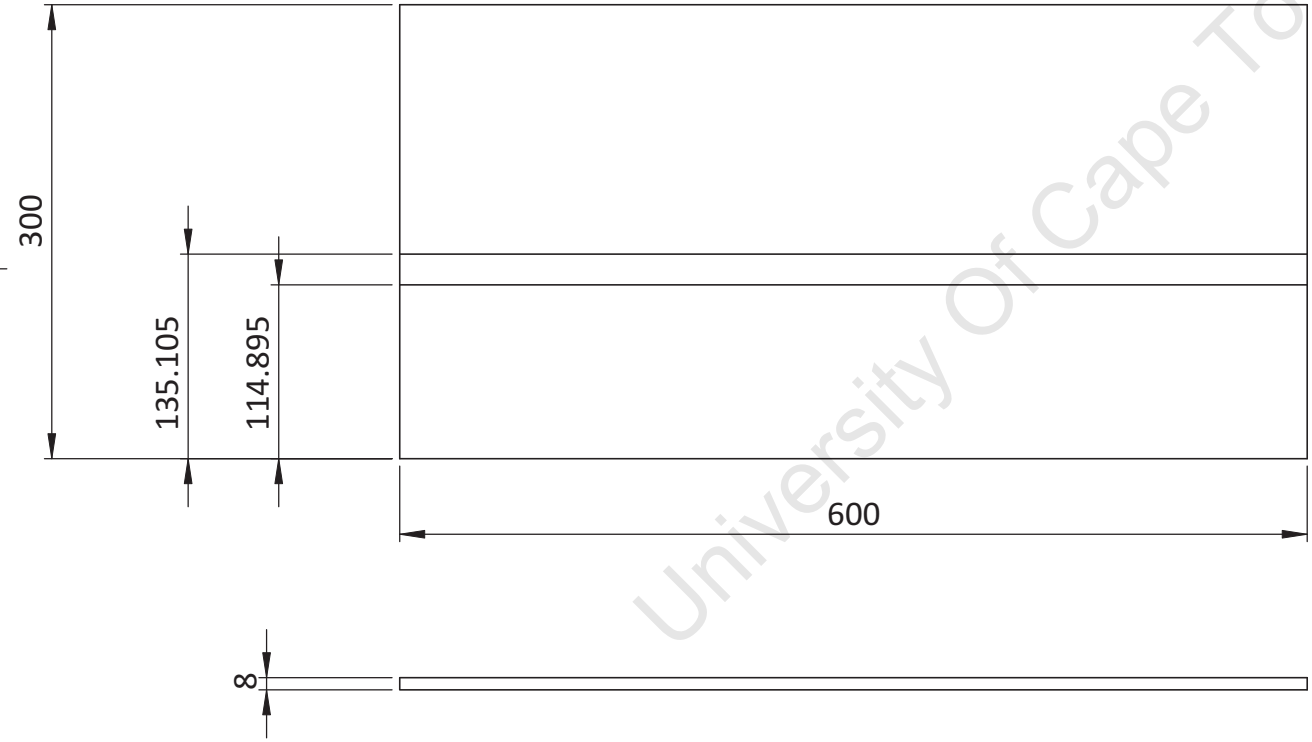

SCALE: 1:5	DRAWING NUMBER: 016
MATERIAL: Aluminium	
TITLE: Flow Base Plate	
AUTHOR: Jordi Reddy	
DATE:	June 2009

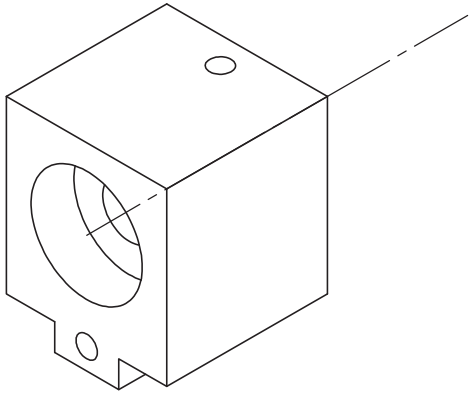

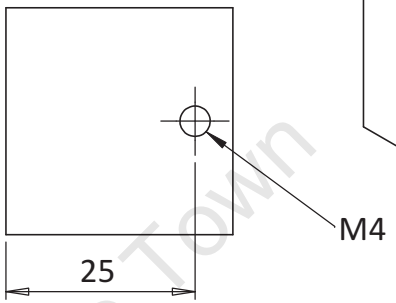

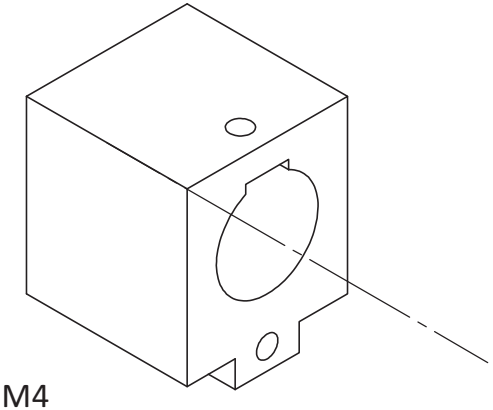

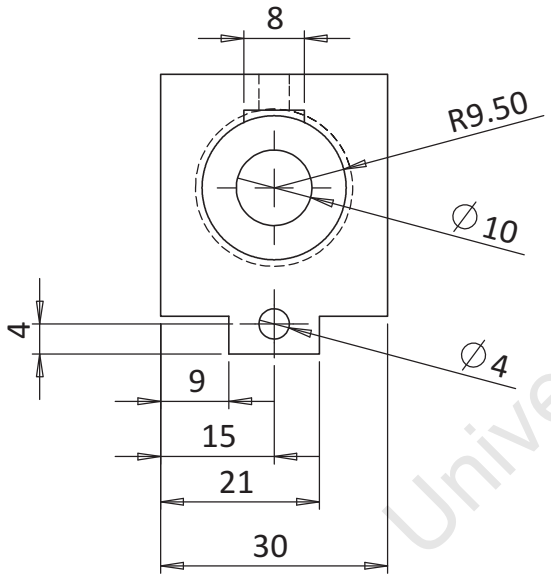

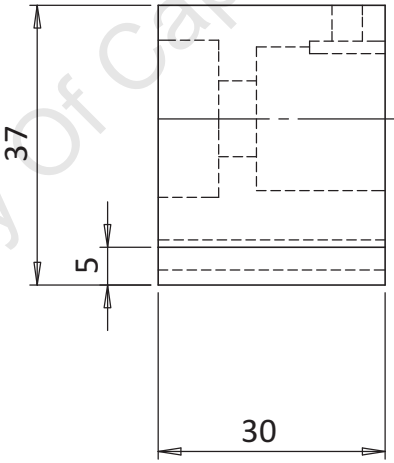

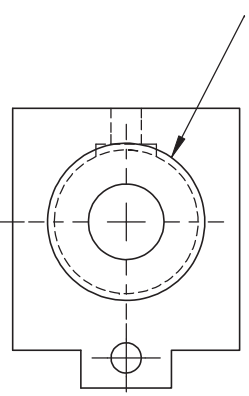

SCALE: 1:1	DRAWING NUMBER: 017
MATERIAL: Stainless Steel 316	
TITLE: Distal Graft Adapter Mount	
AUTHOR: Jordi Reddy	
DATE:	June 2009

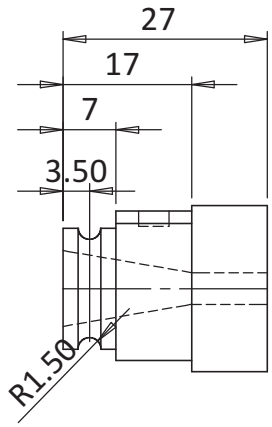

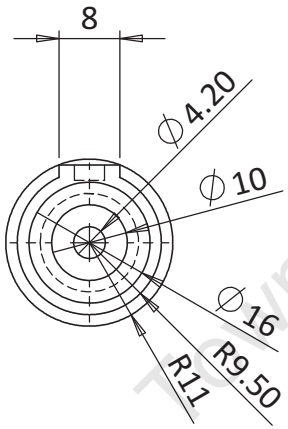

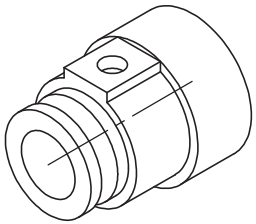

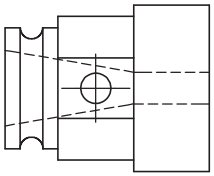

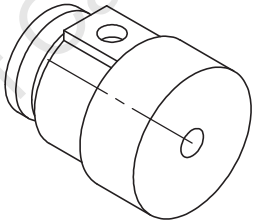

SCALE: 1:1	DRAWING NUMBER: 018
MATERIAL: Stainless Steel 316	
TITLE: Graft Adapter	
AUTHOR: Jordi Reddy	
DATE:	June 2009

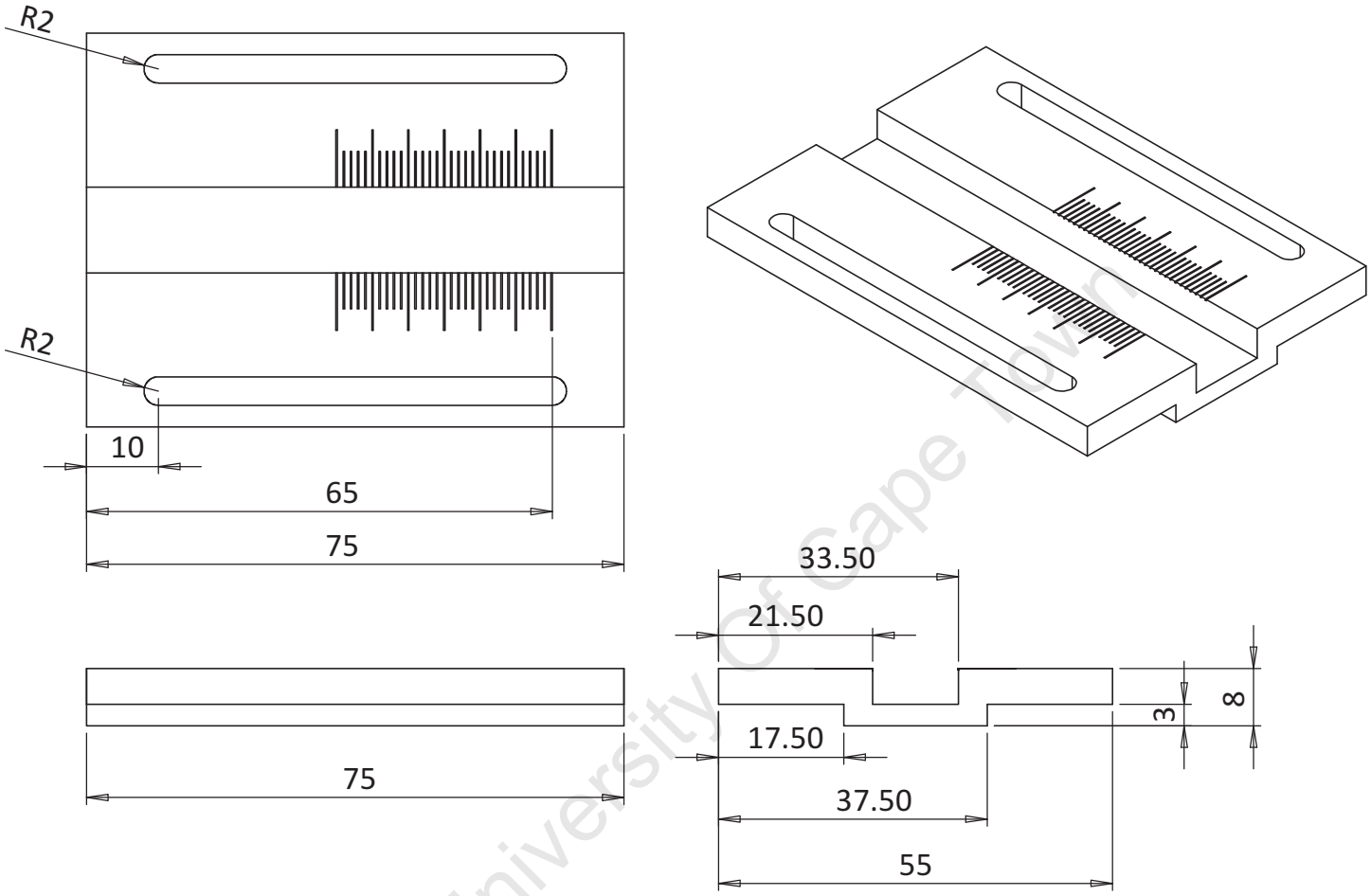

SCALE: 1:1	DRAWING NUMBER: 019
MATERIAL: Stainless Steel 316	
TITLE: Pre-strain Mount Body	
AUTHOR: Jordi Reddy	
DATE:	June 2009

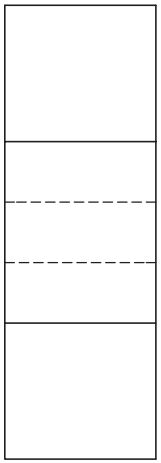

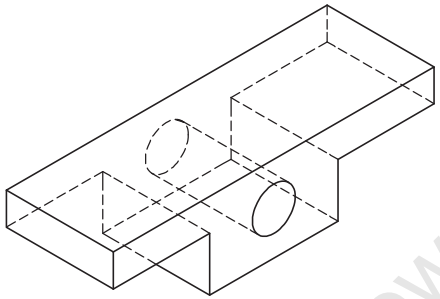

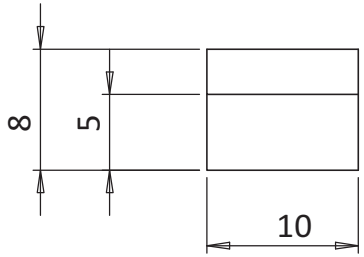

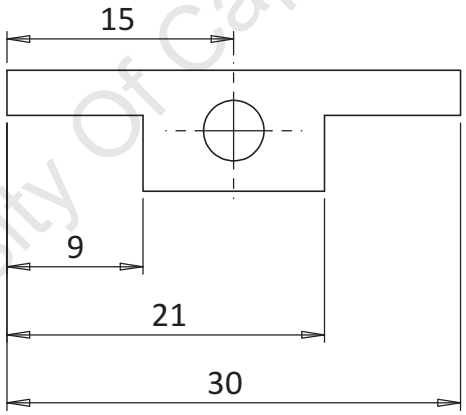

SCALE: 2:1	DRAWING NUMBER: 020
MATERIAL: Stainless Steel 316	
TITLE: Pre-strain Screw Mount	
AUTHOR: Jordi Reddy	
DATE:	June 2009

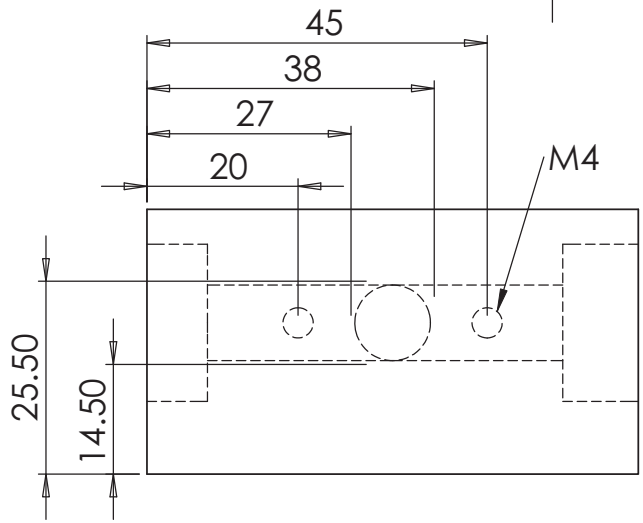

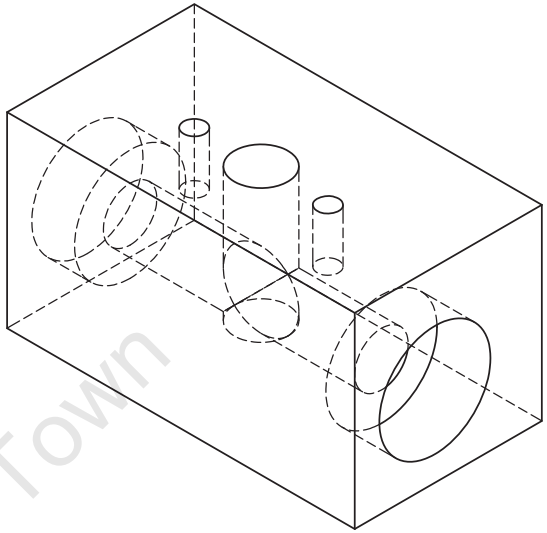

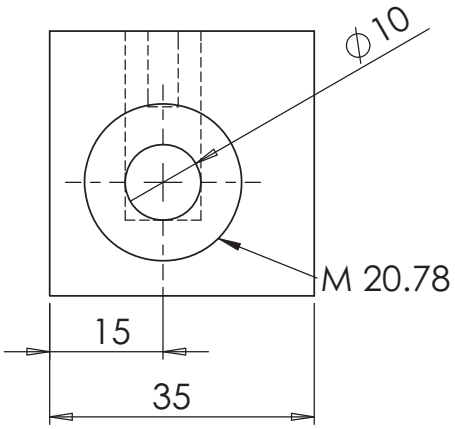

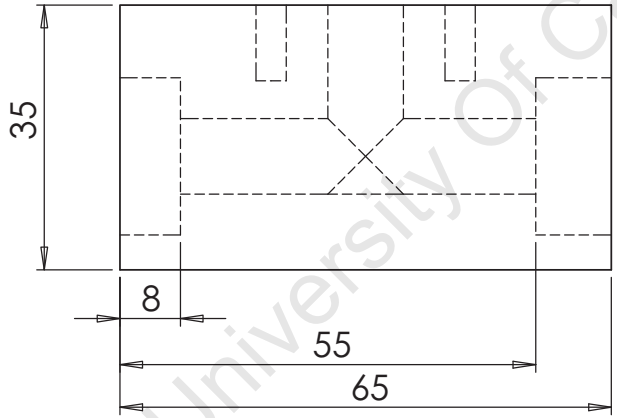

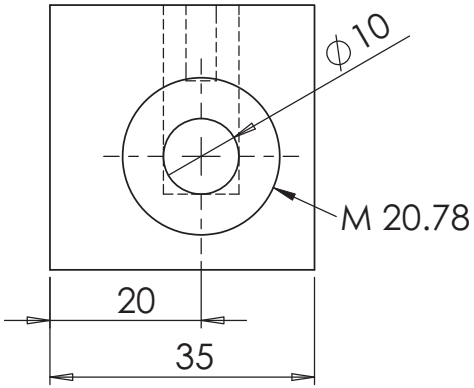

SCALE: 1:1	DRAWING NUMBER: 021
MATERIAL: Perspex	
TITLE: Needle Valve Body	
AUTHOR: Jordi Reddy	
DATE:	June 2009

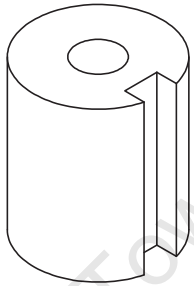

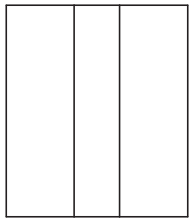

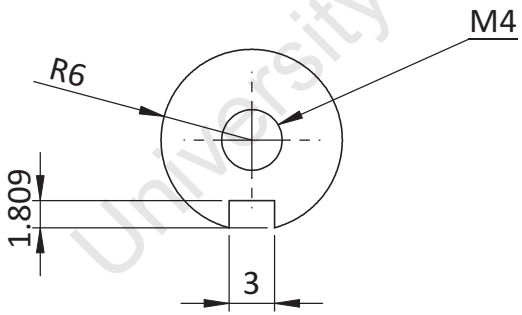

SCALE: 2:1	DRAWING NUMBER: 022
MATERIAL: Teflon	
TITLE: Needle Valve Gate	
AUTHOR: Jordi Reddy	
DATE:	June 2009

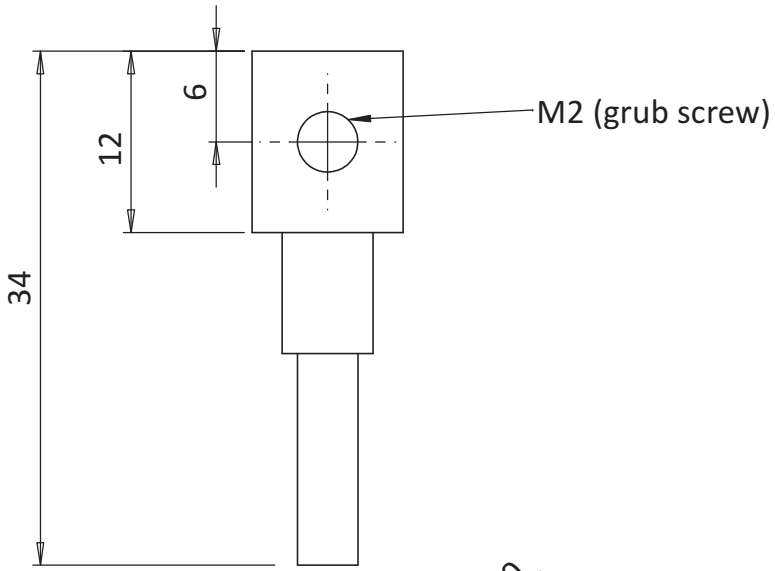

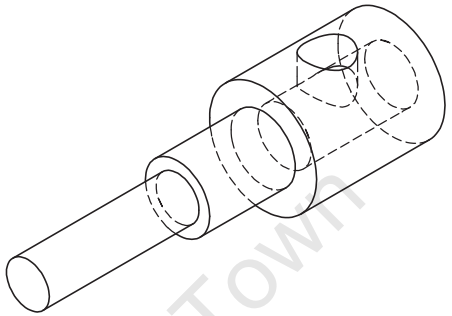

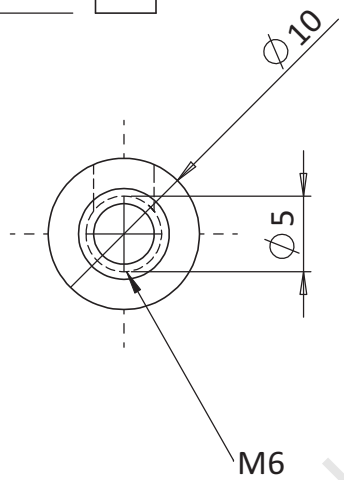

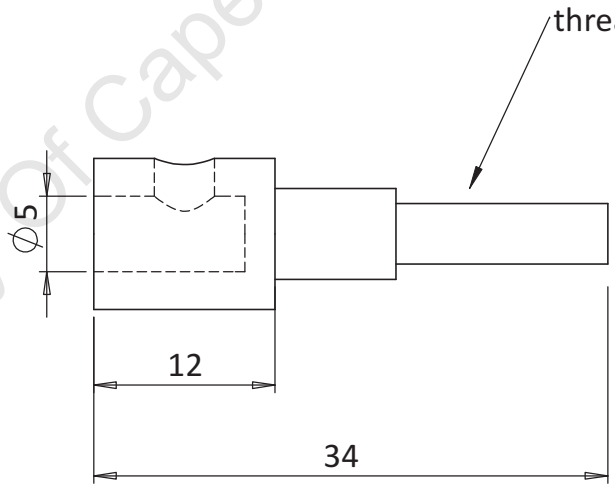

SCALE: 2:1	DRAWING NUMBER: 023
MATERIAL: Stainless Steel 316	
TITLE: Needle Valve Screw	
AUTHOR: Jordi Reddy	
DATE:	June 2009

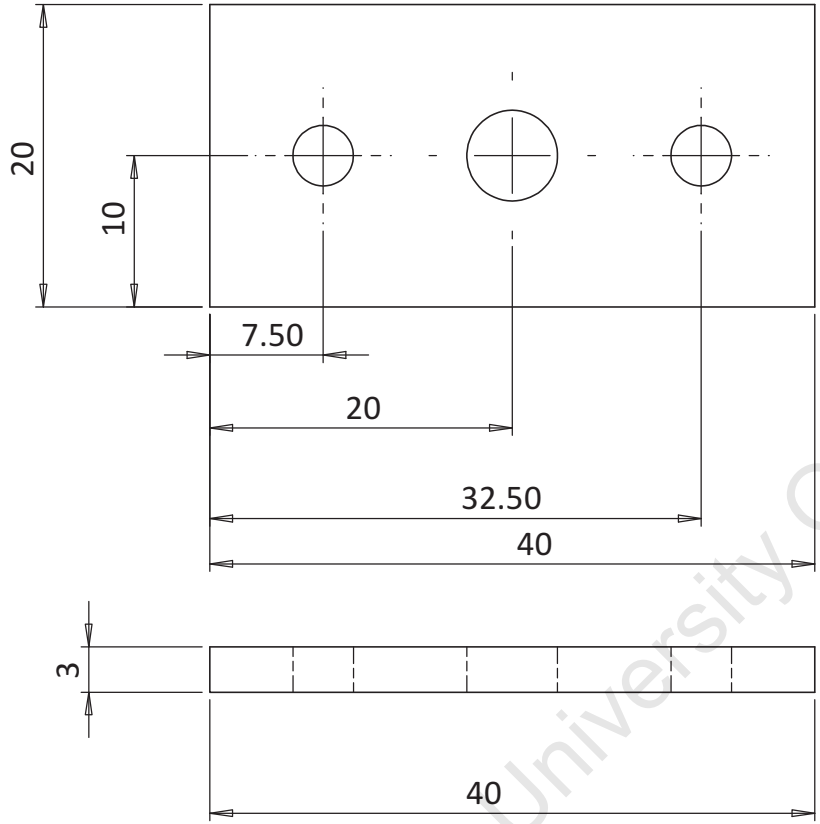

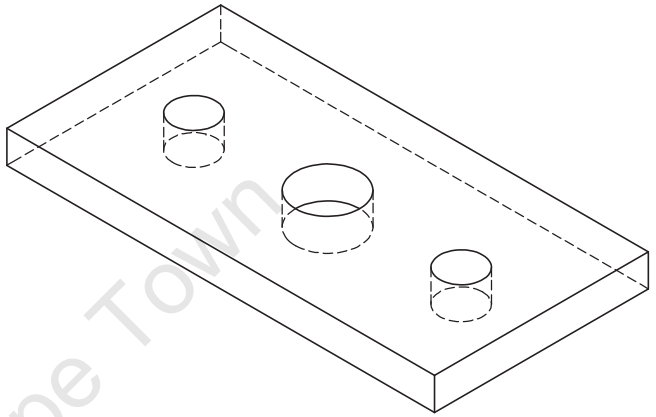

SCALE: 2:1	DRAWING NUMBER: 024
MATERIAL: Stainless Steel 316	
TITLE: Needle Valve Gasket Plate	
AUTHOR: Jordi Reddy	
DATE:	June 2009

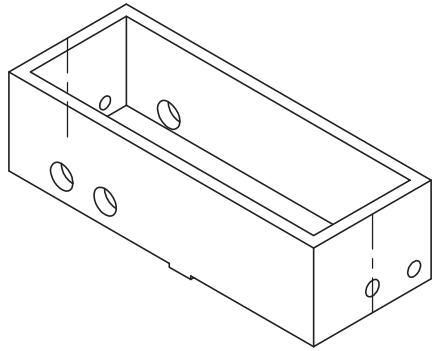

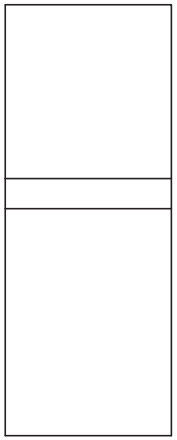

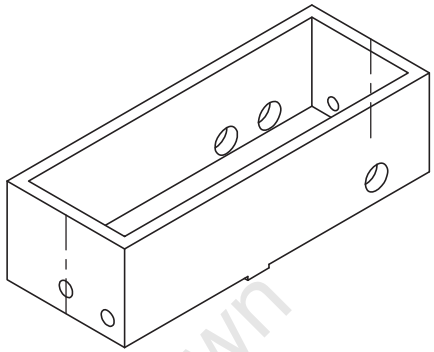

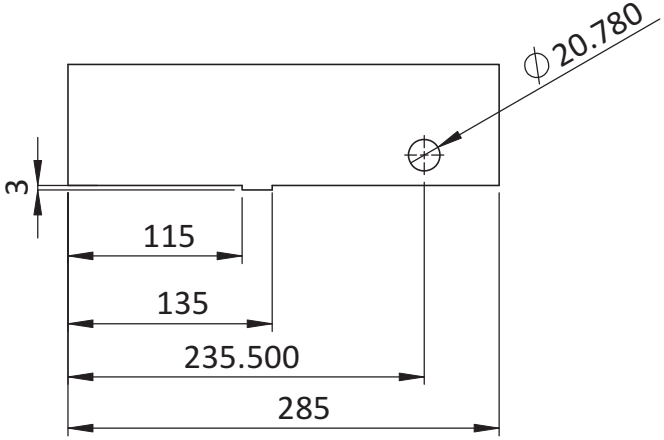

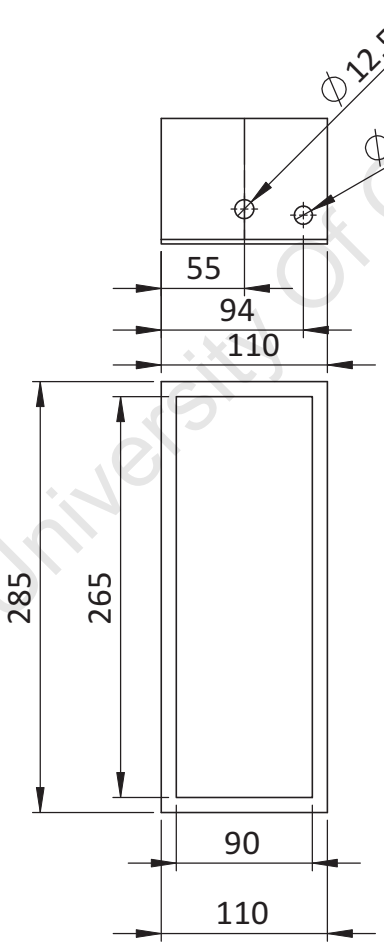

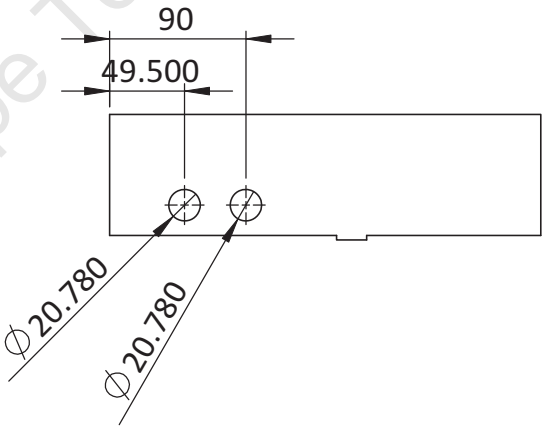

SCALE: 1:5	DRAWING NUMBER: 025
MATERIAL: Perspex	
TITLE: Upper Reservoir	
AUTHOR: Jordi Reddy	
DATE:	June 2009